Miniaturisation des technologies d'imagerie de fluorescence pour assister la chirurgie mini-invasive

Paul Dorval

UNIVERSITÉ DE STRASBOURG

ÉCOLE DOCTORALE MSII

ICube UMR 7357 – Laboratoire des sciences de l'ingénieur, de l'informatique et de l'imagerie

THÈSE présentée par :

Paul Dorval

soutenue le : **25 Février 2015**

pour obtenir le grade de : **Docteur de l'Université de Strasbourg**

Discipline/ Spécialité : Signal, Image, Automatique, Robotique (SIAR) - Image et vision

Miniaturisation des technologies d'imagerie de fluorescence pour assister la chirurgie mini-invasive

THÈSE dirigée par :

M. POULET Patrick	Maître de Conférences-Praticien Hospitalier, Université de Strasbourg

RAPPORTEURS :

M. BOCCARA Claude	Professeur des Universités, ESPCI ParisTech
M. MORDON Serge	Directeur de recherche, INSERM

AUTRES MEMBRES DU JURY :

M. GAYET Brice	Professeur des Universités-Praticien Hospitalier, Université Paris Descartes et Institut Mutualiste Montsouris
M. SOLER Luc	Professeur des Universités-Praticien Hospitalier, Université de Strasbourg
M. UHRING Wilfried	Professeur des Universités, Université de Strasbourg

Remerciements

Le dispositif CIFRE a pour but de sortir le travail de thèse du laboratoire et de créer une synergie entre centres de recherches académiques et entreprises innovantes. Ce travail de thèse a été majoritairement effectué au sein de l'entreprise Fluoptics à Grenoble et c'est tout naturellement que mes premiers remerciements se tournent vers Odile Allard et Philippe Rizo pour la confiance et l'opportunité qu'ils m'ont offert de conduire ce projet. J'exprime tout particulièrement ma gratitude envers Philippe qui a su, tout au long de la thèse, motiver et suivre d'un regard bienveillant le travail accompli.
Je remercie aussi sincèrement Patrick Poulet d'avoir accepté de diriger ce travail et d'avoir partagé avec moi son expertise sur le domaine. Je remercie aussi le laboratoire iCube de Strasbourg pour m'avoir accueilli parmi leurs doctorants.

Je tiens à remercier Claude Boccara et Serge Mordon d'avoir accepté de rapporter ce travail. Je remercie également les autres membres du jury, Brice Gayet, Luc Soler et Wilfried Uhring.

Ma reconnaissance va aussi vers les personnes extérieures ayant participé à ce travail : Fabien Stenard, Gabriele Barabino, Alexandre Filippello, Christian Righini, Ihab Atallah et Jean-Luc Coll notamment pour la validation preclinique et clinique des instruments ; Jean-Marc Dinten, Michel Berger, Patricia Le Coupanec et Charlotte Emain en ce qui concerne les collaborations avec le CEA-LETI.
Alors bien sûr, je remercie chaleureusement mes collègues de Fluoptics. En premier lieu Norman avec qui j'ai énormément appris, puis Stéphanie, Pascal, Yoann, Diane, Anthony, Mathilde, Muriel, Ophélie et tous les autres qui ont permis de rendre ces presque 4 années totalement uniques.

Enfin, je remercie ma famille, mes amis et Laurianne, sans qui tout ça n'aurait pas été possible.

The miniaturization of fluorescence image-guided technologies to assist minimally invasive surgery

Contents

List of Figures

List of Tables

Glossary

CABG: Coronary Artery Bypass Grafting
CCD: Charged-Coupled Devicee
CEA: Comissariat à l'Energie Atomique
CMOS: Complementary Metal Oxide Semi-Conductor
CMOS-APS: Complementary Metal Oxide Semi-Conductor Active Pixel Sensors
CNRS: Centre National de la Recherche Scientifique
CRI: Color-Rendering Index
CE: Conforme aux Egixences
FDA: Federal Drugs Administration
FIGS: Fluorescence Image-Guided Surgery
FPS: Frame Per Second
ICG: IndoCyanine Green
INSA: Institut National des Sciences Appliquèes
Laser: Light Amplification by Stimulated Emission of Radiation
LED: Light-Emitting Diode
HNSCC: Head and Neck Squamous Cell Carcinoma
MPE: Maximum Permissible Exposure
NIR: Near Infra-Red
NUV: Near Ultra-Violet
OD: Optical Density
PCB: Printed Circuit Board
ROI: Region Of Interest
SLN: Sentinel Lymph Node
SLNB: Sentinel Lymph Node Biopsy
SNR: Signal-to-Noise Ratio
USAF1951: United-States Air Force 1951
USB: Universal Serial Bus

Introduction

In the last 10 years, significant improvements have been achieved in all aspects of medical imaging. As a way to create visual representation of the surface or interior of the body or specific organs, medical imaging is a powerful tool to help the physician in his work. In surgery, it gives clues to diagnose disease and guides complex procedures.
Fluorescence image-guided surgery is a particular optical imaging modality. It exploits the properties of light sources in order to image anatomic particularities of tissues thanks to contrast agents, or dyes, previously injected to the patient. This technique gives information in real-time during open surgery to the physician and help him in performing his procedure.
The modality has shown a huge potential in oncology, vascular and lymphatic related surgeries. To be more specific, fluorescence is useful for sentinel lymph node mapping or biopsy in oncologic procedures (breast, skin, gastric and colorectal cancers), perfusion visualization of free flaps in reconstructive surgery, tumor resection and general vascular and lymphatic mapping.

Besides, since 1983 and the first laparoscopic appendectomy, minimally invasive surgical techniques does not cease to develop. The advantages of the method are numerous. First of all, it is noticed a decrease operative trauma with a limited blood loss during surgery. So even though the surgery might take longer in comparison to open procedures, the hospitalization time is always much shorter. With less pain and scarring, the patient bears less post-surgical complications.
Today, the majority of fluorescence image-guided surgery indications are related to open surgery procedures, but the potential of the technology for mini-invasive surgeries is tremendous. Indeed, one of the particularities of mini-invasive surgery is the fact that the surgeon can only rely on the image displayed on the screen and cannot feel the tissue structure as he would do by touching them in an open-surgery procedure. Therefore, complementary information to the anatomical color image is going to become mandatory and NIR fluorescence image-guided

surgery could be the solution. Clinical studies have already presented promising results on indication such as the cholecystectomy or the nephrectomy, which are common mini-invasive surgeries. In these cases, fluorescence imaging is used to image distinctive anatomical part such biliary vessels in the case of cholecystectomy or tumor margins and vascularization for the nephrectomy. Nevertheless, few devices are commercially available for such procedures and the technology is not widely developed in this very demanding field. The direct translation from open to mini-invasive surgeries for the existing fluorescence image-guided devices is not trivial due to their size and overall performance.

Although the potential of fluorescence imaging and mini-invasive procedures seemed promising, challenges have been identified in the translation of the technology from open to mini-invasive procedures. The purpose of the thesis was to first identified the milestones and then addressed them in order to develop a reliable fluorescence image-guided device for mini-invasive surgeries. The obstacles identified to the development were mainly a size issue and a sensitivity problem due to the use of complex optical elements and small image sensors.
This thesis will focus on several subjects. First, the color channel and the way to overlaid the color image to the fluorescence information. Several solution will be presented and a one sensor architecture and a two sensors device will be developed an compared.
A breakthrough in the size of image sensor used will also be exposed. In fact, large scientific image sensor, commonly used in NIR fluorescence imaging, required too much space and cannot be integrated in mini-invasive camera.
The depth of field of the imaging system will also be a problem assessed in the thesis. In general, ergonomics of the fluorescence image-guided devices will be discussed.
Finally, one of the big challenge identified is the need of high framerate acquisition. Because the imaging device has to provide real-time images to the surgeon, the framerate of the system must exceed $25fps$. Moreover, in the case of a single sensor system, a pulsed acquisition mode is envisaged. In this case the system should be able to acquire images at $50fps$ or more. High framerates induce short exposure time and that is, a priori, inadequate with the low fluorescence light emission of the probes imaged.

To solve and progressively address the several issues identified above, the thesis will present the development of three distinctive devices. A first step of miniaturization of the fluorescence image-guided technology for open surgery had been identified as a requirement for further mini-invasive investigation. Based

on this first step, the second development of the thesis is a 2-sensors camera device dedicated to mini-invasive procedures. Then an innovative system able to acquire color images and fluorescence images in the same time with one sensor will be presented.
The chapter 1 of the thesis will present generalities about imaging and especially fluorescence imaging. A survey of existing fluorescence image-guided surgery devices will be exposed. This chapter will clearly set the need for further investigation and the purpose of the developments achieved for this thesis.
The chapter 2 will expose the development of a miniaturized device dedicated to open-surgery and specifically laparotomy, the Fluostick^{TM}. The complete development process will be exposed, as preclinical and clinical evaluations. This development will be a first step, prior of the development of mini-invasive devices.
The chapter 3 will present the development of a 2-sensors fluorescence imaging system for mini-invasive purpose called the FluoMIS^{TM} and directly derived from the development exposed in chapter 2. Characteristics and particularities of mini-invasive modality for fluorescence NIR imaging will be evaluated. Preclinical tests performed with the system will be balanced.
The chapter 4 will introduce a new mini-invasive single sensor fluorescence imaging device development. The goal of this development is to correct the drawbacks of the system presented in chapter 3. Also, it will be exposed innovative achievements as the use of a sequential pulsed acquisition mode.

The conclusion will expose the achievements of the thesis. Also, a discussion will be conducted about the different architectures proposed for a mini-invasive FIGS system. Perspective work and potential studies will end the conclusion.
Appendix will describe characterizations tools involved in the thesis. An image sensor test method will be exposed, as sample results of camera evaluations. A ICG limit of detection determination will be presented and clues about the depth of field and the resolution determination will be given.

Chapter 1

Fluorescence Image-Guided Surgery

What you will find in this chapter:

This chapter is a survey of the specific technology of fluorescence image-guided surgery. It will be exposed the principle of fluorescence, existing fluorescence image-guided surgery systems and major addressed indications. The chapter clearly sets the need for further investigation and the purpose of the developments achieved for this thesis.

Contents

Figures

Tables

1.1 Introduction

In recent years, a lot of improvements have been achieved in all aspects of medical imaging. This chapter will present in details the specific technology of fluorescence imaging. Numerous reviews of the technique have been published [1, 2, 3, 4, 5, 6, 7, 8] and laboratories and companies are working on the subject worldwide. The modality has shown a huge potential in oncology, vascular and lymphatic related surgeries. To be more specific, fluorescence is useful for sentinel lymph node in oncologic procedures (breast, skin, gastric and colorectal cancers in majority, [9, 10, 11, 12, 13, 14, 15, 16, 17, 18]), vascular visualization of free flaps in reconstructive surgery, [19], tumor resection, [20, 21] and general vascular, [22, 23, 24, 25], and lymphatic mapping, [26, 27]. The goal of Fluorescence Image-Guided Surgery (FIGS) systems is to image fluorescent contrast agents, also called probes, previously injected to the patient. To achieve this, the system is able to send specific excitation light absorbed by the probes to be imaged and to collect the subsequent light emitted. Indocyanine Green (ICG) and methylene blue are FDA-approved probes for fluorescence procedures, [28, 29, 30, 31, 32]. Other contrast agents such as Patent Blue V, approved in Europe, have shown a potential for fluorescence image-guided surgeries, [16, 33]. Targeted contrast agents are also under development. They are mostly developed to be tumor specific, [34, 35, 36, 37, 38]. These most common probes emits light in a near infrared (NIR) spectrum region comprised between 650 and $900nm$.
The FIGS system mostly consists in an imaging head linked to one or several control boxes including hardware and software to acquire and display images. Due to their size and weight, most of the available systems on the market are fixed to a mechanical arm and are able to image the surgical field from the top only. The system is built around an imaging sensor, which is, thanks to filters, able to collect specifically the fluorescence light emitted by the excited probes, [39, 40, 41]. The ambient light of the theater, as well as the shadowless surgical light, contain NIR light. It's particularly true for xenon or tungsten type light. Therefore, to perform good fluorescence acquisitions, the light of the operating room must be turned off. Some FIGS systems provide an additional filtered white light which help the surgeon to perform his procedures but will not disrupt the acquisition of fluorescence emission light.

1.2 Fluorescence imaging

1.2.1 Light and living tissues

Medical and optical imaging

Medical imaging, as the process to create visual representation of the body for clinical analysis and medical intervention, is divided into categories according to the electromagnetic spectrum. The figure 1.1 shows the electromagnetic spectrum and names different areas. Medical imaging applications use most of the domains of this spectrum. For instance, radiology deals with the X-rays part of the spectrum, Single Photon Emission Computed Tomography (SPECT) and Positron Emission Tomography (PET) deals with the Gamma-rays part of the spectrum, and Magnetic Resonance Imaging (MRI) with the radio-frequency range.
Fluorescence image-guided surgery, the thematic of this thesis, is part of Optical imaging. Optical imaging modalities focus on the visible part of the spectrum extended to the near-ultraviolet (NUV) and near-infrared areas (NIR).

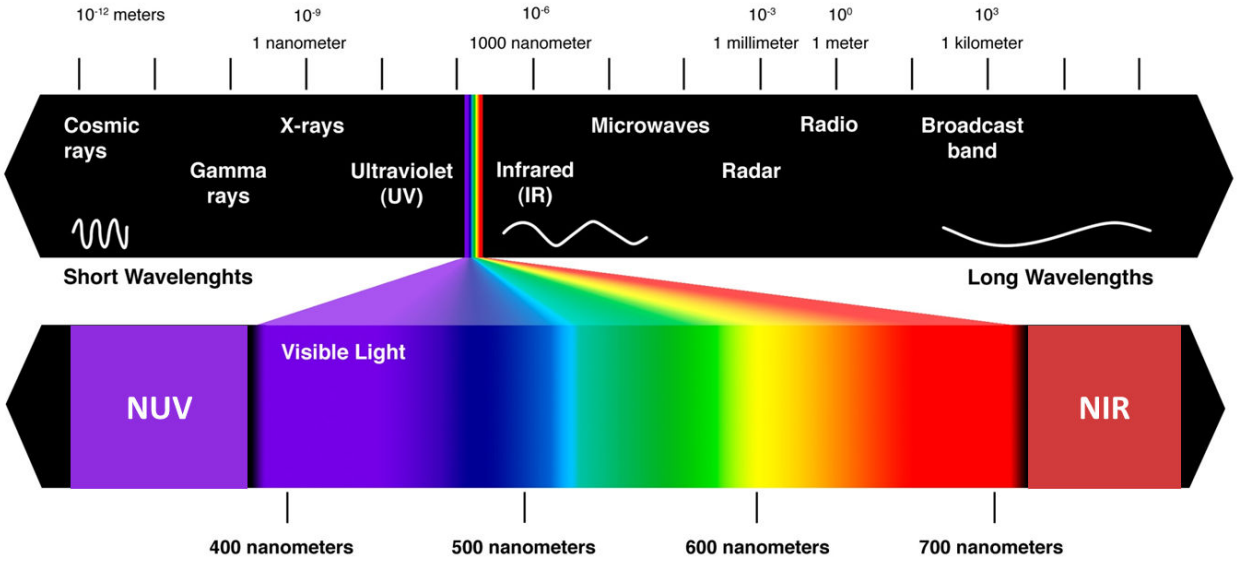

Figure 1.1: Electromagnetic and light spectra

Of course, the first and main in-vivo optical imaging method involve only the eye of the surgeon who is able to distinguish anatomical structures, color and aspects of the tissues and organs thanks to an adequate surgical shadow-less

light and a direct visualization. Nonetheless, the use of special sensors, cameras and lights can bring the surgeon a further level of information.

Light interactions with the tissues

At a microscopic level, two phenomenons describe the light interaction with molecules: the absorption and the scattering. The absorption coefficient, μ_a, of a medium expresses its disposition to block incoming light. In fact, it also expresses how the energy of incoming photons will be taken up by the molecules of the medium considered. The coefficient μ_a is expressed in cm^{-1} and it described by the following equation:

$$\mu_a = \rho_a \sigma_a \tag{1.1}$$

The coefficient ρ_a, expressed in cm^{-3}, is the concentration of molecules in the medium considered. The parameter σ_a is called effective cross-section of a molecule and it expressed in cm^2. The cross section of a molecule is an expression of the theoretical shadow created by the molecule exposed to a beam of light. The following figure, 1.2, is a schematic of the cross-section concept. The molecule is represented by a sphere with a geometrical cross-section A expressed in cm^2, the absorption efficiency coefficient, Q_a is dimensionless.

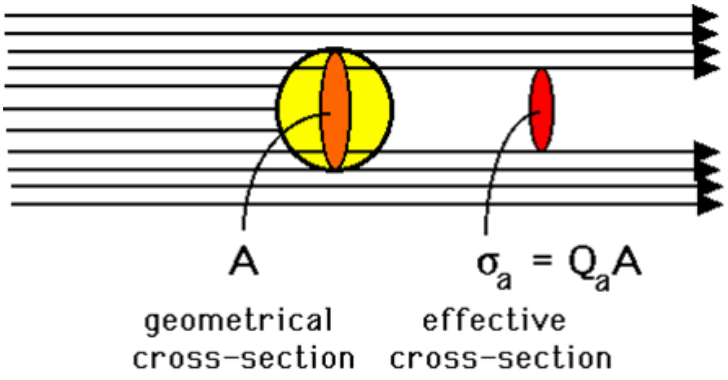

Figure 1.2: Absorption schematic, from [42]

From this absorption phenomenon resulted the Beer-Lambert law which expressed the attenuation of a collimated beam light crossing a non-scattering medium:

$$I(z) = I_0 e^{-\mu_a z} \tag{1.2}$$

The coefficient I_0 is initial intensity of the beam light, I is the intensity at a distance z in the medium expressed in cm.

In order to describe the light interaction with tissues, the absorption is not the only coefficient to take into account. The other phenomenon that will be described here is called the scattering effect. Similarly to the absorption coefficient μ_a, the scattering coefficient μ_s expresses the disposition of a medium to scatter incoming light. The coefficient μ_s is expressed in cm^{-1} and it described by the following equation:

$$\mu_s = \rho_s \sigma_s \tag{1.3}$$

The coefficient ρ_s, expressed in cm^{-3}, is the concentration of molecules in the medium considered. The parameter σ_s is called effective cross-section of a molecule and it expressed in cm^2. The following figure, 1.3, is a schematic of the cross-section concept. The molecule is represented by a sphere with a geometrical cross-section A expressed in cm^2, the scattering efficiency coefficient, Q_s is dimensionless.

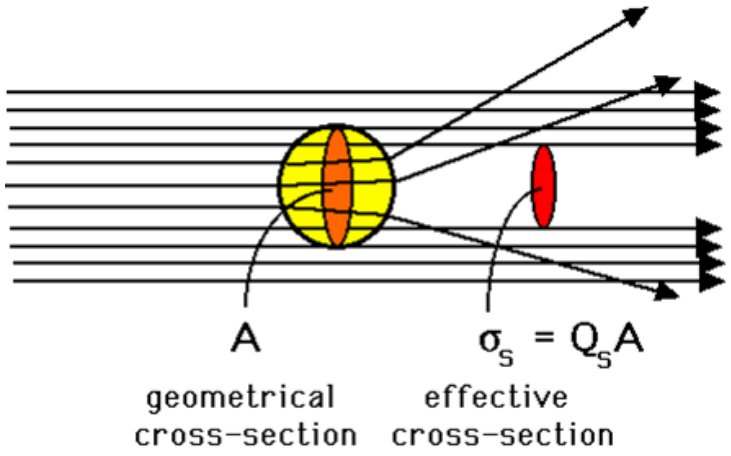

Figure 1.3: Scattering schematic, from [42]

The path of light in a scattering medium is not only described by the scattering coefficient μ_s. Indeed, a scattering event changes the direction by a scattering angle θ. The angular distribution of scattered photons as a function of the angle θ is called the phase function, $f(\theta)$. The phase function depends on the size of the scattering particles. For biological media, it can be expressed by the empiric Henyey-Greenstein law, [43]:

$$f(\theta) = \frac{1}{4\pi} \frac{1 - g^2}{(1 + g^2 + 2gcos\theta)^{3/2}} \tag{1.4}$$

In this equation, g is called the anisotropy factor, defined as the mean value of the cosine of scattering angles, $g =< cos\theta >$. Finally, the scattering properties of

a medium can be expressed by 2 parameters, the scattering coefficient μ_s and the anisotropy factor g. When the medium is highly scattering, these 2 parameters could be expressed by the reduced scattering coefficient μ'_s:

$$\mu'_s = (1 - g)\mu_s \tag{1.5}$$

This coefficient is the opposite of the mean path-length of the light, the limit after that the beam will loose ballistic information.

As a function of its wavelength, incoming light will interact differently with the tissue. The two aspects, important to consider when talking about optical imaging, are the absorption and the reduced scattering coefficients of the tissues. The figure 1.4 gives the absorbance of various tissue and blood components from $100nm$ to $10000nm$. In living issue, the major absorbers are water, lipids, oxyhemoglobin and deoxyhemoglobin. When the absorbance factor is low, the light will be able to penetrate deeper in the tissues, but encountering multiple scattering and following a diffuse transport.
Optical imaging for diagnostic and therapeutic applications in biology and medecine is more efficient in a range spreading from $600nm$ to $1000nm$, where the absorbance coefficient of the tissues is lowest and scattering lower than in the visible range. In fact, it is usually assumed that the reduced scattering coefficient μ_s depends on the wavelength according to a power law:

$$\mu'_s = a.\lambda^{-b} \textit{with } b \textit{ between 0.8 and 1.3, see [44, 45]} \tag{1.6}$$

The window between $600nm$ and $1000nm$ is called the imaging or therapeutic window, [44, 46]. It represents the range where the tissue penetration is greatest. In this window, the absorption coefficient of living tissues are around $0.1cm^{-1}$, corresponding to a path-length of $10cm$ before absorption. The reduced scattering coefficient is of the order of $10cm^{-1}$, corresponding to a mean transport length of $1mm$. Any photon detected after some millimeters of propagation in a tissue encountered many scattering events. Its trajectory is much longer than the straight way, the ratio between the 2 being called the Differential Path-length Factor (DPF), ranging around 10. The penetration depth of optical methods are therefore limited to several centimeters in the NIR range, limiting the optical imaging methods to the examination of small organs or to superficial layers of bigger organs. For fluorescence imaging, we can estimate that the penetration depth is divided by ten, as compared to optical methods detecting scattered photons, giving penetration depth as low as $100\mu m$ in the visible range and up to $3mm$ in the NIR area of the spectrum.

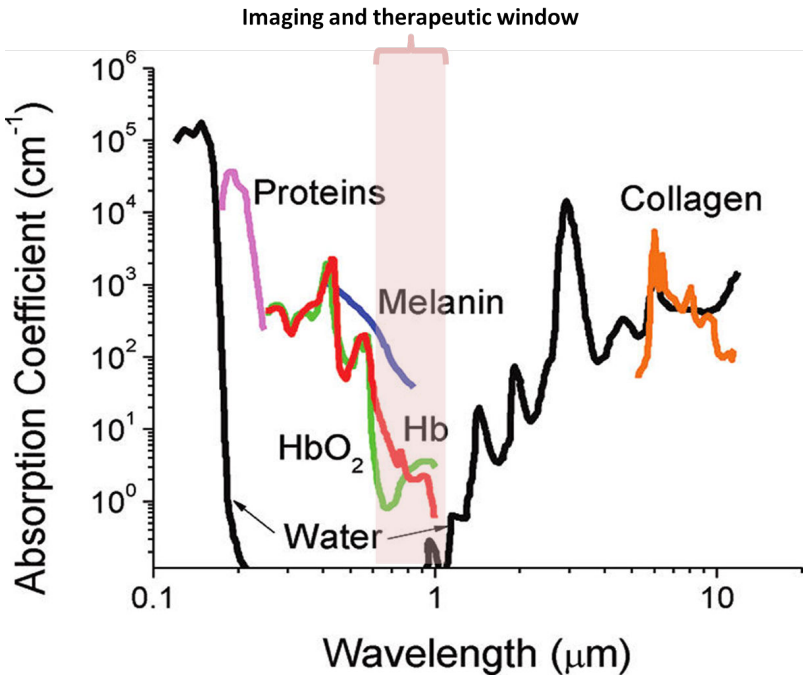

Figure 1.4: Absorption coefficients, from [35]

1.2.2 Fluorescence principle and imaging modality

This thesis will focus on a specific modality of optical imaging called fluorescence imaging. A substance or molecule is called fluorescent when it emits light after it has absorbed light of shorter wavelength. The principle of fluorescence could be explained by a simplified Jablonski diagram, see figure 1.5. A fluorescent molecule absorbs light with specific energy. This energy will set the molecule in an excited state. Then the molecule will try to relax and reach back its fundamental state. By relaxing, the molecule will lose energy. This energy could be expressed by heat and light radiation.

Because the energy of light photons is directly linked to the wavelength through the relation $E = h\nu = \frac{hc}{\lambda}$, where h is Planck's constant, ν the frequency, c the celerity and λ the wavelength, the light emitted by a fluorescent molecule has a higher wavelength than the excitation incoming light. The excitation and the emission wavelengths are not unique and both are distributed along the spectrum. This is explained by the numerous excited states accessible and the various non-radiative relaxation pathways that occur before the radiative emission of fluorescence light. The fluorescence characteristics of a molecule can be described in a spectrum where absorption/excitation and emission are plotted in function

of the wavelength and according to a relative absorption affinity and intensity of emission. Common molecules' spectrum will be presented later in this chapter.

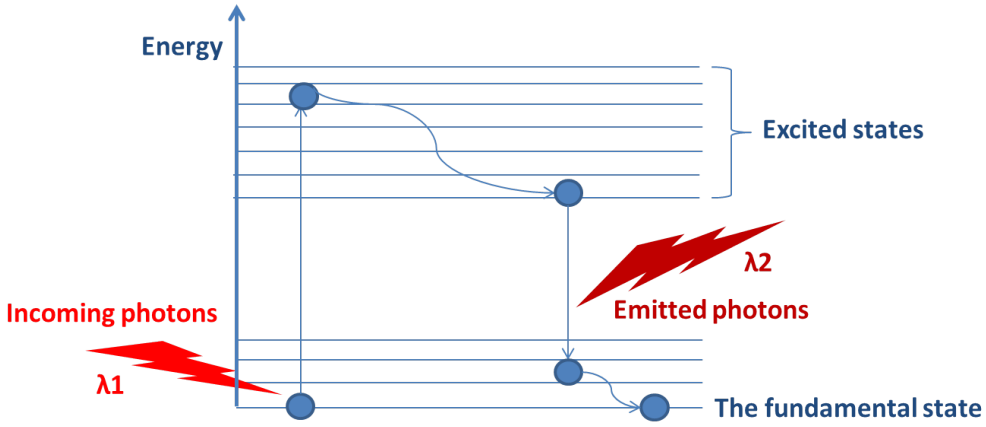

Figure 1.5: Jablonski diagram

Fluorescence in-vivo imaging is a widely develop technique for preclinical investigation purposes. Numerous imaging systems for small animals are available on the market. The table 1.1 presents the main actors on the market. Those systems are mostly designed to image mice or other small animals. They are able to send multiple excitation wavelengths and use switching elements to adapt filtering to the fluorescent probes imaged. As an imaging apparatus, these devices integrate high-end scientific cooled CCD cameras.

Company	**System**
Biospace, France	Photon Imager
Berthold, Germany	NightOWL and LB983
Bruker, Germany	FX Pro, FX MS Pro and Xtreme
Perkin Elmer, USA	FMT1000 to FMT4000
Li-Cor	Pearl Impulse

Table 1.1: The main preclinical in-vivo fluorescence imaging systems

The following figure, 1.6, is a picture of the Bruker system, FX MS Pro. The architecture of the system is common to the other existing devices. The animal is placed in a closed enclosure to perform measurements and no manipulation are allowed during the fluorescence acquisition.

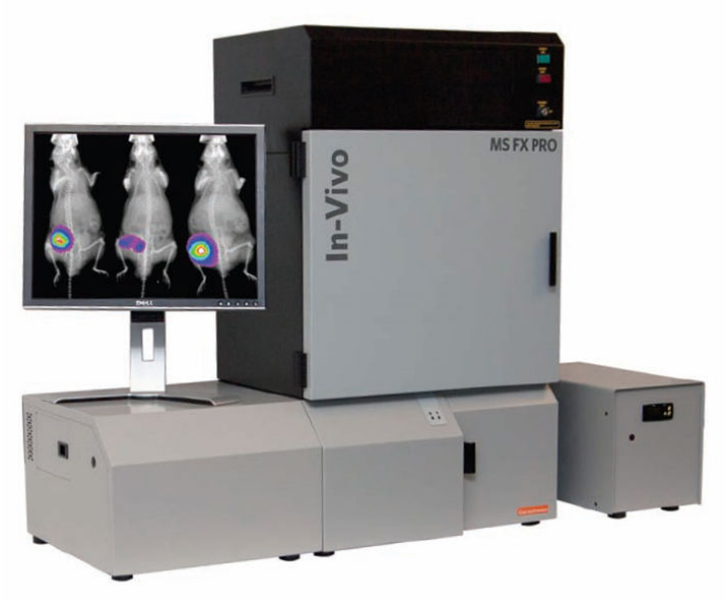

Figure 1.6: The Bruker FX MS Pro, preclinical in-vivo fluorescence system

Concerning medical imaging, the fluorescence could be endogenous or exogenous. Endogenous fluorescence means that some tissues, due to particular molecules, demonstrate autofluorescence properties. Collagen for instance is fluorescent under a blue or near-UV excitation. Nonetheless, most of the autofluorescence of tissues is bounded to the visible part of the spectrum and few autofluorescence artifacts will occurs in the near-infrared therapeutic window described in figure 1.4.
Exogenous fluorescence imaging involves fluorescent contrast agents (also called dyes or probes). These contrast agents are molecules that can be targeted or non-targeted and mostly evolved in the visible and the NIR part of the spectrum. The goal of Fluorescence Image-Guided Surgery (FIGS) systems is to image fluorescent contrast agents previously injected to the patient. To achieve this, the system is able to send specific excitation light absorbed by the probes to be imaged and to collect the subsequent light emitted. As presented before, the NIR area of the spectrum is the more adapted to imaging modalities. FIGS systems mostly deal with NIR localized contrast agents. The figure 1.7 is a schematic of a FIGS system. It mostly consists of a camera able to discriminate the fluorescence emission from the excitation light, a light source to generate the excitation light and filters. Filters are involved to block the excitation light in front of the camera and limit the excitation light to a narrow band of the spectrum. Filters are critical components in a FIGS device. Mostly two types of filters are inte-

grated in such systems. Absorptive glass filters, also called colored filters, are simple and quite cheap. It consists of a glass substrate where various inorganic or organic compounds have been added. Dichroic, or interference, filters are more complex components. They use complex interferential coating on glass or plastic substrate and are usually more selective than colored filters.

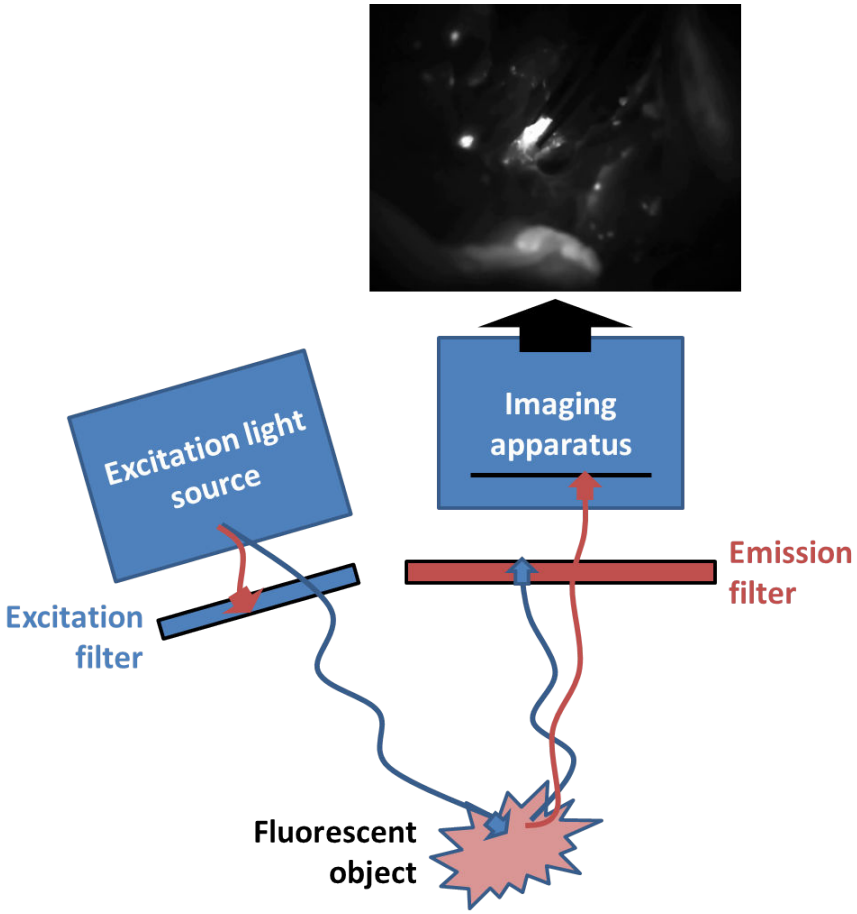

Figure 1.7: Fluorescence imaging principle, FIGS system

The principal approved probes for clinical fluorescence procedures are the Indocyanine Green (ICG), the Methylene blue and the Fluorescein. The ICG and the Methylene blue emit light in a NIR range region comprised between 650 and 900nm. The Fluorescein emits light in the green visible part of the spectrum. Figures 1.8 and 1.9 present the emission and absorption spectrum of ICG and Methylene Blue, the 2 probes which operates in NIR area of the spectrum. This thesis will mostly focus on ICG. ICG is available worldwide for intravenous injection and the main commercial name are:

- Infracyanine® from Serb laboratories, France market

- ICG-Pulsion® from Pulsion, Europe market
- IC-Green® from Akorn laboratories, USA market
- Diagnogreen® from Daiichi Sankyo, Japan market

For lymphatic related indications, which require a subcutaneous injection of ICG, its use is subject to a clinical trial submission.

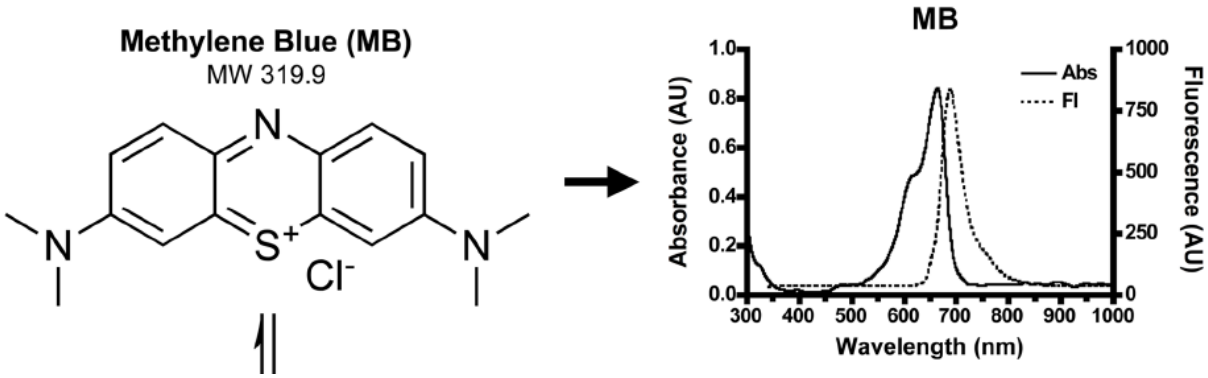

Figure 1.8: On the left, the chemical structure of Methylene Blue is given. On the right, absorption and emission spectrum re displayed, figure from [47]

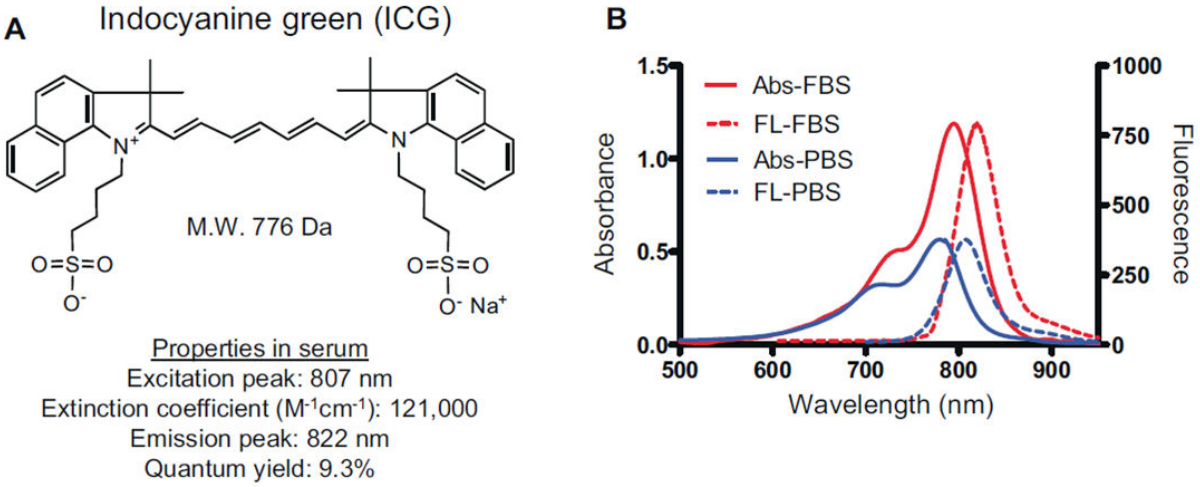

Figure 1.9: On the left, the chemical structure of ICG is given with key optical properties. On the right, absorption and emission spectrum are displayed for ICG diluted in phosphate-buffered saline (PBS) and fetal bovine serum (FBS), figure from [3]

1.2.3 Why fluorescence image-guided surgery ?

The Methylene blue is already used as a simple colored dye in some surgeries, for instance the detection of lymph node. Thanks to its blue color, the surgeon is able to detect high concentration of the product with his eye. The same statement can be made with ICG, which is a green colored dye. It is already an attempt to what fluorescence image-guided surgery is designed for : add contrasts and information to the surgeon's field of view. It is illustrated in figure 1.10. On the left, it is a schematic of the heart as presented in an anatomy book. On the top right, it is the real view of a heart visualized by the surgeon. The goal of FIGS is to give access to the surgeon to extra information such as the position of the vessels or improved differentiation between anatomical structures. On the bottom right, an image of a ewe's heart has been acquired with a FIGS system after an intravenous injection of ICG. Coronary vessels are clearly identifiable.

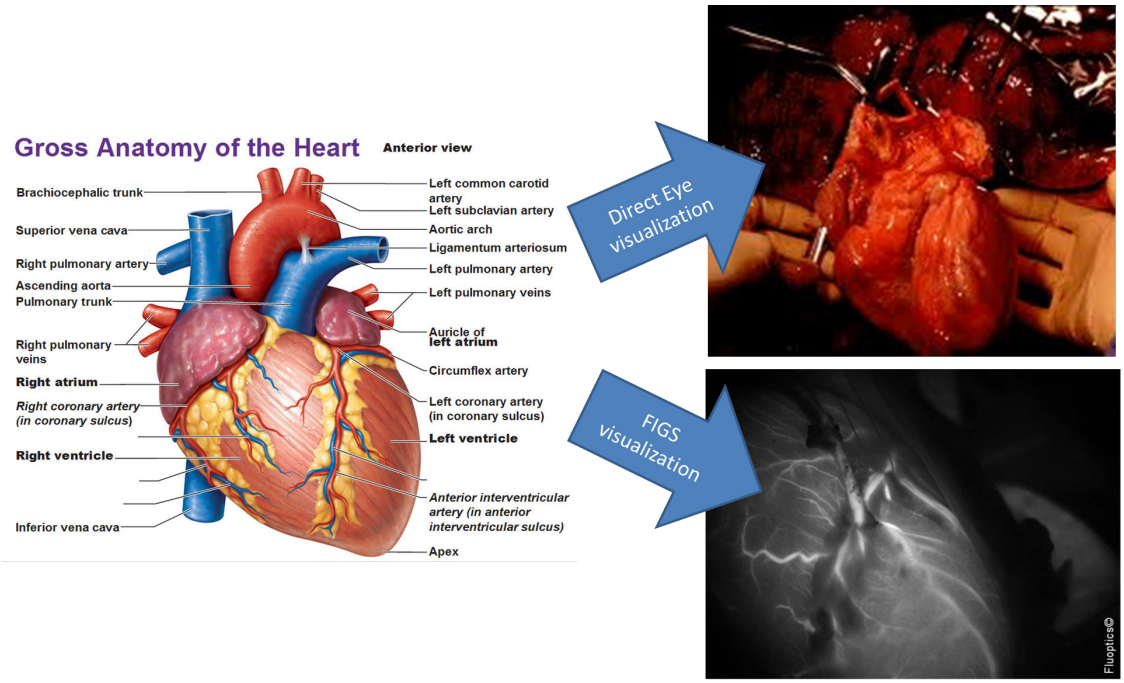

Figure 1.10: The goal of FIGS. Left anatomical representation of the heart, top right surgeon real visualization of the heart, bottom right ewe's heart visualization with the Fluobeam® system

In the case of ICG, NIR FIGS devices have a highly improved contrast in comparison of the eye of the surgeon. What is more, they are able to detect fluorescence signal not only at the surface but few *mm* deeper in the tissues.

Later in this chapter, example of indications using FIGS devices and ICG will be presented.
Perspective also exists with the use of targeted contrasts agents. Some probes under development, coupled to a FIGS system, are able to target specific tumors. For instance, it is the case with Angiostamp^{TM} developed by Fluoptics. Companies as Molecular Probes® and Perkin Elmer ® provide targeted probes for the preclinical market.

1.3 Fluorescence image-guided surgery, a survey

The following section will present a survey of existing Fluorescence Image-Guided Surgery (FIGS) instrumentation. Some typical characteristics of the systems will be presented and compared. Also, a non-exhaustive list of indications will be presented and commented.

1.3.1 Systems

As said before, the devices presented in this thesis mostly focus on the visualization of ICG. Nonetheless, there are not all similar and several parameters could be compared. The table 1.2 presents existing FIGS devices and gives objective information about the fluorescence excitation and emission collection, the typical working distance and field of view of the camera and the presence of an additional color image and white light. A distinction is also made concerning the clinical statue of the devices. Indeed, established company commercialize products for the medical market but laboratories also provide systems to surgeons but only in the context of clinical studies.

System	Manufacturer	Fluorescence Excitation	Fluorescence Signal	Working Distance	Field of view	White light	Color + Fluo	Clinical statue
Photodynamic Eye(PDE®)	Hamamatsu Photonics, Japan	LED 805nm, 4mW/cm^2	>820nm	20cm	9.4×6.9cm	no	no	FDA&CE approved
SPY®	Novadaq Technologies, Canada	Laser 806nm	>835nm	30cm	16.7×12cm	no	no	FDA&CE approved
Fluobeam®	Fluoptics, France	Laser 750nm, 6mW/cm^2	780nm<X<900nm	20cm	from 20×14 to 2.2×1.6cm	yes	no	FDA&CE approved
Artemis®	Quest Medical Imaging, Netherlands	LED&Laser	-	-	-	yes	yes	CE approved
Iridium	Visionsense, Israel	-	-	-	-	yes	yes	CE approved
FLARE™	Israel Beth Deaconess Hospital / Frangioni Labs, USA	LED 745-779nm	800nm<X<848nm	45cm	from 12×9cm to 2.2×1.6cm	yes	yes	Clinical trial
MiniFLARE™	Israel Beth Deaconess Hospital / Frangioni Labs, USA	LED 745-779nm	800nm<X<848nm	30cm	from 12×9cm to 2.2×1.6cm	yes	yes	Clinical trial
T3-platform	SurgOptix, USA	Laser 750nm	-	21cm	from 1.5cm^2 to 107cm^2	yes	yes	Clinical trial
HyperEye®	Mizuho, Japan	LED 760nm	-	-	-	yes	yes	Clinical trial
GXMI navigator	Institute of Automation, China	LED 760nm	-	30cm	25X25cm	Yes	Yes	Clinical trial

Table 1.2: Survey of FIGS systems

In terms of ergonomics, FIGS devices could be classified into two categories. Some of the existing systems are designed to be hand-held directly by the surgeon or by an assistant. Other devices are too heavy and bulky to do so and are integrated into mechanical arms. The figures 1.11 and 1.12 show pictures of the devices.

Figure 1.11: Images of the FIGS systems, mechanical arm-held type. A is the SPY®, B is the Artemis®, C is the FLARE™ and D is the miniFLARE™. See table 1.2 for further details

Figure 1.12: Images of the FIGS systems, hand-held type. A is the PDE®, B is the Hypereye® and C is the Fluobeam®. See table 1.2 for further details

The main actors of the market are the PDE® and the SPY® devices, the SPY® for US market and the PDE® for Asia and Europe markets. The Fluobeam® is the FIGS system developed by Fluoptics and it will be the basis for the developments presented in this thesis. The table 1.3 presents the results of systems comparison performed by Fluoptics. The parameters evaluated were the spatial resolution, the working distance, depth of field and the ICG limit of detection. Methods to determine the resolving power and the ICG limit of detection are presented in appendix B of this thesis. The gap between the limit of detection between the Fluobeam® and the other devices is the more noticeable. It is able to detect quantities of ICG 10 times lower than competitors.

System	Geometric resolution	Nominal working distance	Depth of field	ICG limit of detection
Fluobeam®	$20lp/mm$, i.e. $25\mu m$	$20cm$	$3cm$, autofocus	$0.5pmol$
PDE®	$2lp/mm$, i.e. $250\mu m$	$20cm$	$5cm$, no autofocus	$5pmol$
SPY®	$2.25lp/mm$, i.e. $220\mu m$	$30cm$	$15cm$, no autofocus	$10pmol$

Table 1.3: Performances comparison between the Fluobeam®, PDE® and SPY®

1.3.2 Indications

In the following section will be presented some applications of fluorescence image-guided surgery. This list of indications is not exhaustive and mainly focus on the use of ICG as a contrast agent. The following applications, illustrated by images from the literature acquired with the FIGS systems described in this chapter, will be presented:

- Sentinel Lymph Node mapping and biopsy
- Flap Surgery
- Hepatic Metastases
- Lymphoedema and Lymphatic mapping
- Coronary Artery Bypass Grafting

Sentinel Lymph Node procedure

The Sentinel Lymph Node (SLN) procedure or Sentinel Lymph Node Biopsy (SLNB)is a common act in oncologic surgeries. The so-called sentinel lymph node is the first draining a cancer. It is postulated that it is the first place where metastasizing cancer cells would be found or detected, prior to a global dissemination. Lymph node metastasis is one of the most important signs to stage a cancer and set up an adequate therapy.
The common procedure involves the use of a radioactive colloid, the technetium-99m. This substance, once injected near the tumor, will be rapidly fixed by the first lymph node draining the tumor. Gamma probes are used to detect the technetium and to approximately detect the position of the lymph node. The Methylene blue and the Patent blue V are commonly used in this procedure but

only as a colored visual dye. They are similarly injected in the peri-tumoral area and then fixed by the sentinel lymph node. The dye helps the surgeon to find precisely the position of the node. Allergic reactions has been notified in the literature with blue dyes, [48, 49]. ICG, as a colored dye, has the advantage to be well assimilated by the patient . Nonetheless, its use in subcutaneous injection is currently only possible in the case of a clinical trial.
The exploitation of the fluorescence properties of the dyes already used in the procedure dramatically improve their contrast. Thanks to a FIGS system, the surgeon can detect very low concentration of dye even if the node is covered by few millimeters of tissue. In some particular cases, for instance the SLN procedure for breast cancer, radioactive imaging can be discarded. The node can be found only by the use of ICG and a FIGS system. Figures 1.13 and 1.14 illustrate the detection of the SLN in the case of breast cancer. The figure 1.15 is a SLNB in the case of a bladder cancer.

Figure 1.13: Sentinel Lymph Node (SLN) identification in breast cancer using the PDE®system, [13]

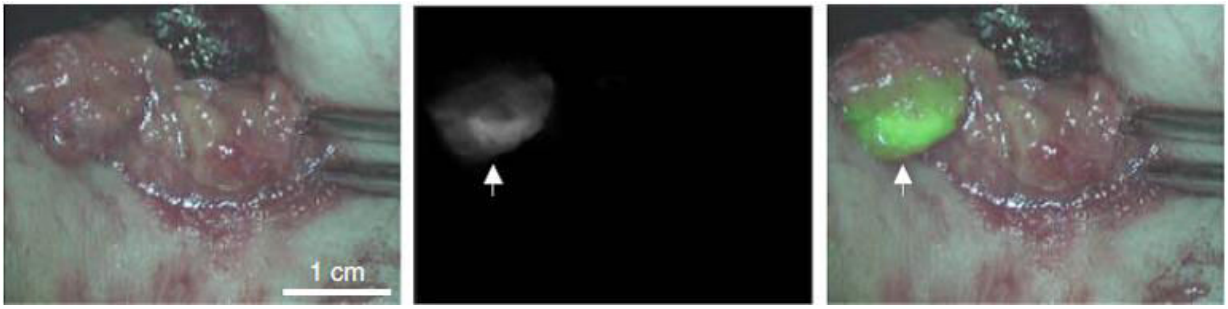

Figure 1.14: SLN biopsy in breast cancer with Flare^{TM}system, [17]

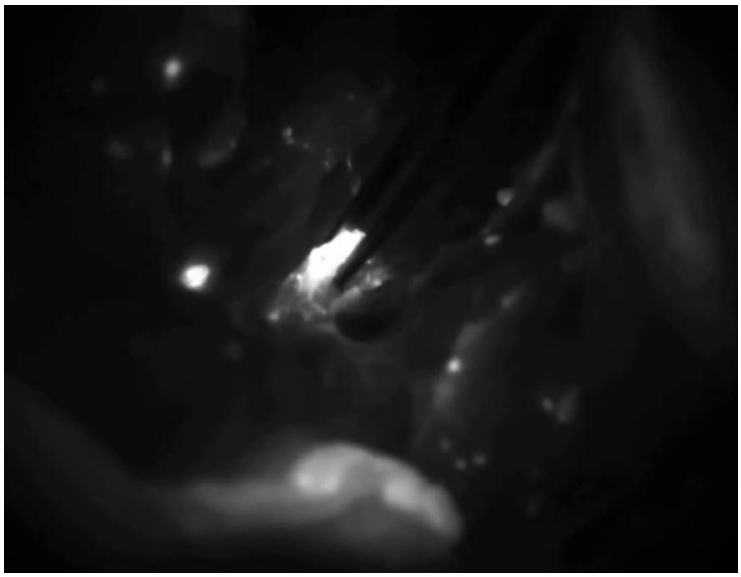

Figure 1.15: SLN biopsy in bladder cancer with the Fluobeam® system

Flap Surgery

Perforator flap surgery is widely used to reconstruct skin defects, like severe burns or excised parts like a breast after a cancer removal. The flap is a vascularized part of the body with skin and fat. It could be localized in the abdomen or lower limbs areas. Once removed, the flap is grafted to the area of the body to be reconstructed. It is important to preserve the vascularization vessels, called the perforator vessels, of the flap during resection in order to correctly perform the graft procedure.
Fluorescence imaging has shown a huge potential for this technique. Indeed, a intravenous injection of ICG and the use of a FIGS system give the surgeon a real-time angiography of the area. The surgeon can easily localizes the perforator vessels that infuse the flap and removed it properly. The figure 1.16 illustrates the dynamic localization of the perforator vessels of a flap before the resection. After an intravenous injection of ICG, the first vessels which appear at the surface of the FLAP are considered as the perforator ones.

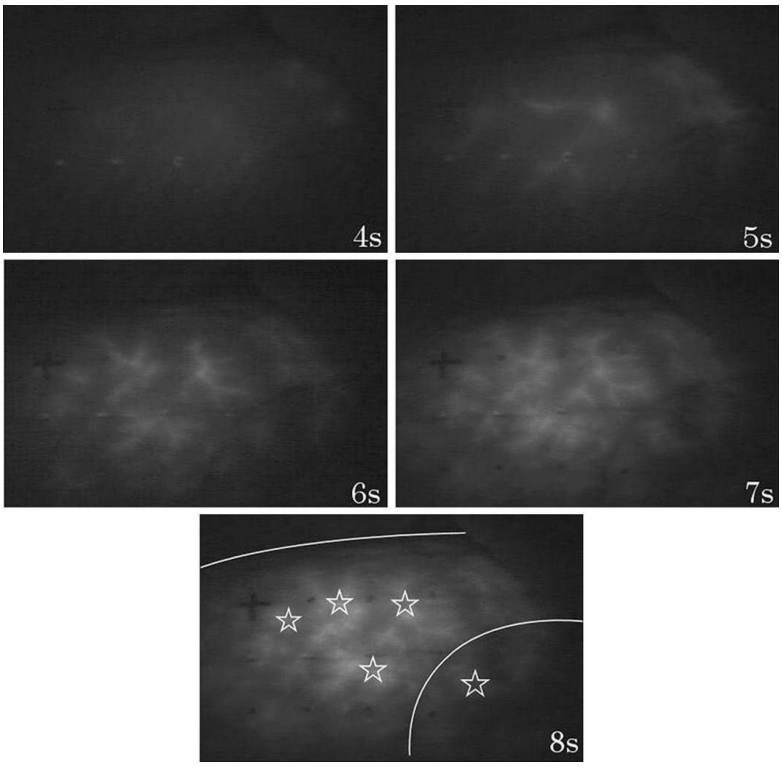

Figure 1.16: Identification of perforator vessels in the flap donor site with the PDE® system, [19]

Hepatic Metastases

After an intravenous injection and a diffusion in the blood, the ICG is accumulated by the liver cells. In healthy liver tissue, the fluorescence ICG distribution is quite uniform on the surface visualized. Studies shown that tumors localized in the liver perturbs the ICG signal and distribution. It results a fluorescence detection and identification of the livers tumors. The fluorescence characteristics change with the type of tumors. For instance, in the case of hepatocellular carcinoma, ICG is strongly fixed inside the tumor. Other example, in the case a metastasis of colon cancer, the ICG is fixed at the margin of the tumor and creates a fluorescent rim around it. The figure 1.17, issued from the work of Ishizawa et al., [21], shows different fluorescent patterns around liver tumors.

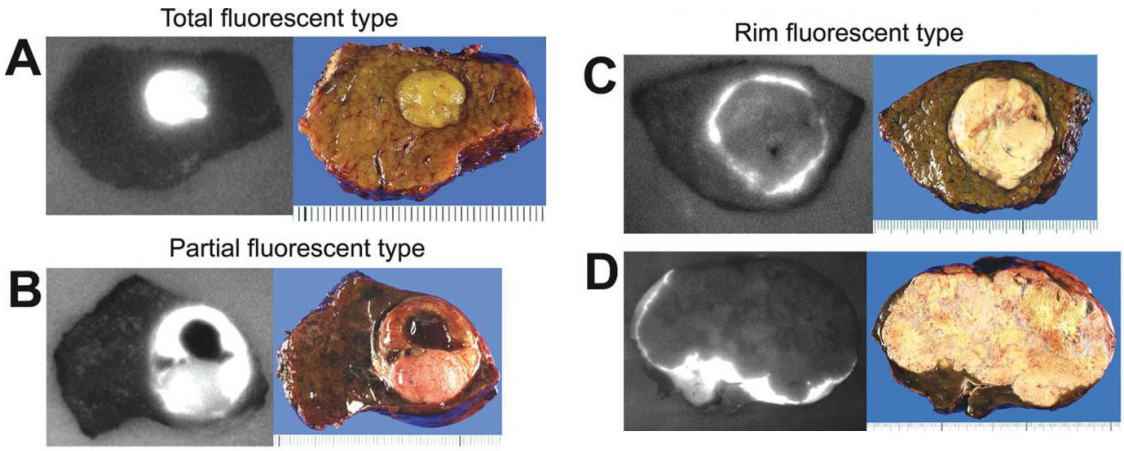

Figure 1.17: Different types of hepatic tumors identified with ICG, PDE®FIGS system, [21]

Lymphoedema

A lymphoedema is a partial or total obstruction of lymphatic system and channels. A previous lymph node resection or the exposition to radiation during therapy cause such alterations. It results a lymphatic retention which could cause more severe affections and injuries. A precise identification of the lymphatic drainage of the lymphoedema is a great advantage in order to cure it. Treatments include non-invasive methods, such compression or exercise, and surgeries such as lymph node grafting or lymphaticovenous anastomosis.
A local injection of ICG and the use of a FIGS system is a very efficient method to map the lymphatic drainage of an area. The figure 1.18 shows an sample acquisition of the surfacic lymphatic drainage of a thigh.

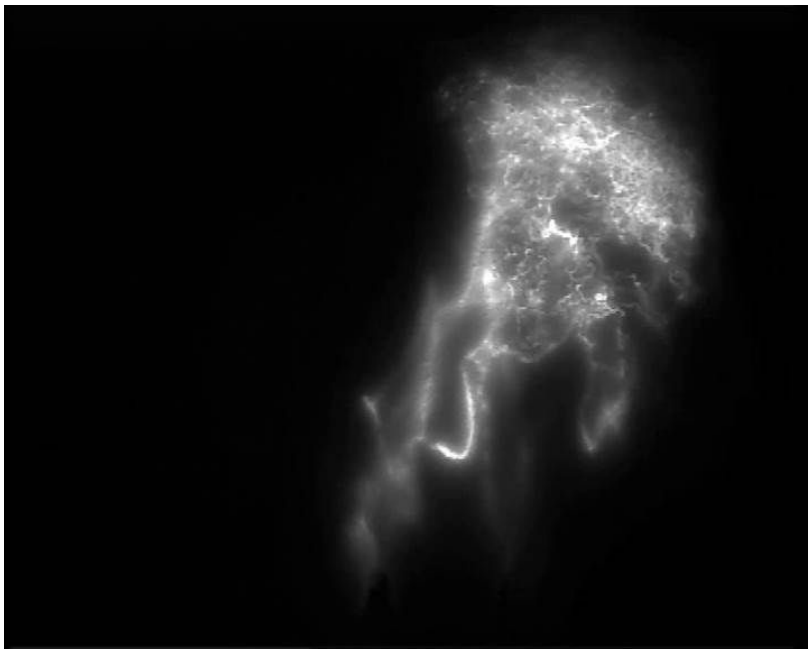

Figure 1.18: Identification of the thigh lymphatic drainage with the Fluobeam®

Coronary Artery Bypass Grafting

The goal of a coronary artery bypass grafting (CABG) is to improve blood flow to the heart. The procedure is needed when coronary arteries are obstructed by plaque and the supply of oxygen to the myocardium is too weak (angina pectoris). The CABG involves veins and arteries that are grafted to coronary vessels to improve the blood flow and the oxygenation of the myocardium.
Fluorescence has shown a huge potential in detecting early coronary bypass graft failures. The flow of a intravenous injection of ICG imaged by a FIGS system gives an indication about eventual leaks or abnormality in the blood flow. Figures 1.19 and 1.20 show images acquired with FIGS systems during CABG.

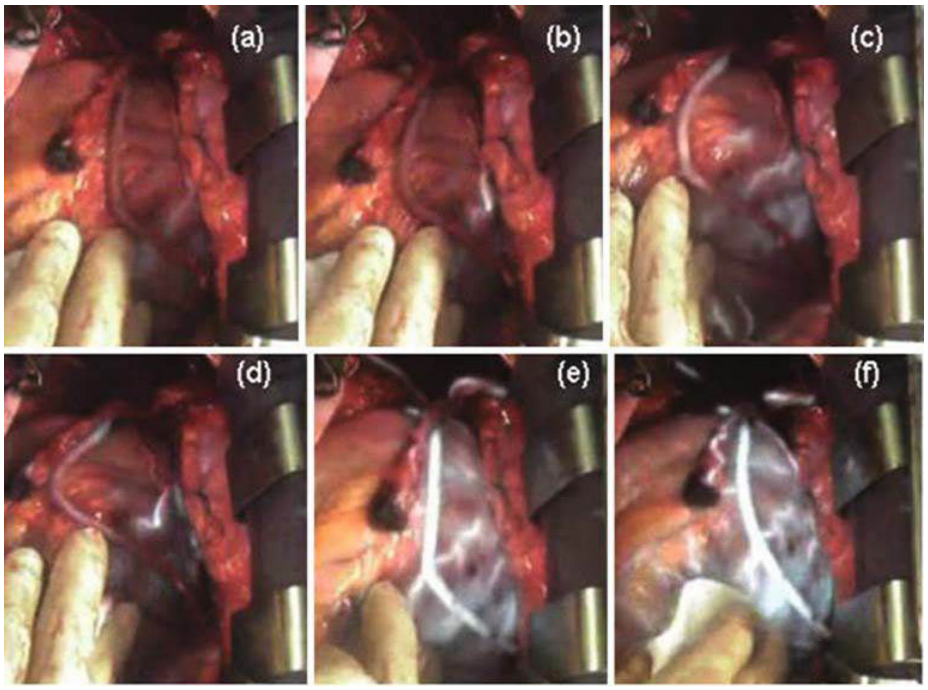

Figure 1.19: Graft assessment with HyperEye®system, [25]

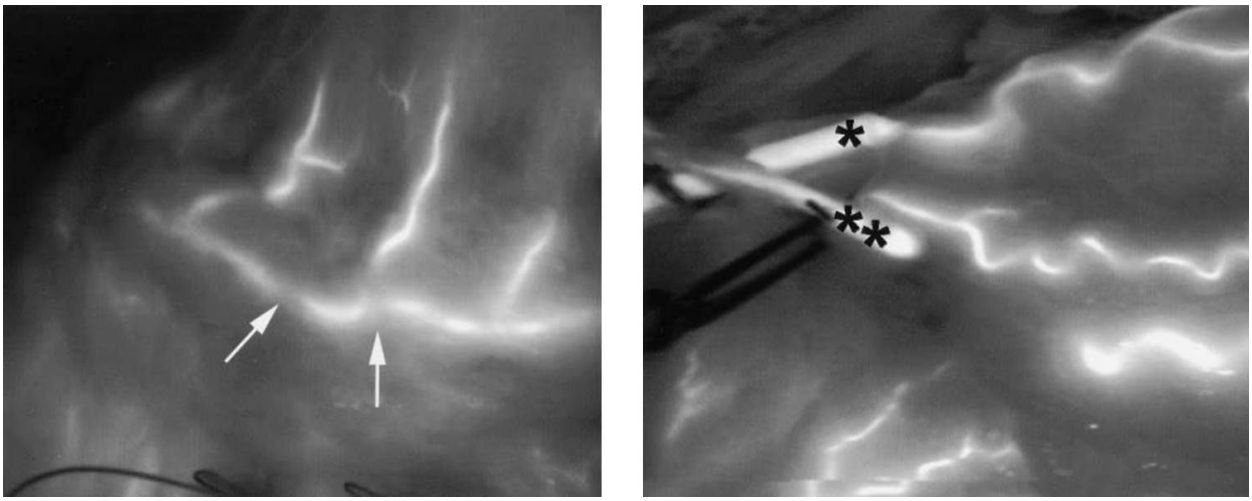

Figure 1.20: Graft assessment with SPY®system, [22]

1.4 Conclusion of the chapter

This chapter presented generalities about imaging and especially fluorescence imaging. The technology of fluorescence image-guided surgery shows a huge potential in several indications, for instance in oncology, vascular and lymphatic related surgeries. Numerous devices exist and address a large scope of indications presented in this chapter. A survey of existing FIGS devices has been exposed and a comparison between the Fluobeam®, developed by Fluoptics, and major actors on the fluorescence market has been presented. Nonetheless, the presented instrumentation is composed of large systems and none seemed to be directly transferable to mini-invasive surgeries. Also, as it will be presented in chapter 2, some open surgeries indications validated on preclinical models cannot be translated to clinic because of the size of the existing devices. The chapter 2 will focus on the miniaturization of a FIGS device for open-surgeries.

Bibliography

[1] R. C. Simon, "Multimodality in vivo imaging systems: Twice the power or double the trouble?" Annual Reviaw of Biomedical Engineering **8**, 35–62 (2006).

[2] A. Taruttis and V. Ntziachristos, "Translational optical imaging," Nucl. Med. Mol. Imaging **199**, 263–271 (2012).

[3] B. E. Schaafsma, J. S. D. Mieog, M. Hutteman, J. R. Van Der Vorst, P. J. K. Kuppen, C. Lowik, J. V. Frangioni, C. J. H. Van De Velde, and A. L. Vahrmeijer, "The clinical use of indocyanine green as a near-infrared fluorescent contrast agent for image-guided oncologic surgery," J. Surg. Oncol. **104**, 323–332 (2011).

[4] S. Keereweer, J. Kerrebijn, P. van Driel, B. Xie, E. Kaijzel, T. Snoeks, I. IQue, M. Hutteman, J. van der Vorst, S. Mieog, A. Vahrmeijer, C. van de Velde, R. de Jong, and L. C., "Optical image-guided surgeryŮwhere do we stand?" Mol. Imaging Biol. **13**, 199–207 (2010).

[5] E. M. Sevick-Muraca, "Translation of near-infrared fluorescence imaging technologies: Emerging clinical applications," Annual Review of Medicine **63**, 217–231 (2012).

[6] S. Gioux, H. S. Choi, and J. V. Frangioni, "Image-guided surgery using invisible near-infrared light: Fundamentals of clinical translation," Mol Imaging **9(5)**, 237–255 (2010).

[7] S. Luo, E. Zhang, Y. Su, T. Cheng, and C. Shi, "A review of nir dyes in cancer targeting and imaging," Biomaterials **32**, 7127–7138 (2011).

[8] G. Themelis, J. S. Yoo, K. S. Soh, R. Schulz, and V. Ntziachristos, "Real-time intraoperative fluorescence imaging system using light-absorption correction," Journal of Biomedical Optics **14(6)** (2009).

[9] J. H. Cornelis, C. van de Velde, J. V. Frangioni, and A. L. Vahrmeijer, "Toward optimization of imaging system and lymphatic for near-infrared fluorescent sentinel lymph node tracer in breast cancer," Annals of Surgical Oncology (2011).

[10] D. H. Suh, K. Kim, and J. W. Kim, "Major clinical research advances in gynecologic cancer in 2011," Journal of Gynecologic Onology **1**, 53–64 (2012).

[11] G. J. Liefers, H. Putter, C. Lowik, J. V. Frangioni, C. J. H., C. van de Velde, and A. L. Vahrmeijer, "Randomized, double-blind comparison of indocyanine green with or without albumin premixing for near-infrared imaging of sentinel lymph nodes in breast cancer patients," Breast Cancer Res Treat **127**, 163–170 (2011).

[12] I. Miyashiro, N. Miyoshi, M. Hiratsuka, K. Kishi, T. Yamada, M. Ohue, and H. Ohigashi, "Detection of sentinel node in gastric cancer surgery by indocyanine green fluorescence imaging: Comparison with infrared imaging," Annals of Surgical Oncology **15**, 1640–1643 (2008).

[13] T. Sugie, K. A. Kassim, M. Takeuchi, T. Hashimoto, K. Yamagami, Y. Masai, and M. Toi, "A novel method for sentinel lymph node biopsy byindocyanine green fluorescence technique in breast cancer," Cancers **2**, 713–720 (2010).

[14] L. M. A. Crane, G. Themelis, H. J. G. Arts, K. T. Buddingh, A. H. Brouwers, V. Ntziachristos, G. M. van Dam, and A. G. J. van der Zee, "Intraoperative near-infrared fluorescence imaging for sentinel lymph node detection in vulvar cancer: First clinical results," Gynecologic Oncology **120**, 291–295 (2011).

[15] M. H. G. M. van der Pas, G. A. M. S. van Dongen, F. Cailler, A. Pelegrin, and W. J. H. J. Meijerink, "Sentinel node procedure of the sigmoid using indocyanine green: feasibility study in a goat model," Surg Endosc **24**, 2182–2187 (2010).

[16] M. Chu and Y. Wan, "Sentinel lymph node mapping using near-infrared fluorescent methylene blue," Journal of Bioscience and Bioengineering **107**, nř4, 455–459 (2009).

[17] S. L. Troyan, V. Kianzad, S. L. Gibbs-Strauss, S. Gioux, A. Matsui, R. Oketokoun, L. Ngo, A. Khamene, F. Azar, and J. V. Frangioni, "The flare intraoperative near-infrared fluorescence imaging system: A first-in-human clinical trial in breast cancer sentinel lymph node mapping," Annals of Surgical Oncology (2009).

[18] W. Kelder, H. Nimura, N. Takahashi, N. Mitsumori, G. M. van Dam, and K. Yanaga, "Sentinel node mapping with indocyanine green (icg) and infrared ray detection in early gastric cancer: An accurate method that enables a limited lymphadenectomy," The journal of cancer surgery **1**, 1–7 (2010).

[19] R. Azuma, Y. Morimoto, K. Masumoto, M. Nambu, M. Takikawa, S. Yanagibayashi, N. Yamamoto, M. Kikuchi, and T. Kisyosawa, "Detection of skin perforators by indocyanine green fluorescence nearly infrared angiography," Plastic and Reconstructive Surgery **122**, 1062–1067 (2008).

[20] Y. Kawaguchi, T. Ishizawa, K. Masuda, and S. Sato, "Hepatobiliary surgery guided by a novel fluorescent imaging technique for visualizing hepatic arteries, bile ducts, and liver cancers on color images," American College of Surgeons **3** (2011).

[21] T. Ishizawa, N. Fukushima, J. Shibahara, K. Masuda, S. Tamura, T. Aoki, K. Hasegawa, Y. Beck, M. Fukayama, and N. Kokudo, "Real-time identification of liver cancers by using indocyanine green fluorescent imaging," Cancer pp. 2491–2504 (2009).

[22] O. Reuthebuch, A. Haussler, M. Genoni, R. Tavakoli, D. Odavic, A. Kadner, and M. Turina, "Novadaq spy : Intraoperative quality assessment in ff-pump coronary artery bypass grafting," Chest **125**, 418–424 (2004).

[23] M. Yamamoto, K. Orihashi, H. Nishimori, S. Wariishi, T. Fukutomi, N. Kondo, K. Kihara, T. Sato, and S. Sasaguri, "Indocyanine green angiography for intra-operative assessment in vascular surgery," European Journal of Vascular and Endovascular Surgery **43**, 426–432 (2012).

[24] M. Yamamoto, S. Sasaguri, and T. Sato, "Assessing intraoperative blood flow in cardiovascular surgery," Surgery Today **41**, 1467–1474 (2011).

[25] T. Handa, R. G. Katare, H. Nishimori, S. Wariishi, T. Fukutomi, M. Yamamoto, S. Sasaguri, and T. Sato, "New device for intraoperative graft assessment: Hypereye charge-coupled device camera system," Gen Thorac Cardiovasc Surg **58**, 68–77 (2010).

[26] J. C. Rasmussen, I. Tan, M. V. Marshall, K. E. Adams, S. Kwon, C. E. Fife, E. A. Maus, L. A. Smith, K. R. Covington, and E. M. Sevick-Muraca, "Human lymphatic architecture and dynamic transport imaged using near-infrared fluorescence," Transl. Oncol. **3**, 362–372 (2010).

[27] M. Marshall, K. E. Adams, S. Kwon, C. E. Fife, E. A. Maus, L. A. Smith, K. R. Covington, and E. M. Sevick-Muraca, "Human lymphatic architecture and dynamic transport imaged using near-infrared fluorescence," Translational Oncology **3**, 362–372 (2010).

[28] T. Desmettre, J. M. Devoiselle, and S. Mordon, "Fluorescence properties and metabolic features of indocyanine green (icg) as related to angiography," Survey of Ophtalmology **45**, 15–26 (2000).

[29] J. T. Alander, I. Kaartinen, A. Laakso, T. Patila, T. Spillmann, V. Tuchin, M. Venermo, and P. Valisuo, "A review of indocyanine green fluorescent imaging in surgery," Int. J. Biomed. Imaging **940585** (2012).

[30] J. V. Frangioni, "New technologies for human cancer imaging," J Clin Oncol **26**, 4012–4021 (2008).

[31] K. Polom, D. Murawa, Young-soo, P. Nowaczyk, M. Hunerbein, and P. Murawa, "Current trends and emerging future of indocyanine green usage in surgery and oncology," Cancer **117**, 4812–4822 (2011).

[32] M. V. Marshall, J. C. Rasmussen, I. C. Tan, M. B. Aldrich, K. E. Adams, X. Wang, C. E. Fife, M. Maus, L. A. Smith, and E. M. Sevick-Muraca, "Near-infrared fluorescence imaging in humans with indocyanine green: A review and update," The Open Surgical Oncology Journal **2**, 12–25 (2010).

[33] F. Tellier, J. Steibel, R. Chabrier, F. X. Blé, H. Tubaldo, R. Rasata, J. Chambron, G. Duportail, H. Simon, J. Rodier, and P. Poulet, "Sentinel lymph nodes fluorescence detection and imaging using patent blue v bound to human serum albumin," Biomed. Opt. Express **3**, 2306–2316 (2012).

[34] D. P. Eisenberg, P. S. Adusumilli, K. J. Hendershott, S. Chung, M. Z. Yu, M. K. Chan, M. Hezel, R. J. Wong, and Y. Fong, "Real-time intraoperative detection of breast cancer axillary lymph node metastases using a green fluorescent protein-expressing herpes virus," Annals of Surgical Oncology **243**, 824–832 (2006).

[35] V. Pansare, S. Hejazi, W. Faenza, and R. Prud'homme, "Review of long-wavelength optical and nir imaging materials: Contrast agents, fluorophores, and multifunctional nano carriers," Chemistry of Materials **24**, 812–827 (2012).

[36] E. Mery, E. Jouve, S. Guillermet, M. Bourgognon, M. Castells, M. Golzio, P. Rizo, J. P. Delord, D. Querleu, and B. Couderc, "Intraoperative fluorescence imaging of peritoneal dissemination of ovarian carcinomas. a preclinical study," Gynecologic Oncology **122**, 155–162 (2011).

[37] G. M. van Dam, G. Themelis, L. M. A. Crane, N. J. Harlaar, R. G. Pleijhuis, W. Kelder, A. Sarantopoulos, J. S. de Jong, H. J. G. Arts, A. G. J. van der Zee, J. Bart, P. S. Low, and V. Ntziachristos, "Intraoperative tumor-specific fluorescence imaging in ovarian cancer by folate receptor-alpha targeting: first in-human results," Nature Medecine **17**, number 10 (2011).

[38] M. Keramidas, V. Josserand, C. A. Righini, C. Wenk, C. Faure, and J. L. Coll, "Intraoperative near-infrared image-guided surgery for peritoneal carcinomatosis in a preclinical experimental model," British Journal of Surgery **97**, 737–743 (2010).

[39] Y. Liu, A. Q. Bauer, W. J. Akers, G. Sudlow, K. Liang, D. Shen, M. Y. Berezin, J. P. Culver, and S. Achilefu, "Hands-free, wireless goggles for near-infrared fluorescence and real-time image-guided surgery," Surgery **149**, 689–698 (2011).

[40] X. Wang, S. Bhaumik, Q. Li, V. P. Staudinger, and S. Yazdanfar, "Compact instrument for fluorescence image-guided surgery," J. Biomed. Opt. **15**, 020509 (2010).

[41] C. Chi, . Du, J. Ye, D. Kou, J. Qiu, J. Wang, J. Tian, and X. Chen, "Intraoperative imaging-guided cancer surgery: From current fluorescence molecular imaging methods to future multi-modality imaging technology," Theranostics **4-11**, 1072–1084 (2014).

[42] S. L. Jacques and S. A. Prahl, "Introduction to biomedical optics," Oregon Graduate Institute, http://omlc.ogi.edu/ (2002).

[43] L. Henyey and J. L. Greenstein, "Diffuse radiation in the galaxy," The Astrophysical Journal **93**, 70 (1941).

[44] E. Hillman, "Optical brain imaging in vivo: techniques and applications from animal to man," Journal of Biomedical Optics **12(5)**, 051402 (2007).

[45] W. F. Cheong, S. A. Prahl, and A. J. Welch, "A review of the optical properties of biological tissues," IEEE Journal of Quantum Electronics **26**, 2166–2185 (1990).

[46] S. Jacques and B. Pogue, "Tutorial on diffuse light transport," Journal of iomedical Optics **13(4)**, 041302 (2008).

[47] A. Matsui, E. Taka, H. S. Choi, V. Kianzad, S. Gioux, S. J. Lomnes, and J. V. Frangioni, "Real-time near-infrared fluorescence-guided identification of the urters using methylene blue," Surgery **148(1)**, 78–86 (2010).

[48] L. Barthelmes, A. Goyal, R. G. Newcombe, F. McNeill, and R. E. Mansel, "Adverse reactions to patent blue v dye e the new start and almanac experience," The Journal of Cancer Surgery **36**, 399–403 (2010).

[49] L. L. Montgomery, A. C. Thorne, K. J. Van Zee, J. Fey, A. S. Heerdt, and P. I. Borgen, "Isosulfan blue dye reactions during sentinel lymph node mapping for breast cancer," Anesthesia & Analgesia **95**, 385–388 (2002).

Chapter 2

The Fluostick^{TM}, a miniaturized hand-held fluorescence image-guided surgery device

What you will find in this chapter:

This chapter exposes the development of a true hand-held FIGS system named the Fluostick^{TM}. The development of the system started in 2011 and reached a CE certification at the end of 2013. It is the first achievement of the thesis. The ways to miniaturize the specific technology of fluorescence imaging will be investigated. Preclinical and clinical studies have been conducted. The clinical evaluation includes surgical resections of liver metastases of colorectal cancers.

Contents

Figures

Tables

2.1 Introduction

The chapter 1 of this thesis presents in details the specific technology of fluorescence imaging. The modality has shown a huge potential in oncology, vascular and lymphatic related surgeries, [1]. Devices have been specifically developed for the visualization of ICG in sentinel lymph node in oncologic procedures (breast, skin, gastric and colorectal cancers in majority), vascular visualization of free flaps in reconstructive surgery, tumor resection and general vascular and lymphatic mapping, [2, 3, 4].

The survey of FIGS systems presented in chapter 1 presented their common architecture which mostly consists in an imaging head linked to one or several control boxes including hardware and software to acquire and display images. Due to their size and weight, most of the available systems on the market are fixed to a mechanical arm and are able to image the surgical field from the top only. The system is built around an imaging sensor, which is, thanks to filters, able to collect specifically the fluorescence light emitted by the excited probes. The ambient light of the theater, as well as the shadowless surgical light, contain NIR light. It's particularly true for xenon or tungsten type light. Therefore, to perform good fluorescence acquisitions, the light of the operating room must be turned off. Some FIGS systems provide an additional filtered white light which help the surgeon to perform his procedures but will not disrupt the acquisition of fluorescence emission light.

A breakthrough is still needed in the design of fluorescence imaging devices to make them easy to use for everyday surgery. Such procedures, as the resection of peritoneal carcinomatosis using fluorescence imaging have been successfully experimented in preclinical model, [5]. The same statement could be made about head and neck cancer procedures. Nevertheless, because of the size of existing instrument, they cannot be used for similar indications on humans. Most of available devices for clinical investigations or everyday procedures are too bulky to image the sides of cavities or specific organs, [6, 7, 8]. Nonetheless, the sensitivity and the overall imaging performances of existing instrumentation are now the basis for the further developments of fluorescence image-guided surgery systems, [9, 10, 11, 12, 13].
The miniaturization of fluorescence imaging technologies is the purpose of some studies and prototypes have been developed for specific indications. Head and neck cancers is one of the field where decreased footprint of fluorescence imaging

system is required, [14, 15, 16]. Some others miniaturization of fluorescence technology projects have been described, especially for in-vivo microscopy applications, [17, 18]. Finally, developments for preclinical procedures or clinical studies only have been achieved, but none have reached an approval yet, [19, 20, 21, 22]. The purpose of this study is to describe the development approach and the first results of what is now a CE-marked, miniaturized, hand-held, fluorescence image-guided surgery system, the Fluostick^{TM}.

2.2 The miniaturization of existing technologies

2.2.1 Purpose of the development

In a miniaturized system, we will mostly consider the miniaturization of the terminal head of the system, also called the optical head. Indeed, it's the only part of the FIGS system which will enter the sterile zone and the working field of the surgeon. Currently, most of the existing FIGS instruments approved for operating room are dealing with all the constraints explained here except one, the footprint. Actually, current devices are addressing vascular applications where the size of the instrument, fixed to a mechanical arm, does not really matter. In these applications a wide field should be imaged. Nevertheless, in lymphatic or some cancer related surgeries, liver cancer for instance, we should be able to image the sides of the cavities or organs. None of the existing instruments are able to do this.
We identified a real need for surgeons to use smaller and lighter fluorescence imaging devices. Nevertheless, it's important to notice that the primary goal of such a development is to design an effective, approved and reliable fluorescence imaging device for surgery.

The second design goal is to improve the size and the maneuverability of the fluorescence imaging system and to develop a real hand-held system for surgery. Some existing systems for other modalities have been taken as references, ultrasound and gamma detection systems. By reducing the size of fluorescence imaging devices, the aim is to promote fluorescence imaging surgery for indications where size matters.
A picture of the final CE-certified system is shown in figure 2.1. The system is composed of a control box linked to the miniaturized optical head through a custom cable. In the operating room, the camera head and the cable are slipped in a sterile drape cover with an optical windowed tip. The control box is set on a table at 1.5 meter from the surgical field, in the non-sterile zone of the theater.

The control box is linked to a computer thanks to an RJ45 cable, and a specific software drives the system, displays the images live and is able to back up data.

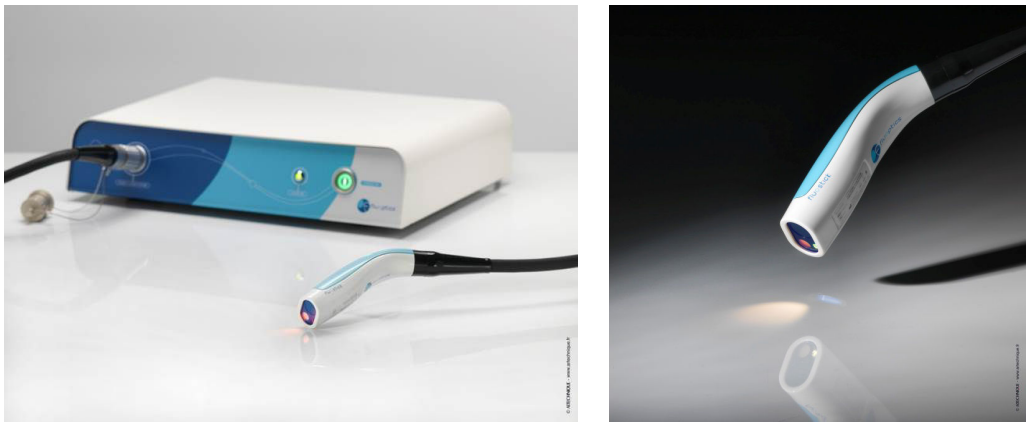

Figure 2.1: The control box and optical head of the Fluostick^{TM} imaging system (left) and detailed view of the miniaturized optical head (right)

2.2.2 Camera

One of the very first aspect to consider before designing a FIGS system is the camera. It is the central element of the design and the system is built around it. The camera is composed of an imaging sensor and electronics linked to the sensor. The camera could be packaged or not. The low quantity of emitted light, and its spectrum characteristics are limiting parameters for common imaging sensors. Two main technologies currently coexist. One, called Charged-Coupled Devices (CCD) is particularly adapted to low signal and high dynamic acquisition. The other technology, named CMOS Active Pixels Sensors (CMOS-APS) is adapted to small and low-powered devices. A lot of improvements have been achieved lately in the field of CMOS-APS technology, especially about noise and overall sensitivity. Other technologies exist, as Electron-Multiplying CDD or other image intensifier approaches, but lead to significant challenge in terms of integration, noise and resolution degradation. Also the cost is generally high because those sensors have a low diffusion on the market. In order to select a sensor for fluorescence imaging purpose, several characteristics have to be evaluated :

- The quantum yield of a sensor expresses its ability to detect light at a specific wavelength. It is the ratio between the incoming photons, at a specific wavelength, and the electron/hole pairs created by the sensor.
- The well capacity of a sensor's pixel is directly linked to the dynamic of signal acquired.
- Another aspect which must be examined is the overall noise of a sensor. This aspect is important to consider because very low light signals with long exposure time will have to be acquired in fluorescence imaging. The Appendix A of this thesis presents in details the characteristics of an image sensor and the way to evaluate them.

For miniaturization purposes, it is important to consider the electronics linked to a sensor. A native digital sensor will need important electronics to acquire the signal and send it through a digital connection (USB or Ethernet for instance). Analog sensors have the advantage to require few electronics integrated directly behind the sensor. Digital sensors and cameras require more space to be integrated. Analog is the choice made for the Fluostick^{TM}. Some of electronics could be deported from the terminal head to the control boxes but signals have to be sent very properly through at least 5 meters of cable required between the sterile and the non-sterile zone. The sensor chosen is a CCD sensor with an optimized response in the NIR region of the spectrum. The reference is the Sony ICX659ALA. With a 1/3 inch size and a definition of 752x576px, it offers a pixel size of 6.5μm and a high well capacity directly linked to a good dynamic range. A specific integration of the sensor has been done by NET Gmbh for this project.
The whole camera, sensor linked to electronic, is comprised in a rectangle of 40×20mm with a terminal circular tip of 20mm diameter. The figure 2.2 shows the size of the camera in comparison with the other elements of the optical head. It also provides information on the overall inner architecture of the Fluostick^{TM}.

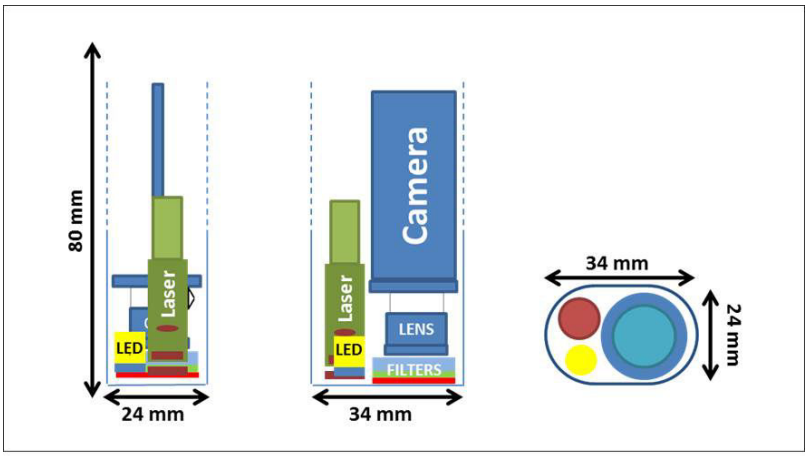

Figure 2.2: Layout and architecture of the Fluostick^{TM}optical head

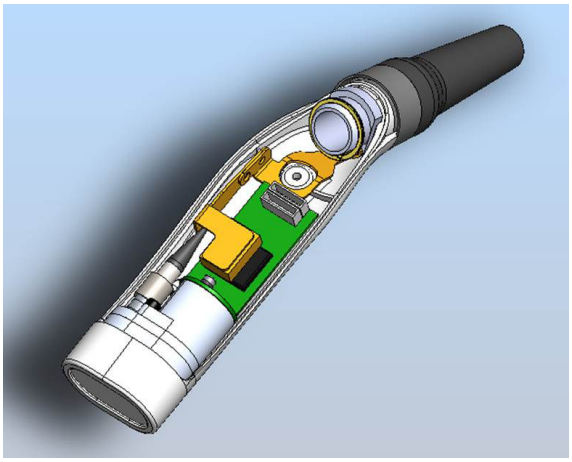

Figure 2.3: 3d sample of the mechanical integration of the Fluostick^{TM}

2.2.3 Optics, Filtering and Excitation

As explained before, the FIGS system must provide light to excite the fluorescent contrast agent and should also help the surgeon to perform his procedure by providing additional white light. There are several ways to generate light. In the medical field, for powerful white light emission, the LED technologies are more and more used instead of older and less reliable techniques such as Xenon lamps. Latest advances in the LED field allow to generate a huge amount of light with tiny and low-powered components.
The ways to generate excitation light are different due to its characteristics. Indeed, excitation light should be restricted to a narrow band of the absorption

spectrum because of the characteristics of the fluorescent probes. Moreover, the excitation light has to be quite powerful to be efficient for fluorescence imaging purpose, especially in the NIR spectrum where fluorescence yield are low. Using Laser technologies is the easiest way to produce these types of light. Nevertheless, the use of filtered LED is not prohibited and can be found in numerous FIGS devices such as the PhotoDynamic Eye of Hamamatsu or the HyperEye of Mizuho . The great advantage of Laser technology for miniaturization purpose in comparison to LED is that it can be efficiently coupled to an optic fiber and deported to a remote box. The system can be more compact and heat dissipation is facilitated.

After generating the excitation light, the second functionality of a FIGS system is to be able to collect the tiny amount of light emitted by the fluorescent probes. The whole acquisition chain has to be optimized for the emission spectrum of the considered probe. We will focus on the most common fluorescent probe, the Indocyanine Green (ICG), a product approved for vascular procedures. The emission spectrum of ICG starts at $700nm$ and end at $850nm$ (Near-Infrared Light, NIR). Therefore, in order to perform a good acquisition, all the parts of this chain must be optimized for the NIR region of the spectrum. The particularity of a fluorescence imaging system in comparison to a simple camera is its ability to discriminate fluorescence emission from other types of incoming light. To do so, filters are placed in front of the lens of the system. These filters are critical components of the system and have to be able to isolate fluorescence emission light from the powerful excitation and white lights which illuminate the working field.

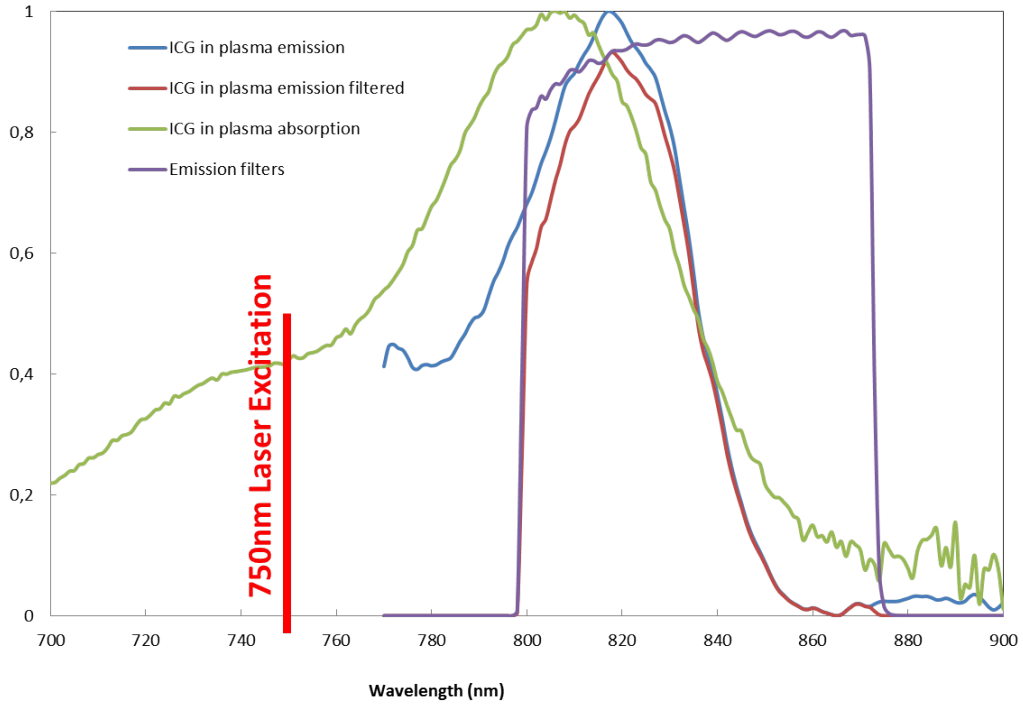

Figure 2.4: Explanation of the filtering used in the Fluostick^{TM}, overlaid with ICG emission and absorption in plasma, convolution of the ICG emission and filters

The filtered light emitted by the fluorescent probe first crosses the optical lens of the system. The selection of a lens impacts in many ways the performances and the maneuverability of a FIGS system. The lens has to be able to collect the maximum of the incoming photons from the surgical field. Several parameters are important to consider. First, the F-number is the ability of the lens to collect light. The lower the F-number, the higher the amount of light collected by the lens. Then, the focal length determines the field of view of the lens. The combination of these two parameters, knowing the working distance, will define the ability of the system to collect light from a determined field of view. Another aspect that can be evaluated from these parameters is the depth of field of the system. This is particularly important for a miniaturized system, supposed to be hand-held. An increased depth of field will help the surgeon to focus on the regions of interest. Considering miniaturization purposes, the size of the lens is important to take into account, knowing that, for a constant imaged circle, the smaller the F-number, the larger the size of the lens is. In appendix B, section B.3 presents theoretical statements about the depth of field of a system.

The Fluostick^{TM}is a fix-focus imaging system. The lens behind the camera is S-mounted and NIR optimized. A trade off is found between the F-number of the lens and the focal length to preserve the depth of field of our imaging device. It is particularly important considering the fact that the system is hand-held and not attached to a mechanical arm. The working distance can be adjusted between $5cm$ and $10cm$ in production.
The excitation light of the system is provided by a $750nm$ laser located in the electrical box. An optical fiber drives it to the head of the system. At the tip of the system, the fiber is expanded by an optical combination and spread quite uniformly and with no speckle to the imaged field. The optimized optical combination makes of Fluostick^{TM}a class1 Laser system. Custom filtering is placed in front of the lens and is optimized to collect ICG emission from $795nm$ to $875nm$. The figure 2.4 shows the filtering used in the device. The filtering is overlaid with ICG absorption and emission in plasma.

2.2.4 Ergonomics and conclusion on miniaturization purpose

After investigation, the oblong format has been chosen for being the best compromise to fit the sensor, the laser excitation and the white light illumination together. The oblong section fits a rectangle of $34\times24mm$. The figure 2.3 displays the inside of the optical head and the disposition of the components. A curved shape has been given to the optical head with the purpose to make it easier to handle. Moreover, the profiles of the system have been designed to fit the hand. A triangle form is created to help the prehension of the optical head. Some cross-sections of a 3D-model of the optical head are shown in figure 2.5. The system is $140mm$ long. The weight of the system is $150gr$. The whole design is thought to make the surgeon able to grip the system and acquire images in every situation.
Another aspect which have been considered for ergonomics purpose is to limit the frame rate of the camera at $25fps$. In fact, a lower frame rate would disturb the surgeon in his procedure. Time gap between the effective acquisition and the image displayed should not exceed $50ms$. Because the camera implemented is analog, one image is composed of two interlaced frames, acquired one after the other. It means that the exposure time of the system will not exceed $20ms$ in order to reach the $25fps$ requirement. A short exposure time is a constraint for a FIGS system but is compulsory for a hand-held camera and this is even more critical for fix-focused devices.

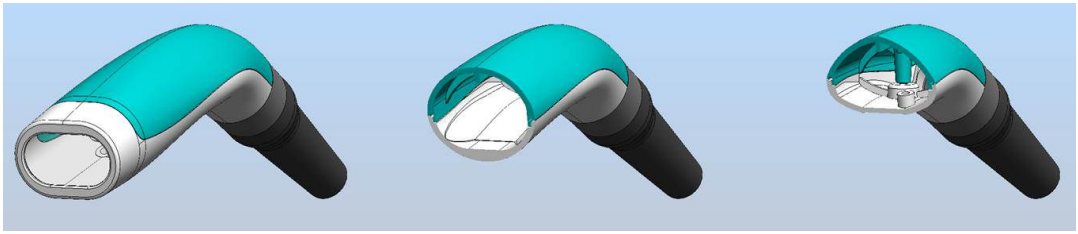

Figure 2.5: Cross sections of the Fluostick^{TM}imaging head

The table 2.1 displays the different aspects to be considered before designing a FIGS system. The different options are characterized by their miniaturization factor, their price and their relative fluorescence efficiency.

Design Feature	**Different solutions to consider**	**Miniaturization and Integration factor**	**Price**	**Fluorescence performance**
Camera	Analog CCD camera	+++	+++	+
	Digital CMOS camera	+	+	−
	Digital CCD camera	−	−	−−
	Digital sCMOS and sCCD camera	−−−	−−−	+++
Fluorescence excitation	LEDs	+	++	+
	LASER	+++	−−	+++
Optics	Fix focus S-mount, high F#	+++	+++	+
	Fix-focus C-mount, low F#	−	−	+++
	Zoom/Autofocus lens	−−	−−	++
Ergonomics	System on an arm	−−−	−−−	+++
	Full hand-held system	+++	+	+
	Hybrid system arm and hand-held	+	−	++

Table 2.1: Summary of the features to consider when developing a FIGS system

2.3 Evaluation of the system

2.3.1 Imaging and Fluorescence performance

Thanks to an optimized design, the Fluostick^{TM}can be considered as a true hand-held system. Because it's a FIGS system, the imaging performances are the first aspects to be considered for evaluation.
At a $10cm$ working distance, the laser illumination is $12.5mW/cm^2$ at $750nm$. At a $5cm$ working distance, the laser illumination goes up to $25mW/cm^2$ at $750nm$, which is very comfortable for real-time and fast ICG visualization. Theoretically, the excitation power could reach the value of $50mW/cm^2$ at a $5cm$

working distance but $25mW/cm^2$ is the highest value available in order to keep the system class1 in terms of Laser safety. In most of the cases, a FIGS system does not authorize the surgeon to keep the surgical shadowless light on, which could contain NIR light, during NIR acquisitions. The white light emission of the Fluostick^{TM}is able to provide a high quality white light with a $4000lux$ power at $10cm$ working distance and a very high Coloring Rendering Index (CRI) of 93. The characteristics of the light, especially for the CRI which must exceed 90, comply with the IEC60601-1-41 standards for medical and surgical lights.

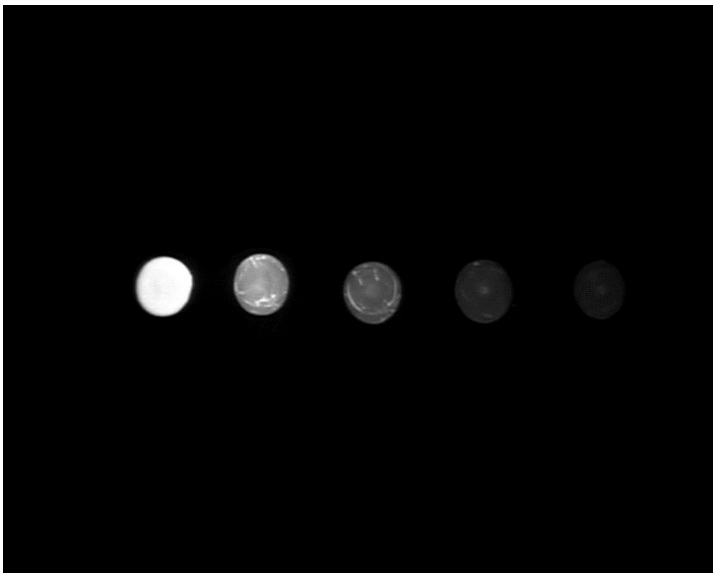

Figure 2.6: Image acquired with the Fluostick^{TM}during the drops test. The working distance is $7cm$ and the excitation power density $18mW/cm^2$. Quantities of ICG visualized are, from left to right, $1000pmol$, $100pmol$, $50pmol$, $10pmol$ and $5pmol$.

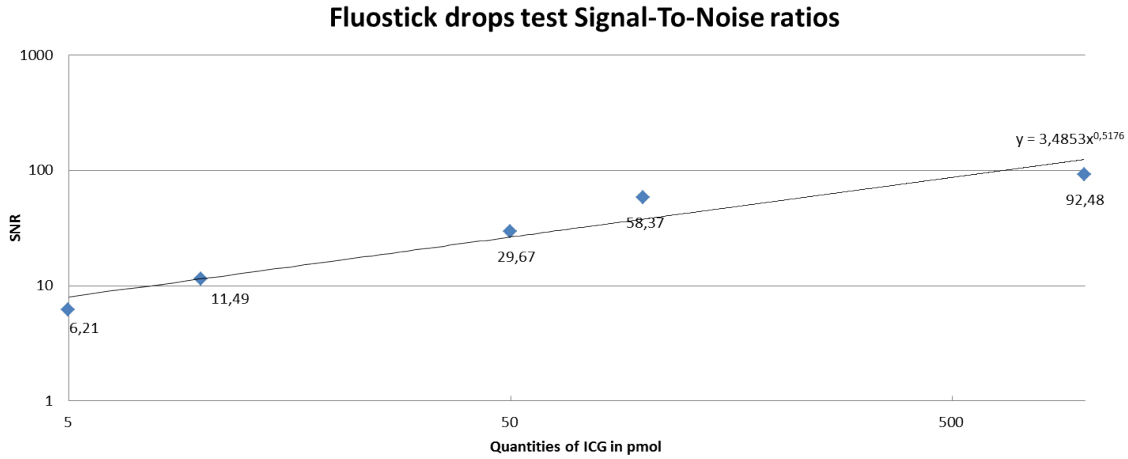

Figure 2.7: Signal to Noise Ratio for 5, 10, 50, 100 and 1000 pmol of ICG

The system is able to image properly a quantity of ICG down to $5pmol$ of product in solution with a very low background. The figure 2.6 shows the results of imaging 5 different $10\mu L$ drops of ICG. Description of the test method is made in Appendix B, section B.1. Thanks to a very low background, the values of Signal to Noise Ratio (SNR) are high, see figure 2.7. The SNR values follow a theoretical curve which would be function of $\sqrt{Fluorescence\ Signal}$. It is explained by the fact that the photon emission follow a Poisson distribution and the theoretical SNR value should be $N/\sqrt{N}$, where N the signal. Statements about the response of an imaging system is given in appendixB.
The spatial resolution of the image is around $70\mu m$. The figure B.2 shows an image of an USAF1951 resolution chart acquired with the Fluostick^{TM}. In this figure, to the well displayed group 2, element 6, corresponds a resolution of $70.1\mu m$. Description of the method of resolution determination is given in Appendix B, section B.2 of this thesis.The table 2.2 presents Fluostick^{TM} review of performance.

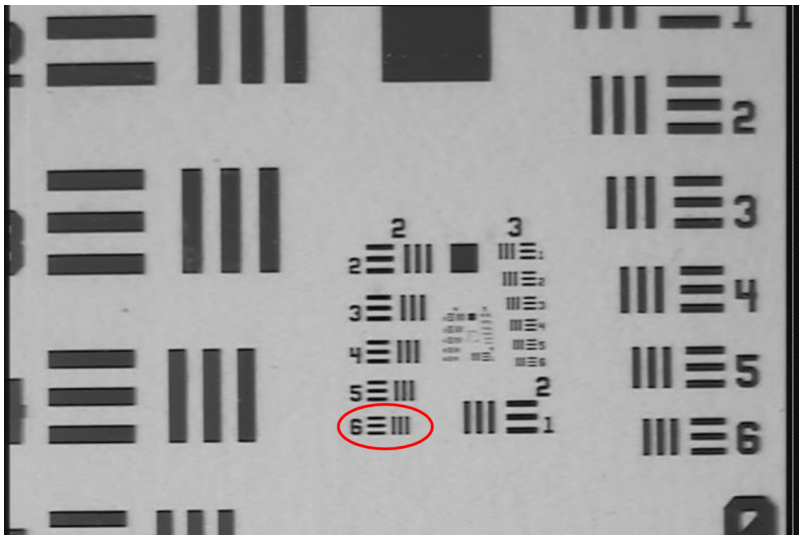

Figure 2.8: Image of an USAF1951 resolution chart acquired with the Fluostick^{TM}

Footprint	$34\times24mm$
Length	$140mm$
Weight	$150gr$
Working distance	50 to $100mm$
Field of view	$40\times30mm$ at $100mm$ working distance
Depth of field	$15mm$
ICG limit of detection	$5pmol$
Excitation	$25mW/cm^2$ at $50mm$, $12.5mW/cm^2$ at $100mm$
F number	1.8
Optical resolution	$70\mu mol/L$
Sensor definition	$752\times 576px$
Sensor characteristics	High NIR optimized monochrome CCD, $25fps$
White light intensity	$4000lux$
White light temperature	$4000K$
White light color rendering index	93
Dynamic range	8 bits

Table 2.2: Specifications of the Fluostick^{TM} imaging system

2.3.2 Preclinical evaluation

A first preclinical evaluation has been performed with the Fluostick^{TM} at the Albert Bonniot Institute in Grenoble, France. The model used was mice with peritoneal tumors. An intravenous injection of a targeted NIR fluorescent probe had been performed prior to the test. The probe, called Angiostamp^{TM}, is developed by Fluoptics and has similar fluorescence characteristics than ICG. Preclinical evaluations are compulsory in order to optimize the characteristics of our

fluorescence system. The particularity of preclinical studies is that they require a high level of sensitivity in comparison to surgeries procedure. The observation that the Fluostick^{TM} has been successfully evaluated in these conditions stresses the fact that its performance will be good enough for surgery. The figure 2.9 shows sample images acquired with the Fluostick^{TM} on these mice models.

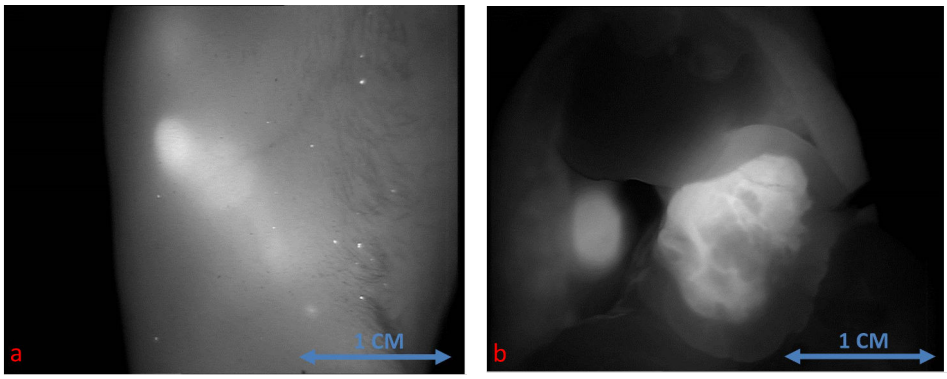

Figure 2.9: Fluostick^{TM} on Mice model, peritoneal tumors under the skin(a) and open(b)

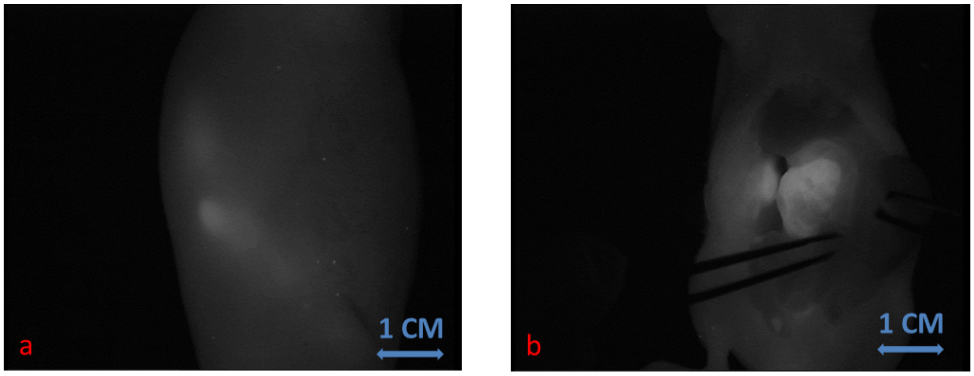

Figure 2.10: Fluobeam^{TM} on Mice model, peritoneal tumors under the skin(a) and open(b)

The images presented in figure 2.10 have been acquired during the same preclinical test session. Subjectively, the overall image quality and fluorescent SNR seems equivalent between the Fluostick^{TM}and the Fluobeam®. In chapter 1 of this thesis, it has been presented that the Fluobeam^{TM} is an accurate FIGS system, at least in comparison with the PDE® and the SPY®, the main actors of the market.

Still at the Albert Bonniot Institute, further investigations used the Fluostick^{TM} to guide head and neck squamous cell carcinoma (HNSCC) resection in an optimized orthotopic animal model for head and neck cancer. A systemic administration of Angiostamp^{TM}800, an RGD-based probe that targets $\alpha\nu\beta3$ integrin, has been performed in nude mice presenting orthotopic HNSCC tumors developed after intra-oral implantation of tumor fragments obtained from subcutaneous tumors derived from a human HNSCC. These tumors had a positive expression of $\alpha\nu\beta3$ integrin. Tumor resection was performed with and without the help of Fluostick^{TM}. NIR optical imaging guided surgery using Fluostick^{TM} helped to detect fluorescent cancer residues that could remain unidentified if resection was done exclusively under visual guidance, cf. figure 2.11. These residues were measured and analyzed microscopically and it have been revealed that Fluostick^{TM} could detect fluorescent cancer foci as small as $185\mu m$. The detection of these residues had a positive impact on the recurrence free survival rate of mice in comparison with mice which underwent tumor resection without the help of Fluostick^{TM}. This preclinical stage is an important step before testing Fluostick^{TM} in HNSCC resection in humans

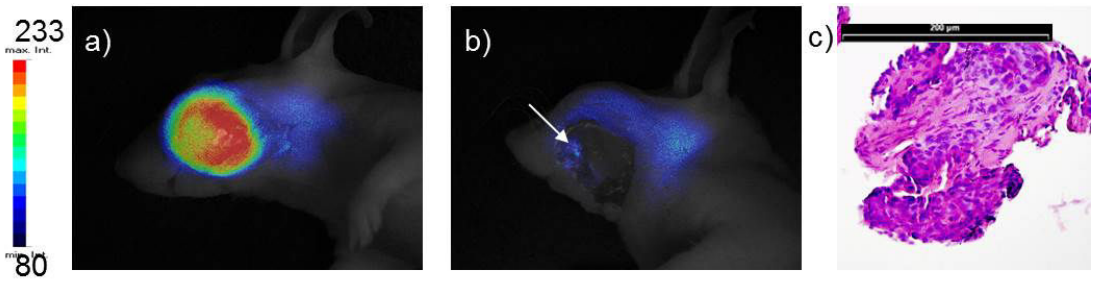

Figure 2.11: Fluostick^{TM} guided resection of HNSCC after systemic administration of Angiostamp^{TM}800. a) Fluorescence of HNSCC orthotopic tumors. b) Fluorescent residues (arrow) unintentionally left behind after total macroscopic resection of the tumor. c) Microscopic analysis of fluorescent residues (H.E. staining) revealed foci of squamous cell carcinoma, from [23].

2.3.3 Clinical evaluation

The Fluostick^{TM} has been developed in accordance to the IEC60601-1 standard and received a CE mark in December 2013. Thanks to this approval, the system is currently used in Europe in operating rooms for tumors resection and lymphatic

procedures. The size of the Fluostick^{TM} allows the surgeon to take the system in one hand and move with the other hand structures in order to find region of interest. It's particularly true in head and neck, colorectal or liver cancer related surgeries.
The figure 2.12 shows sample images acquired with the Fluostick^{TM} in vivo in the theater. These images are a good example of the use of the device in the operating room. On the left, the surgeon has detected a tumor lesion on the liver of his patient previously injected with ICG. The pictures on the right show the actual aspect of the tumor and the fluorescence image acquired with the Fluostick^{TM}. The margin of the tumor are clearly visible thanks to the fluorescence.

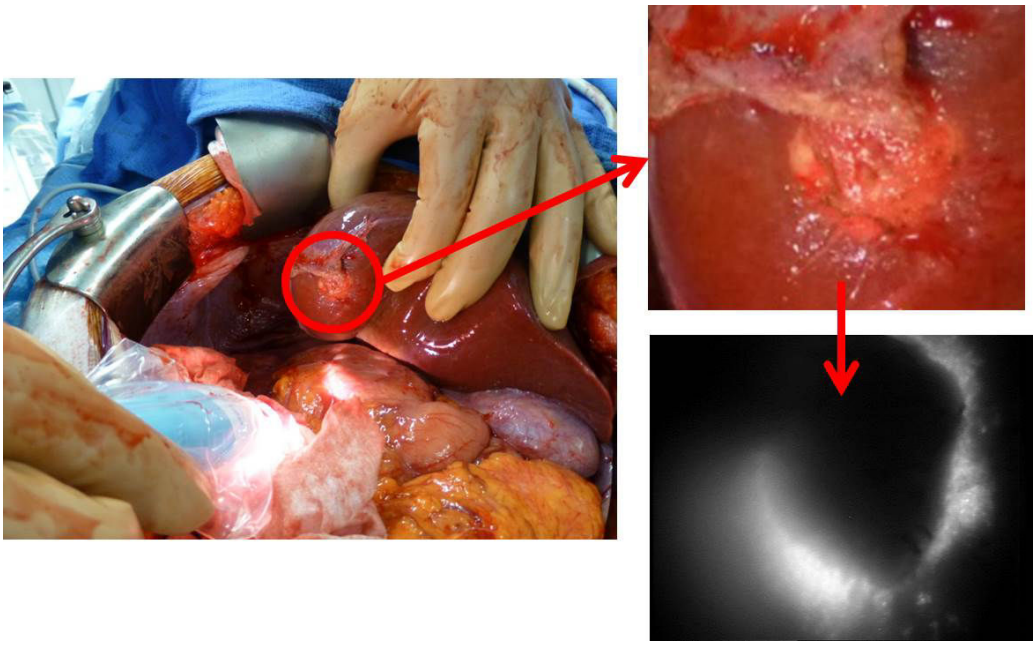

Figure 2.12: Liver tumor imaged with the Fluostick^{TM}

A clinical trial was conducted with the Fluostick through 2013 and 2014 (Clinical Trials identifier NCT01982227). Between 30 and 40% of patients with colorectal cancer develop metastatic disease intraperitoneally. The optimal treatment of this disease combines surgery and chemotherapy but requires resection of all lesions larger than $2mm$. ICG has an affinity for tumor tissues and the interest of its use has been demonstrated for the detection of SLN and some liver surgeries, see 1.3.2 in Chapter 1 of this thesis. The ability of ICG to detect peritoneal carcinomatosis in humans has never been evaluated. The study aimed to evaluate the diagnostic performance of fluorescence in the detection of malignant cells in peritoneal carcinomatosis of colorectal origin compared with patholog-

ical analysis. The trial was driven by Pr. Gabriele Barabino and Alexandre Filippello, intern in surgery at the CHU Saint-Etienne, France. The design of the Fluostick^{TM}had been validated by Pr. Barabino prior to the trial, and then successfully fit his demands. 10 patients were included in the trial.
For each case, a classic exploration of the abdominal cavity, based on pre-operative data, was performed and the presence of tumors was checked for 13 delimited areas. Then, the same exploration was performed for the 13 areas with the Fluostick^{TM} imaging system. Further investigation in fluorescence were done on the pieces resected from the patient and additional fluorescent nodules were identified and analyzed. The results obtained with the Fluostick^{TM} were equivalent to the classic surgery procedure. Some tumor nodules not detected in the classic way had been identified fluorescent on resected pieces and analysis revealed them as malignant. The figure 2.13 and figure 2.14 show the Fluostick^{TM} used during abdominal cavity inspection. The shape of the system was there a clear advantage in comparison to existing instrumentation. The system authorizes a visualization of the organs and the sides of the cavity. The surgeon noticed the rapidity of the method thanks to the accurate design of the system.

Figure 2.13: Per-operative peritoneal carcinomastosis resection with the Fluostick^{TM}

Figure 2.14: Per-operative peritoneal carcinomatosis resection with the Fluostick^{TM}

The figure 2.15 illustrated the use of the Fluostick^{TM}on further fluorescent investigation on rested pieces.

Figure 2.15: Study of anatomical pieces from a carcinomatosis resection with the Fluostick^{TM}

2.4 Conclusion of the chapter

The main objective of this study was to illustrate the development and the design of a miniaturized palm-sized FIGS system and to display sample results of its preclinical and clinical evaluations. The performances of the Fluostick^{TM} are similar to those currently demonstrated by existing devices. The system has been successfully validated in operating room and showed its potential for numerous applications such as liver tumors resection or vascular related surgeries. The choices we made for design purpose, such as the curved shape or the sensor technology will help us in developing new solutions for minimally invasive surgery and other modalities where fluorescence imaging is barely developed.
In fact, chapter 3 will show the development of a FIGS system dedicated to mini-invasive procedures directly based on results presented above. The main breakthrough achievement of this chapter concern the use of a small analog sensor which demonstrated its ability to acquire accurate fluorescence images.

Bibliography

[1] A. Taruttis and V. Ntziachristos, "Translational optical imaging," Nucl. Med. Mol. Imaging **199**, 263–271 (2012).

[2] J. C. Rasmussen, I. Tan, M. V. Marshall, K. E. Adams, S. Kwon, C. E. Fife, E. A. Maus, L. A. Smith, K. R. Covington, and E. M. Sevick-Muraca, "Human lymphatic architecture and dynamic transport imaged using near-infrared fluorescence," Transl. Oncol. **3**, 362–372 (2010).

[3] F. P. R. Verbeek, J. R. van der Vorst, B. E. Schaafsma, M. Hutteman, B. A. Bonsing, F. W. B. van Leeuwen, J. V. Frangioni, C. J. H. van de Velde, R. Swijnenburg, and A. L. Vahrmeijer, "Image-guided hepatopancreatobiliary surgery using near-infrared fluorescent light," J. Hepatobiliary Pancreat. Sci. (2012).

[4] T. Handa, R. G. Katare, H. Nishimori, S. Wariishi, T. Fukutomi, M. Yamamoto, S. Sasaguri, and T. Sato, "New device for intraoperative graft assessment: Hypereye charge-coupled device camera system," Jpn. A. Thorac. Surg. **58**, 68–77 (2010).

[5] M. Keramidas, V. Josserand, C. Righini, C. A.and Wenk, C. Faure, and J. L. Coll, "Intraoperative near-infrared image-guided surgery for peritoneal

carcinomatosis in a preclinical experimental model," Brit. J. Surg. **97**, 737–743 (2010).

[6] S. L. Troyan, V. Kianzad, S. L. Gibbs-Strauss, S. Gioux, A. Matsui, R. Oketokoun, L. Ngo, A. Khamene, F. Azar, and J. V. Frangioni, "The flare tm intraoperative near-infrared fluorescence imaging system: A first-in-human clinical trial in breast cancer sentinel lymph node mapping," Ann. Surg. Oncol. (2009).

[7] J. S. D. Mieog, S. L. Troyan, M. Hutteman, K. J. Donohoe, J. R. van der Vorst, A. Stockdale, G. J. Liefers, H. S. Choi, S. L. Gibbs-Strauss, H. Putter, S. Gioux, P. J. K. Kuppen, Y. Ashitate, C. W. Lowik, V. Smit, R. Oketokoun, L. H. Ngo, C. J. H. van de Velde, J. V. Frangioni, and A. L. Vahrmeijer, "Toward optimization of imaging system and lymphatic tracer for near-infrared fluorescent sentinel lymph node mapping in breast cancer," Ann. Surg. Oncol. (2011).

[8] G. Themelis, J. S. Yoo, K. S. Soh, R. Schulz, and V. Ntziachristos, "Real-time intraoperative fluorescence imaging system using light-absorption correction," J. Biomed. Opt. **14**, 064012 (2009).

[9] M. Yoshida, K. Kubota, J. Kuroda, K. Ohta, T. Nakamura, J. Saito, M. Kobayashi, T. Sato, Y. Beck, K. Y., and M. Kitajima, "Indocyanine green injection for detecting sentinel nodes using color fluorescence camera in the laparoscopy-assisted gastrectomy," J. Gastroenterol. Hepatol. **27**, 29–33 (2012).

[10] S. Keereweer, J. Kerrebijn, P. van Driel, B. Xie, E. Kaijzel, T. Snoeks, I. IQue, M. Hutteman, J. van der Vorst, S. Mieog, A. Vahrmeijer, C. van de Velde, R. de Jong, and L. C., "Optical image-guided surgeryŮwhere do we stand?" Mol. Imaging Biol. **13**, 199–207 (2010).

[11] T. Sugie, K. Kassim, M. Takeuchi, T. Hashimoto, K. Yamagami, M. Y., and M. Toi, "Novel method for sentinel lymph node biopsy by indocyanine green fluorescence technique in breast cancer," Cancers **2**, 713–720 (2010).

[12] G. van Dam, G. Themelis, L. Crane, R. Harlaar, Pleijhuis, W. Kelder, A. Sarantopoulos, J. de Jong, H. Arts, A. van der Zee, J. Bart, P. Low, and V. Ntziachristos, "Intraoperative tumor-specific fluorescence imaging in ovarian cancer by folate receptor-alpha targeting: first in-human results," Nat. Medecine **17**, 1315–1320 (2011).

[13] S. Gioux, H. S. Hak Soo Choi, and J. V. Frangioni, "Image-guided surgery using invisible near-infrared light: Fundamentals of clinical translation," Mol. Imaging **9**, 237–255 (2010).

[14] P. M. Lane, T. Gilhuly, P. Whitehead, H. Zeng, C. F. Poh, S. Ng, P. M. Williams, L. Zhang, M. P. Rosin, and C. E. MacAulay, "Simple device for the direct visualization of oral-cavity tissue fluorescence," J. Biomed. Opt. **11**, 024006 (2006).

[15] C. F. Poh, S. P. Ng, P. M. Williams, L. Zhang, D. M. Laronde, P. Lane, C. MacAulay, and M. P. Rosin, "Direct fluorescence visualization of clinically occult high-risk oral premalignant disease using a simple hand-held device," Head Neck Surg. (2007).

[16] D. Roblyer, R. Richards-Kortum, K. Sokolov, A. K. El-Naggar, M. D. Williams, C. Kurachi, and A. M. Gillenwater, "Multispectral optical imaging device for in vivo detection of oral neoplasia," J. Biomed. Opt. **13**, 024019 (2008).

[17] K. K. Ghosh, L. D. Burns, E. D. Cocker, A. Nimmerjahn, Y. Ziv, A. El Gamal, and M. J. Schnitzer, "Miniaturized integration of a fluorescence microscope," Nat. Methods **8**, 871–878 (2011).

[18] D. Shin, M. Pierce, A. Gillenwater, and R. Richards-Kortum, "A fiber-optic fluorescence microscope using a consumergrade digital camera for in vivo cellular imaging," OSA/BIOMED/DH (2010).

[19] J. W. Kakareka, T. E. McCann, N. Kosaka, M. Mitsunaga, N. Y. Morgan, T. J. Pohida, P. L. Choyke, and H. Kobayashi, "A portable fluorescence camera for testing surgical specimens in the operating room: Description and early evaluation," Mol. Imaging Biol. **13**, 862–867 (2011).

[20] S. Gioux, J. G. Coutard, M. Berger, H. Grateau, V. Josserand, M. Keramidas, C. A. Righini, J. L. Coll, and J. M. Dinten, "Fluostic: miniaturized fluorescence image-guided surgery system," J. Biomed. Opt. **17**, 106014 (2012).

[21] X. Wang, S. Bhaumik, Q. Li, V. P. Staudinger, and S. Yazdanfar, "Compact instrument for fluorescence image-guided surgery," J. Biomed. Opt. **15**, 020509 (2010).

[22] Y. Liu, A. Q. Bauer, W. J. Akers, G. Sudlow, K. Liang, D. Shen, M. Y. Berezin, J. P. Culver, and S. Achilefu, "Hands-free, wireless goggles for near-infrared fluorescence and real-time image-guided surgery," Surgery **149**, 689–698 (2011).

[23] I. Atallah, J. Coll, C. Milet, M. Keramidas, S. Guillermet, A. Hurbin, and C. A. Righini, "Optimisation d'un modele animal pour le cancers des vads et apport de l'imagerie en fluorescence dans l'exerese tumorale," in "Societe francaise d'ORL," (2013).

Chapter 3

From the Fluostick^{TM} to the FluoMIS^{TM}, a fluorescence mini-invasive surgery device

What you will find in this chapter:

This chapter will present the development of a fluorescence imaging system for mini-invasive surgeries, the FluoMIS^{TM}. The development is directly based on the Fluostick^{TM}. The chapter will also describe the specificities of mini-invasive surgeries and stress the main challenges of the translation of fluorescence image-guided surgery technologies for mini-invasive procedures. Sample results obtained during the use of fluorescence imaging in procedures such as the cholecystectomy in preclinical models will be presented.

Contents

Figures

Tables

3.1 Introduction

Since 1983 and the first laparoscopic appendectomy, minimally invasive surgical techniques does not cease to develop. By 1986, it was estimated that more than 1 million laparoscopic sterilizations were being performed in the United States alone, [1]. In 1987, Mouret performed the first cholecystectomy with CCD laparoscopic device, [2, 3]. The advantages of the method are numerous. First of all, it is noticed a decrease operative trauma with a limited blood loss during surgery. So even though the surgery might take longer in comparison to open procedures, the hospitalization time is always much shorter. With less pain and scarring, the patient bears less post-surgical complications.
Today, the majority of fluorescence image-guided surgery indications are related to open surgery procedures, but the potential of the technology for mini-invasive surgeries is tremendous. Indeed, one of the particularities of mini-invasive surgery is the fact that the surgeon can only rely on the image displayed on the screen and cannot feel the tissue structure as he would do by touching them in an open-surgery procedure. Therefore, complementary information to the anatomical color image is going to become mandatory and NIR fluorescence image-guided surgery could be the solution. Several studies focused on the reliability of fluorescence information in mini-invasive procedures, [4, 5, 6, 7, 8, 9, 10, 11, 12, 13].

Most of existing instrumentation for fluorescence imaging in mini-invasive surgeries are not able to provide simultaneously a color image and a fluorescence image in a common way for surgeon. Moreover, the fluorescence limit of detection remains quite low and systems are not ready for specific targeting fluorescent probes. The utility of fluorescence has been tested during cholecystectomy[14, 15, 16, 17, 18, 19, 20] and other indications, such as hepatic and oncologic related procedures, [21, 22, 23, 24, 25, 26].
The development of the FluoMIS^{TM}will be a first step in the comprehension of the in-games of fluorescence imaging for mini-invasive surgeries. The goal of the development is to rapidly develop a system able to acquire simultaneously a color and a fluorescence image to gain feedback about the utility of fluorescence imaging for mini-invasive surgery.
The chapter will present quantitative figures about the gap that exists in terms of ICG limit of detection between open and mini-invasive systems. Then, the technical development of FluoMIS^{TM} will be exposed. Finally, results of two preclinical evaluations on pigs will be presented.

3.2 The purpose of the development and the particularities of mini-invasive procedures

3.2.1 The purpose of the development

As said previously, fluorescence image-guided surgery has shown a huge potential for open surgery. Nonetheless, with respect to the increasing number of mini-invasive procedures, the question of the use of fluorescence imaging for this type of surgery must be addressed. The aim of fluorescence image-guided surgery is to provide the surgeon with additional information that cannot be seen in direct visualization of the operating field. It is easy to understand that additional information will be also useful in procedures where there is no direct eye visualization of the operating field.

According to the bibliography and thanks to discussions with surgeons, an added value to the use of fluorescence in mini-invasive procedures have been identified for several applications. The applications include cholecystectomy and liver tumors resections.

The purpose of the development of the FluoMIS™was to rapidly develop a FIGS system, based on existing instrumentation and dedicated to mini-invasive surgery. The goal was to develop a system able to acquire simultaneously a fluorescence image and a color image of the operating field. The work achieved with the development of the Fluostick™imaging system is the starting point for the design of the FluoMIS™.

A particular procedure has been selected for evaluation of the system. The aim is also to valid the relevance of fluorescence imaging for this procedure. The procedure selected is called the cholecystectomy and will be explained later on this chapter.

3.2.2 Minimally invasive surgery

In coelioscopy, rigid laparoscopes are the standard. Some of existing systems are qualified of video-laparoscopes, it means that the sensor of the system is placed at the distal part of the rigid laparoscope. The Olympus company is the main manufacturer of such devices.

Nevertheless, most of the rigid laparoscopes available on the market are not video laparoscopes. The common laparoscope is an optical element used to deport the image from the inside of the body to the terminal upper part of the system, also called the ocular, where a camera would be attached to acquire images. As

defined here, the laparoscope is called a rod-lens system. The figure 3.1 describes the characteristics of such a system. A lens at the tip of laparoscope build an image which is deported to the upper part of the laparoscope thanks to relay lenses. At the top of the laparoscope, the ocular, an output lens combination gives back the image at an infinite focal plan.
The laparoscope is also used to conduct the light emitted by the imaging system to inside the body. Optical fibers drive the light from top to bottom.

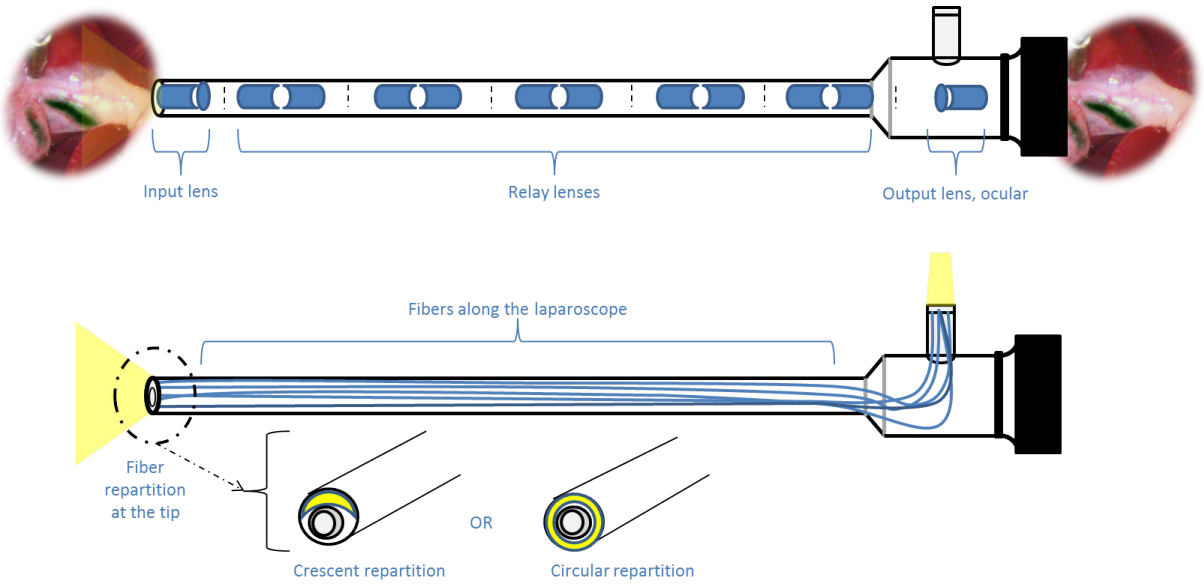

Figure 3.1: Schematic of a standard laparoscope, rod-lens system and fibers repartition

In common laparoscopic procedures, camera and light cable are linked to the laparoscope. The camera is held directly by the surgeon or by an assistant. The camera is mostly linked to a control box. The light cable is linked to an other box where the white light, compulsory to acquire images in the cavities, is generated. As said before, some systems, such the ones developed Olympus company, use image sensor at the distal tip of the laparoscope. In this case, the camera and the laparoscope are one entity that cannot be separated, see figure.

3.2.3 Translation from open surgery to mini-invasive surgery

The Fluorescence image-guided surgery has been well characterized for open surgery. Nevertheless, the specificities of mini-invasive systems make the translation of the technology challenging. This section will presents the main differences between open and mini-invasive procedures concerning FIGS systems.

Near-infrared sensitivity

As presented before, see figure 3.1, the rigid laparoscope is made of a lot of optical parts. Knowing the fact that a non Anti-Reflection coated optical surface will reflect 4% of the incoming light, the multiple optical interfaces present in a laparoscope will decrease the level of fluorescence signal transmitted to the sensor placed behind it. The goal of the following experiment is to show how the use of a rigid laparoscope impact fluorescence imaging and fluorescence emission collection.
We compare the overall sensitivity in ICG visualization of a FIGS system for open surgery and the same instrumentation but using a laparoscope. The methods implies drops of $10\mu L$ of ICG at different concentrations. Description of the test method is made in Appendix B, section B.1. The goal of the test is to show how the use of a laparoscope impact the fluorescence image-guided surgery in terms of limit of detection and reliability.

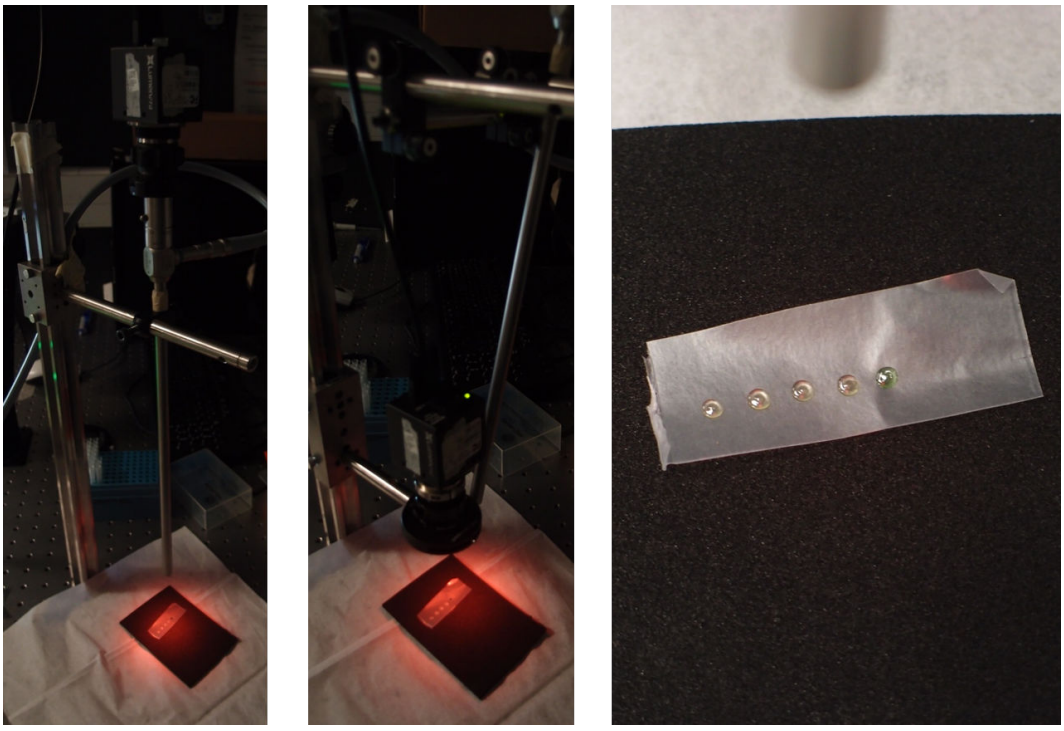

Figure 3.2: On the left, the experimental setup for laparoscopes comparison. Middle, the corresponding setup for the open surgery evaluation. Right, the five drops of ICG disposed on Parafilm®(Pechinet USA) from left to right, 5$pmol$, 10 $pmol$, 50 $pmol$, 100 $pmol$ and 1000 $pmol$

To achieve this goal, only the lens change between the systems we compare.

The upper part of the experimental FIGS system is comprised of a Lumenera camera LM265, from Lumenera Corp, Canada, which integrates a Sony monochrome CCD sensor ICX285. This sensor has been widely used in fluorescence imaging and other applications because of his high overall sensitivity and his low noise. The definition of the sensor is 1392x1040px for a 2/3$inch$ size. The emission filter used to collect the fluorescent light emitted by the drops of ICG is the FF01-776 interferencial filter from Semrock®, USA. The excitation light is provided by a 2W, 750nm Laser provided by the company LDX Optronics Inc, USA. The Laser power excitation is set to 15mW/cm^2 at the surface of the drops for all the setups.
For the optical installation which carries out the role of FIGS system for open surgery, a Xenoplan lens from Schneider Gmbh has been chosen. This lens has a 18mm focal length and a F1.8 maximal optical aperture. For test consideration and reliability, the aperture of the lens has been limited to F5.6. Indeed, in order to set correspondence between the setups, the signals acquired here should not be saturated. Concerning the experimental setup for the mini-invasive system, a video coupler from Precision Optics Corporation USA, a.k.a POC, has been chosen. The focal length of the video coupler is 30mm. The figure 3.2 shows the experimental setup.
Three different laparoscopes have been evaluated for the mini-invasive version of the experimental setup. The table 3.1 presents the references chosen and the main characteristics of the scopes. All the references are 10mm diameter and 0° laparoscopes which is the standard for coelioscopy procedures.

Manufacturer	**Reference**	**outer diameter**	**Lens diameter**	**Overall length**	**fiber output repartition**	**NIR optimized**
Storz Gmbh	Hopkins II 26003AGA	10 mm	3 mm	40 cm	circular	Yes
Precision Optics Corporation	6711-801	10 mm	2 mm	37 cm	circular	No
Schoelly Gmbh	SIS000034-pro1	10 mm	2 mm	43 cm	crescent	Yes

Table 3.1: The three different laparoscopes use for the experiment

The figure 3.3 shows samples of images acquired during the experimentation. For each configuration, images of the drops of ICG have been taken at seven different exposition times, 10, 20, 30, 40, 50, 100 and 150ms. The signal to noise ratio (SNR), is calculated from each image acquired and for each drop of ICG

on the image. The SNR is calculated from the formula below :

$$SNR = \frac{\text{ICG mean drop signal} - \text{Noise mean signal}}{\text{Noise deviation}}$$

Thanks to this approach, the ratio between the SNRs gives us a good indication of the differences in term of sensitivity between the systems.

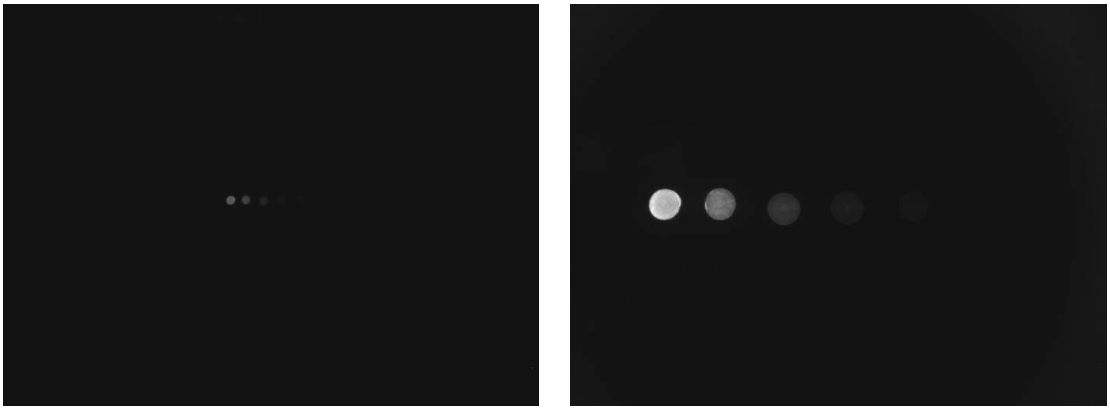

Figure 3.3: Left, the drops of ICG acquired with the experimental system plus the Storz laparoscope at $150ms$ exposure time. Right, the drops of ICG acquired with the experimental system in the open configuration at $50ms$ exposure time

The figure 3.4 displays the results of the calculation of the SNRs for each systems at $20ms$ exposure time. The $20ms$ exposure time has been chosen here because it is coherent with a real time imaging use of the system. The systems using the POC and the Schoelly's laparoscopes are not able to detect the drops of ICG with the concentration of $0.5\mu mol/L$ and $1\mu mol/L$. Nonetheless, the limit of detection is similar between the open surgery setup and the system using the Storz laparoscope. Calculation has been performed to determine the ratios between the systems. Also, because we clearly know the aperture of the open surgery setup, F5.6, we are able to give an equivalent in term of optical aperture for each configuration evaluated. Some other known references for open surgery have been added, such as the Fluostick$^{\text{TM}}$, previously presented in the chapter 2 of this thesis.

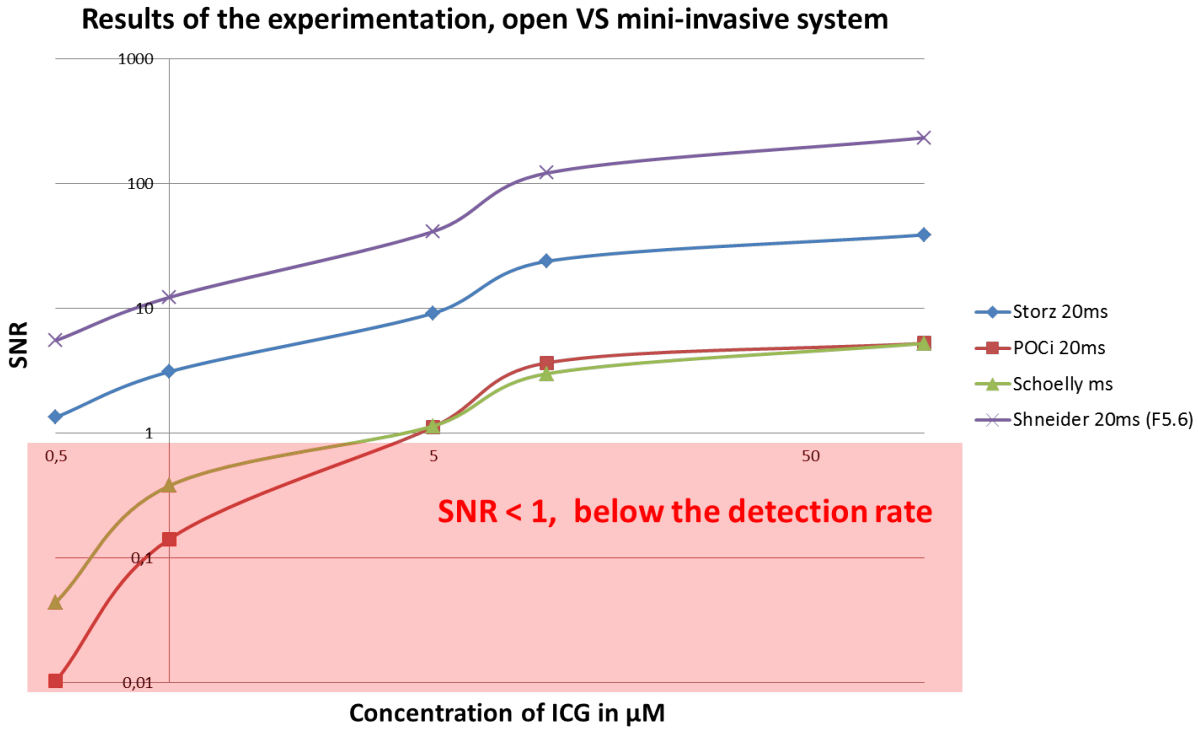

Figure 3.4: Results of the experimentation, comparison between laparoscopes and a open surgery FIGS system

	Open surgery setup	**Mini invasive setup - Storz**	**Mini invasive setup - POC**	**Mini invasive setup - Schoelly**	**Fluostick^{TM}**
SNR Ratio	1	1/5	1/62	1/48	12
Ratios with the Fluostick^{TM} taken as reference	1/12	1/63	1/745	1/571	1
Corresponding optical aperture (normalized F-number)	F5.6	F12.7	F45	F38	F1.8

Table 3.2: Results of the experiment. Corresponding F-numbers are given in front of calculated SNR ratios

The table 3.2 exposes the results of the experimentation. It clearly show the gap in sensitivity that exists between open surgery and mini-invasive systems. Considering the Fluostick^{TM}as a reference system for open surgery, the ratio of collected light arriving on the sensor of the system is 63 between open surgery and the best mini-invasive setup. The challenge is real if the goal is to reach the same limit of detection between open and mini-invasive procedures. The Storz laparoscope appears as the best choice for the development of a mini-invasive instrumentation for fluorescence imaging.

Ergonomics

It is also important to notice the difference that exists between existing FIGS systems and current standards in mini-invasive surgery. The mini-invasive system is dedicated to be held by the surgeon and is manipulated all along the surgery. It is not the case for FIGS system for open procedures which are not used during all the surgery time and are not real hand-held system or are integrated in a mechanical arm. An improvement is required concerning the ergonomics of the system.
The figure 3.5 shows a non-exhaustive list of the FIGS systems for open surgery available today on the market, see chapter 1 for further details. Systems are bulky and heavy in comparison to common laparoscopic cameras which are palm-sized system. The figure 3.6 shows one of the current laparoscopic system from Olympus, the EndoeyeHD® camera. This difference is partly due to the use of big cooled CCD cameras for the detection of the fluorescence signal. For laparoscopic cameras, sensors are rarely larger than $1/2inch$ and only few electronics can be embedded in the head of the system. One challenge identified for the translation to the technology from open to mini-invasive surgeries is to reach a similar fluorescence sensitivity with the use of low-end sensors and electronics.

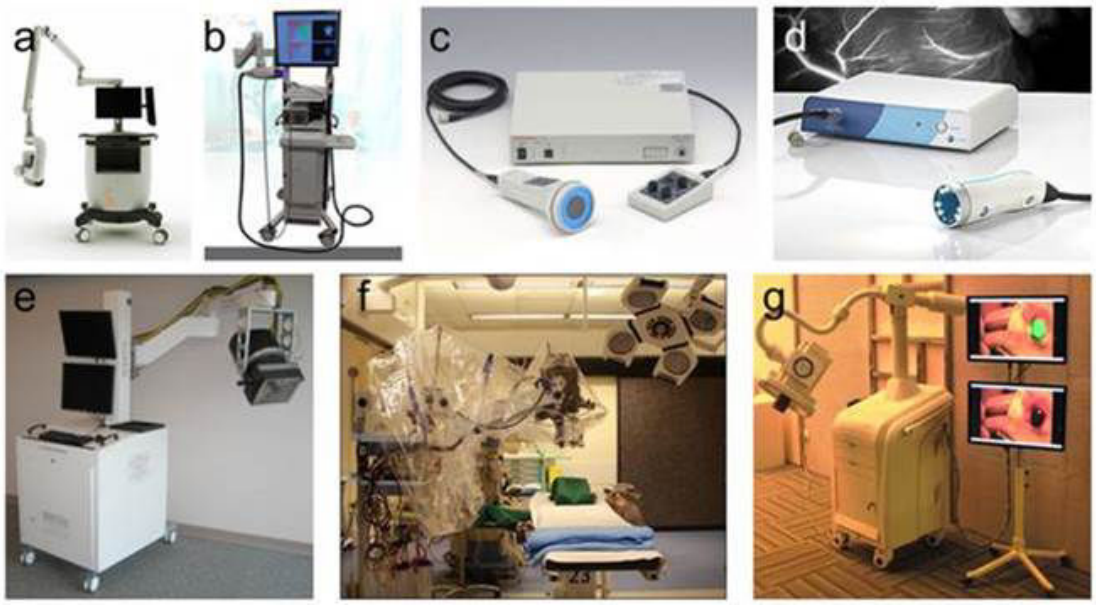

Figure 3.5: Several FIGS systems for open surgery available on the market. a is the Novadaq SPY^{TM} system, b is the Artemis^{TM} system, c is the Hamamatsu PDE^{TM} , d is the Fluobeam® from Fluoptics, e is the FLARE^{TM} imaging system, f and g are labs systems from Technische Universitat Munchen and Institute of Automation of Chinese Academy of Sciences. Figure issued from [27]

Figure 3.6: Picture of the Olympus EndoeyeHD system

3.2.4 Fluorescence imaging and digestive coelioscopy

According to interview with surgeons, the main possible applications of fluorescence imaging for mini-invasive procedures in digestive coelioscopy are listed below:

- **Biliary surgeries**
  The cholecystectomy is the resection of biliary vesicle, also called the gallbladder or cholecyst. The gallbladder stock and releases the bile produced by the liver into the small intestine. Several clinical aspects can conduct the surgeon to take the decision to remove the biliary vesicle. Mostly, a cholecystectomy is performed when little stones, called gallstones, block the vesicle.
  During the cholecystectomy, the surgeon has to cut the cystic canal, which is the output canal of the gallbladder. The problem which could occur is a unintentionally total or partial section of the common biliary hepatic canal. The hepatic canal come from the liver and drain other fluid to the small intestine. Both canals merge before reaching the intestine. Even if it is a quite rare complication (approximatively 5 per 1000 cholecystectomies performed), it results severe injuries for patients.
  Nowadays, cholecystectomies are mostly mini-invasive procedures. There are approximately 750 000 cases of laparoscopic cholecystectomy performed each year in USA, [14]. Standard rigid laparoscopy systems are used to perform the surgery. Once removed, the vesicle is evacuated by the laparoscope's hole. The procedure is common and the anatomy of the region is not very complex. The problem is partly due to modality of imaging. Because the laparoscope goes a lot of time inside from outside of the body during the operation, the surgeon might lose his marks and unintentionally hurt a biliary vessel during the resection. Indeed, the configuration of the cystic and the hepatic canals junction could be tricky due to anatomy variations, see figure 3.7
  Thanks to a prior IV injection of ICG to the patient ($5mg/kg$, from 2 to 8 hours before the surgery), the surgeon will be able to image the bill duct which would have accumulated ICG from the liver. The biliary vessels will be clearly visible during operation and mistakes would be avoided.

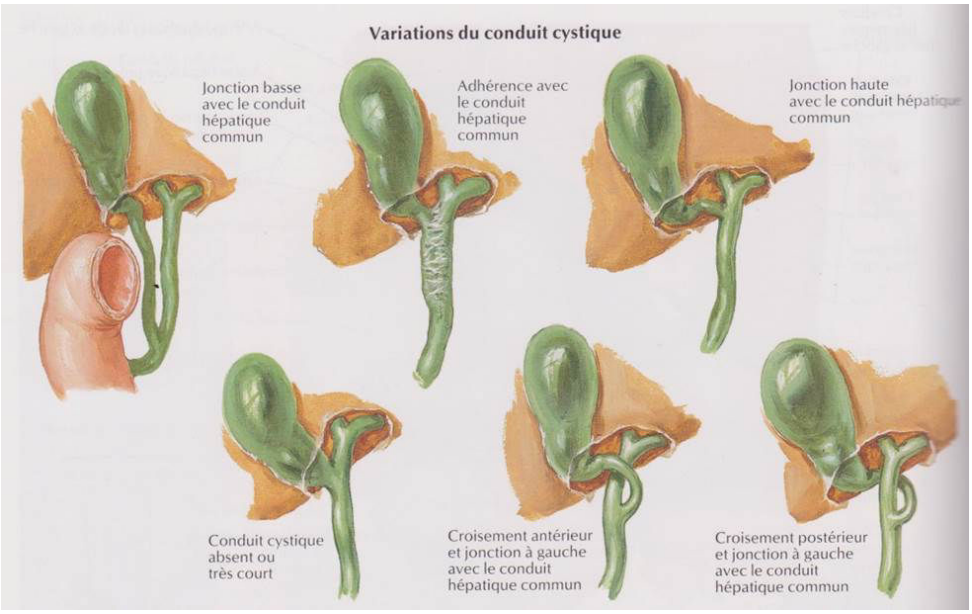

Figure 3.7: Anatomy of the gallbladder, cystic canal and biliary hepatic canal configuration, [28]

- **Hepatic surgeries**
  Some hepatic surgeries involve partial or total resection of one or several segments of the liver. For instance, in a oncologic procedure, a whole segment of the liver should be removed if tumors are inside. Fluorescence imaging is useful to discriminate the different segments of the liver. One segment of the liver could be identified, positively or negatively, by fluorescence. Positively, the portal branch of the segment of the liver is identified, clamped and punctured with a needle for the ICG injection. Only this segment will be fluorescent and the other not. Negatively, still the portal branch of the segment of the liver clamped, an intravenous injection of ICG is performed. In this case, all the liver will be fluorescent except the segment that should be removed.

- **Organs vascularization**
  Similarly to the hepatic surgeries with an intravenous injection of ICG, fluorescence imaging could be useful in order to evaluate the vascularization of an organ or a tissue, for instance in reconstructive surgeries or wound care. In numerous cases, the good vascularization of an organ means a good functionality.

- **Partial nephrectomy**
  A partial nephrectomy is the resection of a kidney tumor without removing the total kidney. The aim of the surgery is to cure the cancer and to preserve the maximum of healthy kidney tissue. After an IV injection, the ICG is cleared by hepatic metabolism and reach the kidney via lymphatic drainage. All the kidney will express ICG fluorescence under an appropriate excitation light except the renal tumors which would have a reduced expression of ICG, [29]. Fluorescence is useful to preserve the maximum of healthy renal tissue by delimiting the margin of the tumor. Also, it helps in limiting injuries and blood loss thanks to rapid identification of vessels.

3.2.5 Fluorescence and minimally invasive surgery, existing instrumentation

In the following section, it will be presented a survey of existing FIGS systems and solutions for mini-invasive procedures. The survey will not be exhaustive but it will show the variety of approach in the development of such systems. It is now clearly established that fluorescence imaging could be very useful in mini-invasive procedures. Several systems have been developed during the past five years. Some of the big actors of the mini-invasive market, Storz and Olympus companies, have designed their own devices. Specialists of fluorescence imaging, such as the company Novadaq or laboratories have also contributed to the emergence of FIGS systems dedicated to mini-invasive surgeries.

Major companies

Major actors of the mini-invasive surgery market have investigated the question of fluorescence image-guided surgery. Olympus company has developed a prototype able to give an image of ICG fluorescence visualization. The device does not offer simultaneously the color and the fluorescence images. The figure 3.8 presents an image acquired with the system.
The system developed by Storz Gmbh is similar to the Olympus one in the fact that it provides fluorescence and color image sequentially and not simultaneously. Nevertheless, the Storz device is a commercialized product under the reference D-light P system.

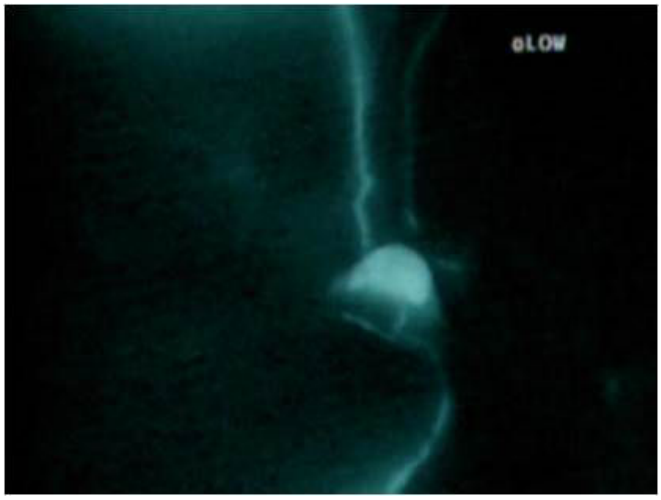

Figure 3.8: A Sentinel Lymph Node procedure performed with the Olympus laparoscopic prototype, [4]

Fluorescence imaging specialists

Some companies specialized in FIGS devices also proposed a mini-invasive system. It is the case for Novadaq and Quest medical. Novadaq has developed two distinctive devices for mini-invasive procedures. One is called the Firefly® and is dedicated to an integration into the DaVinci® surgical robotic system (Intuitive Surgical Inc., USA). It furnishes a fluorescence in false color overlaid to a black and white anatomical background. The Pinpoint® is the other mini-invasive device of Novadaq. It provides a true color+fluorescence image to the surgeon. The figure 3.10 is an example of images acquired with the Firefly® system. The figure 3.9 presents acquisitions performed by the Pinpoint®system.

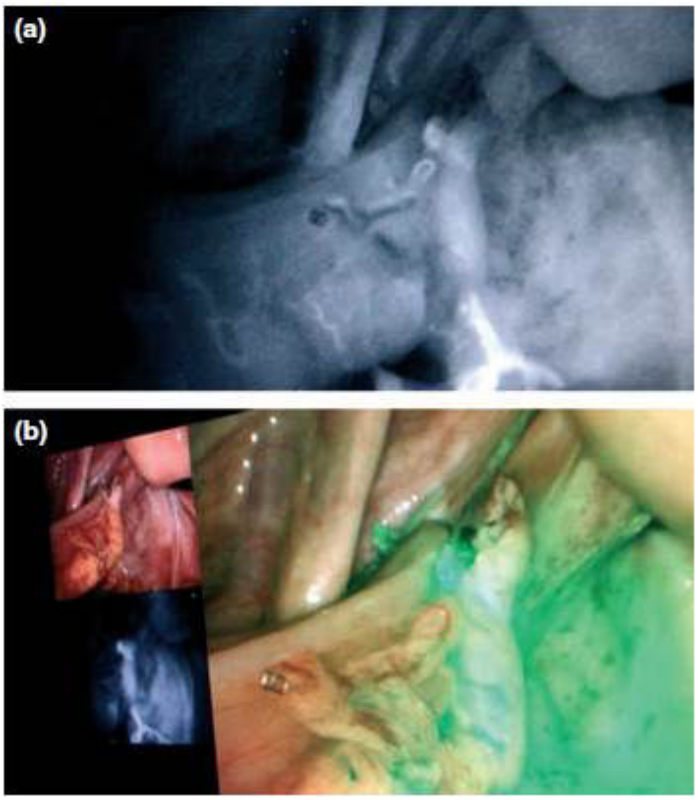

Figure 3.9: Raw fluorescence image (top) and screen-shot of the display (bottom) of the Pinpoint system during the construction of colorectal anastomosis, [6]

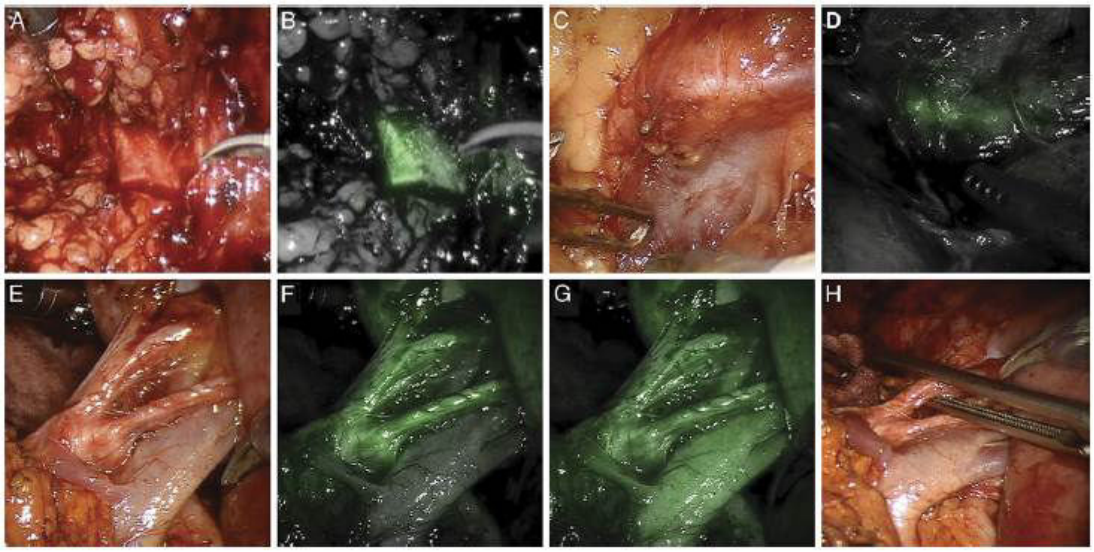

Figure 3.10: Identification of renal structures during a partial nephrectomy performed with the DaVinci® Surgical System, [12]

Labs developments

Laboratories also participate in the development of FIGS for mini-invasive surgeries. The figure 1.14 shows images acquired with an experimental setup derivate from the Flare^{TM} FIGS system. These types of systems help in developing the indications of the technology in the case of clinical trials but they are far from an everyday clinical product in terms of integration, ergonomics and general safety.

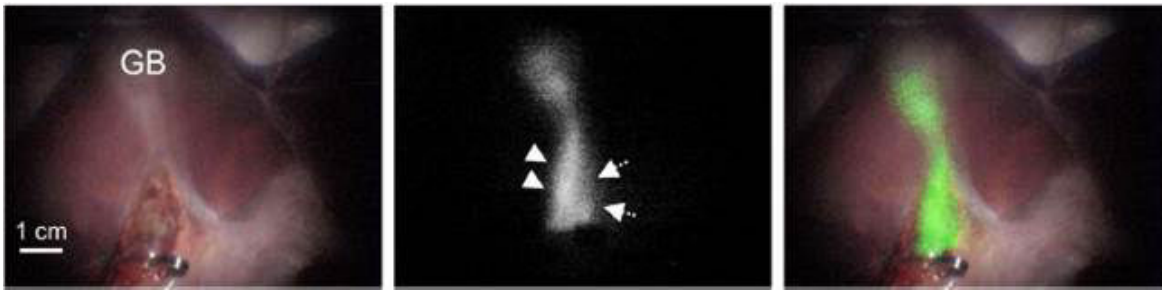

Figure 3.11: Imaging of the with the bile duct FLARE system for laparoscopy, [8]

3.3 The technical development of the FluoMIS™

3.3.1 Build on existing material

The work and the technologies involved in the development of the Fluostick™are the basis for the setup of a innovative FIGS system for mini-invasive surgery. The elements which are the most important to consider in the Fluostick™are the whole fluorescence acquisition channel, comprising optic, filters and camera.

Optics and camera

The camera selected for the fluorescence channel is the same as the one integrated in the Fluostick™imaging system. The camera is analog, few electronics are embedded behind the sensor. The sensor is a Sony ICX659ALA. It is a $1/3inch$ sensor with an optimized response in the NIR region of the light spectrum. The definition is $752\times576px$ and the pixel size $5.3\mu mol/L$. The camera has been developed specifically by NET Gmbh for this project.

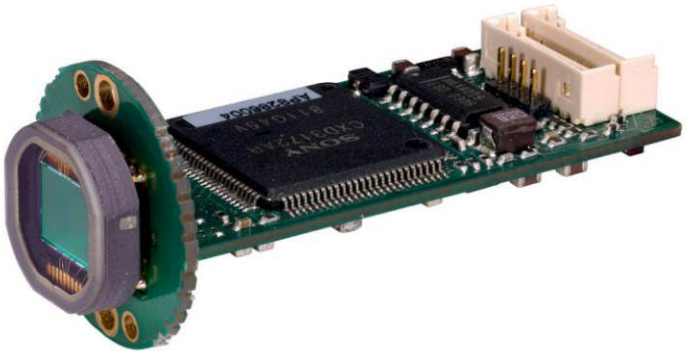

Figure 3.12: The fluorescence channel specially designed camera

The $750nm$ Laser excitation of the Fluostick™is also used for the FluoMIS™ development. Clinical evaluation of the Fluostick™ has confirmed the filtering methods and the references chosen. The filtering strategy filtering will stay the same for the FluoMIS™. The main difference will reside in the fact that filters will be now placed between the lens and the sensor of the system rather than in front of the lens.

Size and overall design

Figures in chapter 2 shows the inner architecture and the outer shape of the Fluostick™, see figures 2.2 and 2.3. The system was designed to perfectly fit

the hand of the surgeon. Also, clinical validation and electrical and safety tests sessions have been performed and validated the design. The mechanics of the FluoMIS^{TM} will be based on the Fluostick^{TM} achievements in this point. The main aspects that will be similar for the new development are :

- The overall size and shape
- The camera integration
- The filtering method
- The cable gland and the cable itself

3.3.2 Specific development for the FluoMIS^{TM}

Two main changes have been operated between the Fluostick^{TM}device, designed for open surgeries, and the FluoMIS^{TM}system, made for mini-invasive procedures. The first change is to add a color channel in the optical head. Indeed, the goal of the system is to be able to acquire simultaneously a fluorescence image and a color image. The second change is about the generation of the light by the system. In fact, in a FIGS system for open surgery such the Fluostick^{TM}, the excitation light and the additional white light are emitted directly by the optical head. In a mini-invasive system, the white light is usually generated by a separated box linked to the laparoscope thanks to an optical fiber cable. For the FluoMIS^{TM}, the light box must be able to generate white light and excitation light and mix them into the optical cable.

The color channel, the design of the optical head

The optical head of the FluoMIS^{TM} is a trade off between existing solutions, the fluorescence acquisition channel is similar to the one used in the Fluostick^{TM} system, and new achievements, the addition of a color channel in a constrained volume. The following section will describe the development of the optical head and will give description of the optical and mechanical specificities of the system. The first goal of a laparoscopic device is to provide a color image to the surgeon. There is several way to combine color and fluorescence acquisition on a FIGS system. The chapter 4 of this thesis will present one original way to acquire color and fluorescence information with one image sensor. For the FluoMIS^{TM}, in order to keep the system simple, the choice was made to use a second sensor in the system to acquire color image. A dichroic filter is used to split the fluorescence information from the white light and both sensors work simultaneously.

The sensor selected for the color channel of the system is the Sony CCD sensor ICX639BKA. This reference is very similar to the black and white sensor used for the fluorescence channel, reference ICX659ALA. These sensors have the same package and the same pixel matrix (same number of pixels, 756×572, and same pixel size, 6.5μm). Only the top layer of the image sensor differ, the color sensor use a YeCyMgG Bayer type filter. It means that every pixel of the sensor is dedicated to a color, yellow, cyan, magenta or green. This choice was made to simplify the overlay of the fluorescence and color information. Also, the same electronics can be used to drive both sensors.

The figure 3.13 displays sample images of the mechanical 3D model of the FluoMIS^{TM}. The goal of the mechanical integration of the sensors is to give the same optical path for both white and fluorescence lights. Possible adjustments has been designed. Indeed, because of the numerous optical elements used in the system, laparoscope, video-coupler and filter, the white light and the fluorescence light will not be focused at the same distance. It is a consequence of chromatic aberrations and the difference of dispersion in the optical glass elements between visible and NIR light. Mechanically, the possibility has been given to the length of the color optical path to be adjusted. Also, in order to simplify the software requirements for the system and avoid complicated alignment and adjustment algorithms, sensors can be aligned pixel to pixel during production.

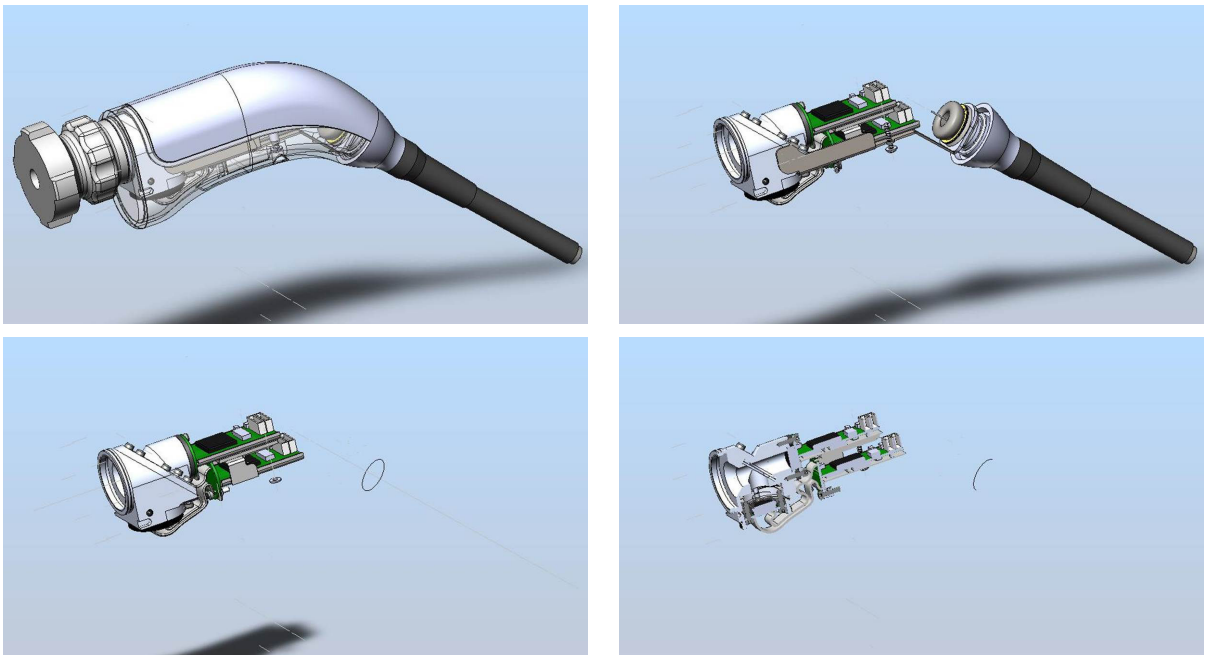

Figure 3.13: Views of the mechanical conception of the FluoMIS^{TM}optical head

Sensors are disposed with an angle of 90^o one to the other. The dichroic filter is placed between the sensors in order to have the same optical path between the last lens of the video coupler and the top glass of both sensor. The reference of the dichroic filter used is the 801nm Fluorescence dichroic Filter from Edmund Optics. The description of the filter used is given below, see figures 3.15.

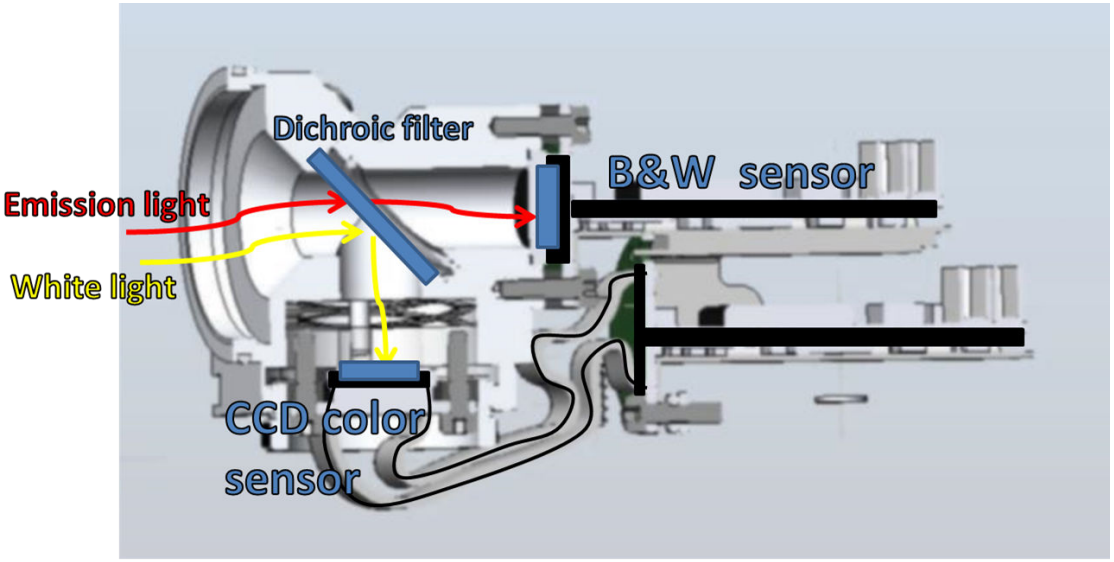

Figure 3.14: Inner architecture of FluoMIS^{TM}optical head

The figure 3.14 is a schematic displaying the position of the different elements in the FluoMIS^{TM} optical head. The video coupler, used to link the laparoscope optic to imaging head, has been specifically designed for his project. Indeed, because a dichroic filter in the optical path between the video coupler and the sensor must be added, an extra back focal length in comparison of the standard C-mount optics is required. The standard C-mount back focal length is around $20mm$. For the FluoMIS^{TM}, the back focal length of the video coupler used is about $35mm$.

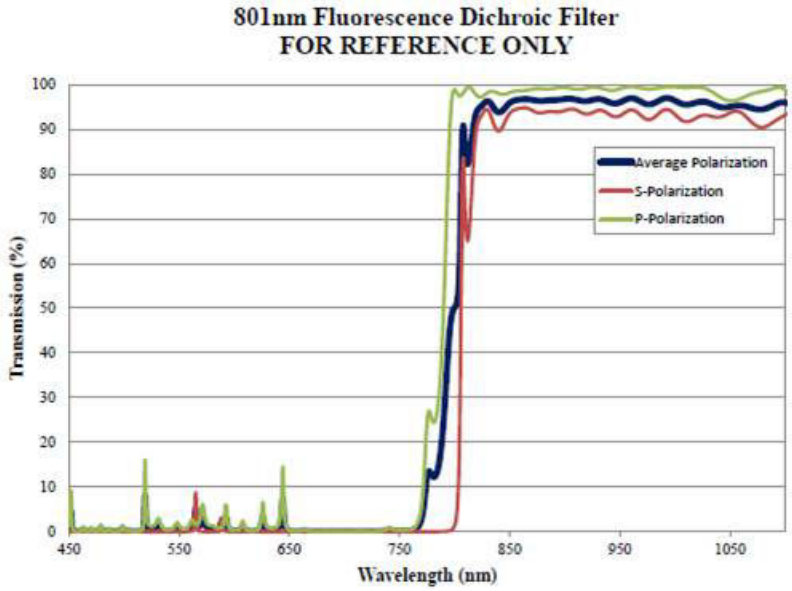

Figure 3.15: FluoMIS dichroic filter, optical head

The development of a specific light box

The global architecture of the FluoMIS^{TM} is similar to existing systems dedicated to mini-invasive procedures. In such systems, the white light needed to acquire images is generated by a separate electrical box. Then, the light is send to the laparoscope thanks to a specific fiber or water cable. Because the FluoMIS^{TM} is dedicated to fluorescence imaging, not only white light is needed on the operation field but also excitation light for the fluorescent contrast agent. The development of the specific light box of the system, generating white and excitation lights, is described below.

As said before, the starting point for the development of the FluoMIS^{TM} is the Fluostick^{TM}. The Fluostick^{TM} is driven by a control box where the excitation light is generated by a Laser at a 750 nm wavelength. The choice was made for the development of the FluoMIS^{TM} to keep this control box and to try to use it with few modification. The mechanical enclosure of the specific light box is the same as the one of the control box. In a normal use, the light box is placed on the control box. The camera is linked to the control box and the light cable is linked to the light box.

The Laser is driven from the control box to the light box thanks to an optical fiber at the back of the system. Also, a SubD9 cable has been added, near the optical fiber, to transmit commands and security signals between the boxes. The

white light is generated inside the light box by a LedEngine module from Schott company, see figure 3.16. This module consists of 7 LEDs disposed on a fan-cooled PCB. A condenser is placed in front of the PCB to collect the maximum amount of light from the LEDs.
A cubic optical combination comprises of a Mightex lens holder, reference LCS-BC25-9999, used to hold a dichroic glass, mixes the white light with the excitation light. Input and output lenses are used to condensate the light into the output $5mm$ diameter light cable. Filters are used to discriminate the lights, references will be given below. The figure 3.17 explains the system and gives the position of the optical elements.

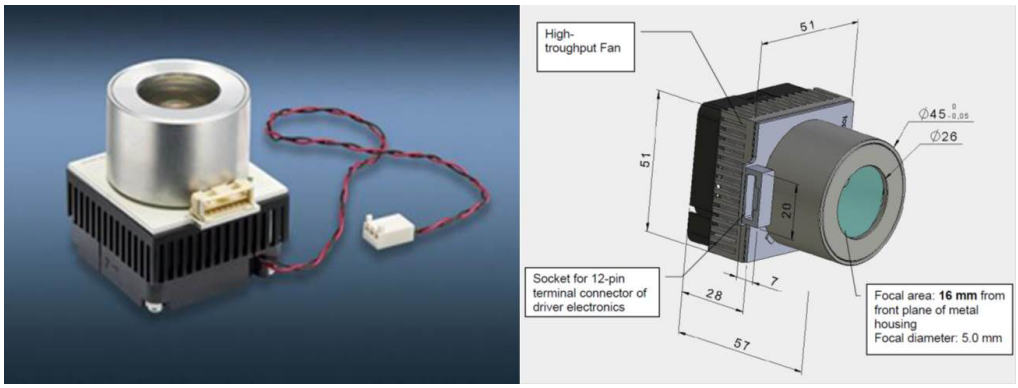

Figure 3.16: Views of the Schott LedEngine

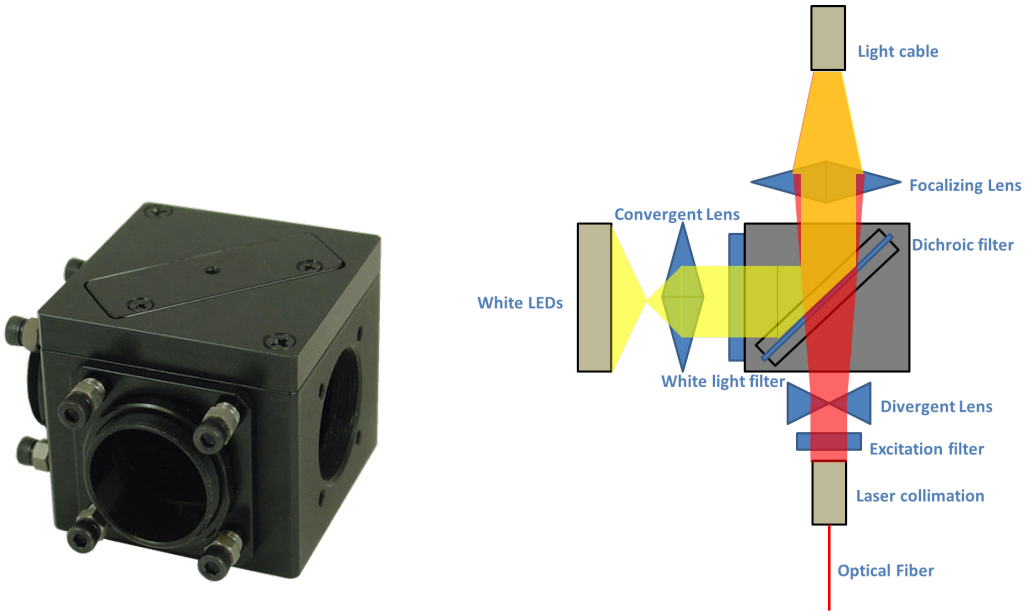

Figure 3.17: Left, picture of the Mightex beam-splitter holder. Right, description of the optical combination used to mix white light and excitation light

As said before, the position of the specific filters used in the light box are given by the figure 3.17. The characteristics of these filters are given by the figure 3.18. An interferential excitation filter, from the Semrock company, is used to avoid parasite light and is placed between an optical combination used to expand the Laser beam from $200\mu m$ to $4mm$ and a divergent lens used to adjust the laser beam to the diameter of the output light cable. The reference of the excitation filter is FF01-747/33-25.
In order to avoid near-infrared light emitted by the LEDs which could disturb the measurement of the fluorescence signal, a filter is placed between the white light emission and the dichroic separator. The filter, referenced by Semrock, is interferential. The reference is FF01-750/SP-25. The filter cuts the emission of light beyond $730nm$.
The dichroic separator is used to mix white light and excitation light. The filter is transparent to radiation beyond $700nm$. The light emitted between 400 and $700nm$ is reflected by the filter. The filter is referenced by Semrock by the number FF01-705/Di01. Finally, the output of the light box is a slightly divergent beam of white light and excitation light mixed. The diameter of the beam is $5mm$ at the position where the light cable is set when plugged into the light box. In order to well fit the light cable to the box, a specific connection has been designed. One piece, attached to the light cable is screwed to the box and guarantee the exact

position of the light cable.

For security and ergonomics reasons, an electromechanical system is used to detect the presence of the light cable. When unplugged, the white light and Laser emission are shut down.

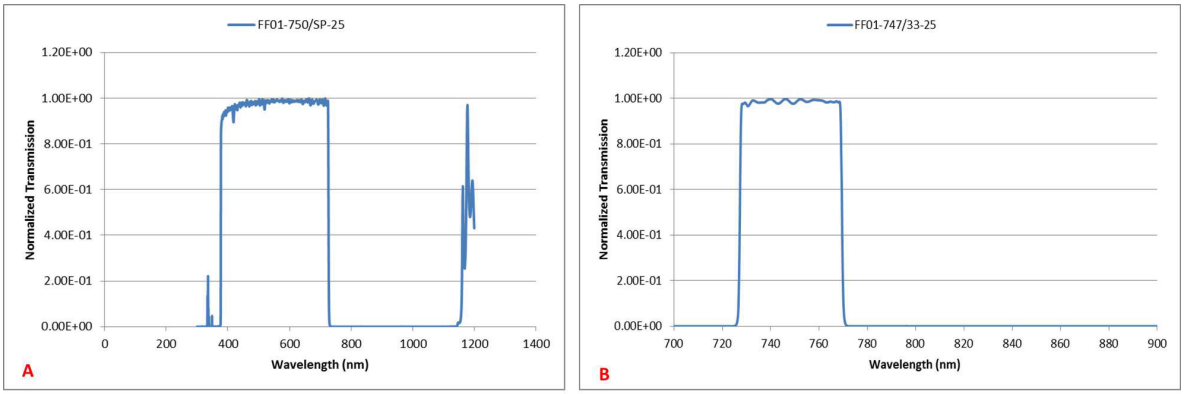

Figure 3.18: Filters used in the light box. A is filter used in front of the white light source. B if the excitation filter.

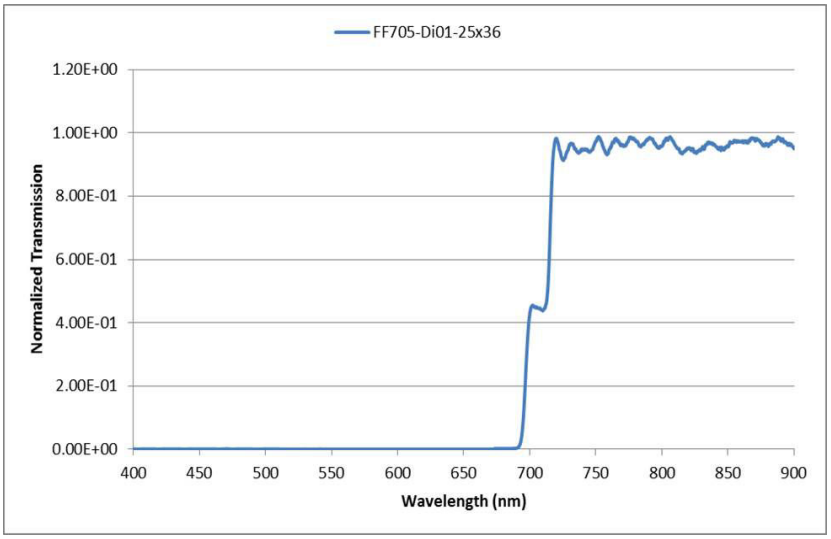

Figure 3.19: Transmission characteristics of the dichroic filter used in the light box.

The figure 3.20 is a picture of the inner structure of the light box.

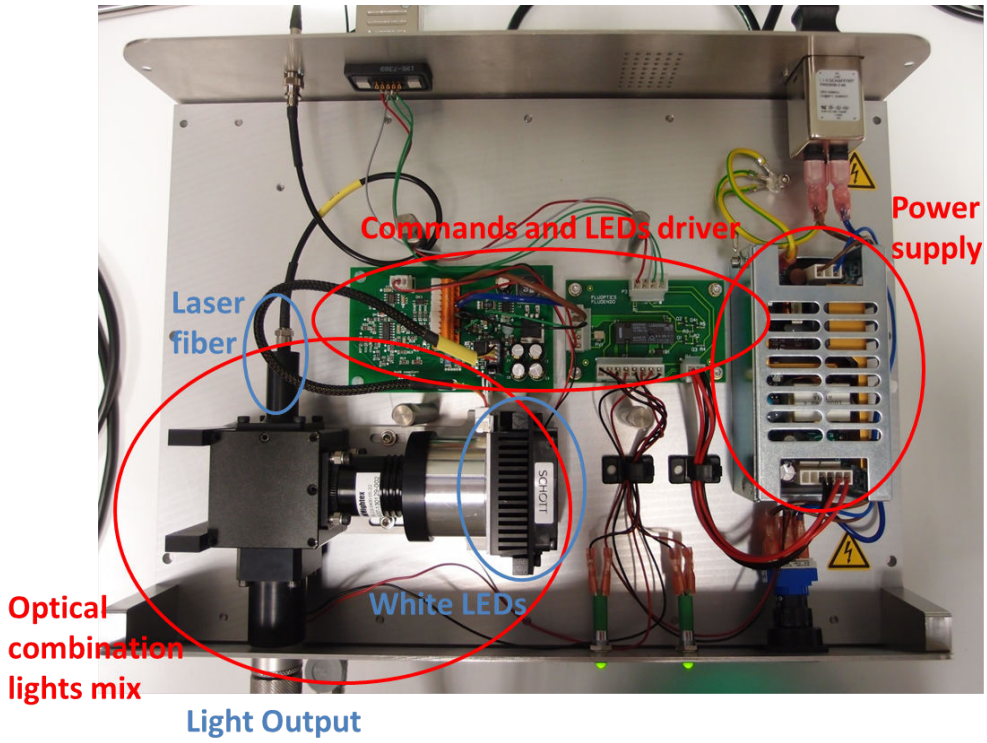

Figure 3.20: View of the inner architecture of the FluoMIS^{TM}light box

3.3.3 Final specifications

The following tabs and graphs detail the overall performance of the FluoMIS^{TM} imaging system :

- White light characteristics, spectral data
  The figure 3.21 shows spectrum characteristics of the white light emitted by the system. The measurement presented has been taken at a $5cm$ distance from the tip of the laparoscope with a spectroradiometer Spectbos1201 from the JETI Gmbh company. At this working distance, the power of the white light is approximately $50000lx$ at a $4450K$ color temperature.

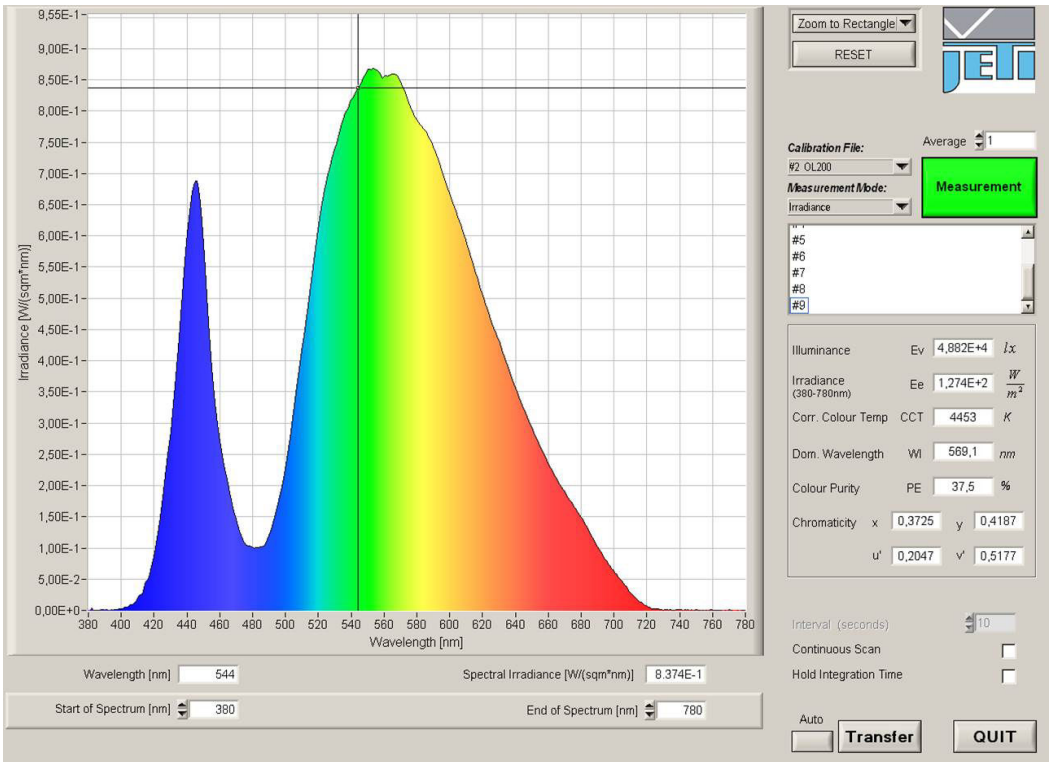

Figure 3.21: White light spectrum

- Excitation light characteristics
  The FluoMIS^{TM}has been developed with the same exigence in term of risk management as the Fluobeam®, a CE/FDA certified commercialized medical device. Because we use a Laser excitation light, some aspects are very important to consider to make the system safe for the patient and the surgeon. Also, we have to consider the fact that the distal tip of the laparoscope will enter in contact with patient's tissues.
  The Laser safety standard IEC60825 is applicable to all medical device using Laser emission. Knowing our configuration, two types of risk have to be considered in order to set the power of the Laser emission, i.e. the ocular risk for the operator and the maximal tissue admission for the patient.
  For the tissue, the standard gives us a limit to not exceed knowing the Laser wavelength. For $750nm$, the limit is $2520W/m^2$. So, for one square centimeter the maximum of Laser power admissible by the tissues is $252mW$.

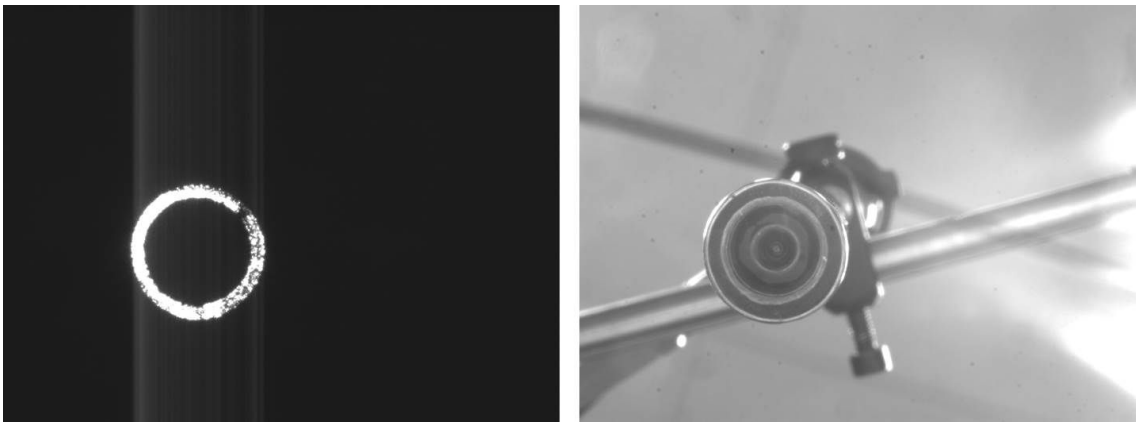

Figure 3.22: Two images of the laparoscope output, on the left the Laser is ON, on the right the laser is OFF

The figure 3.22 shows two images of the tip of the laparoscope. In one image the Laser is ON, in the other the Laser is OFF. Thanks to these acquisition and knowing the outer diameter of the laparoscope, the surface of emission of the Laser could be precisely determined. This surface will be the one which could be in contact with patient's tissues during operation. Calculation gives an accessible surface of $24.54mm^2$. So, the maximum emission power out of the laparoscope is about $62mW$. A power meter with a detector of $1cm^2$ is used to set and measure the power out of the laparoscope.
This output power gives the following power density at several working distances : $1.5mW/cm^2$ at $10cm$, $3.5mW/cm^2$ at $7cm$ and $5mW/cm^2$ at $5cm$ working distance. The standard IEC60825 gives us the Maximum Permissible Exposure (MPE) for the ocular risk at a $750nm$ wavelength for a given output diameter. The emission surface calculated above can be interpreted as a circle with a $5.59mm$ diameter. As set, the system is a class1 Laser system and completely safe for the patient and the surgeon.

- Resolution Measurements thanks to the USAF1951 resolution chart give the value of $140\mu m$ as the optimal resolution for the system at a $5cm$ working distance. Details about the method of determination of the resolving power is given in the appendix B, section B.2. The figure 3.23 shows an image of the resolution target on the color channel only and on the merge fluorescence and color channel. In this image, the fluorescence image is printed in green and color channel still appear black&white. The

figure shows the efficiency of the mechanical fusion of the two channel. The distortion is low on the edges of the images and the fusion is good on almost all the field of view.

Figure 3.23: Views of a USAF1951 standard resolution target. On the left, the color channel only. On the right, color and fluorescence channel (green) using an additional NIR light

3.4 Evaluation of the system

3.4.1 Performances

An evaluation of the ICG limit of detection of the system has been performed. The methods implies drops of $10\mu L$ of ICG at different concentrations. Description of the test method is made in Appendix B, section B.1. The quantities of ICG imaged are respectively $1000pmol$, $100pmol$, $50pmol$, $10pmol$ and $5pmol$. The figure 3.24 shows sample images of the test. It is an image of the 5 drops of ICG at a $3cm$ distance in fluorescence only and with the fusion mode fluorescence plus color image. At this distance, the laser power density emitted by the system is $6.5mW/cm^2$. Only the highest quantities of ICG are detected by the system. The 50, 10 and $5pmol$ drops of ICG are below the detection rate of the FluoMIS^{TM}. At a $8cm$ working distance, the Fluosick^{TM} is able to detect all the ICG drops. A comparison of the systems is presented in the chapter 4 of this thesis.

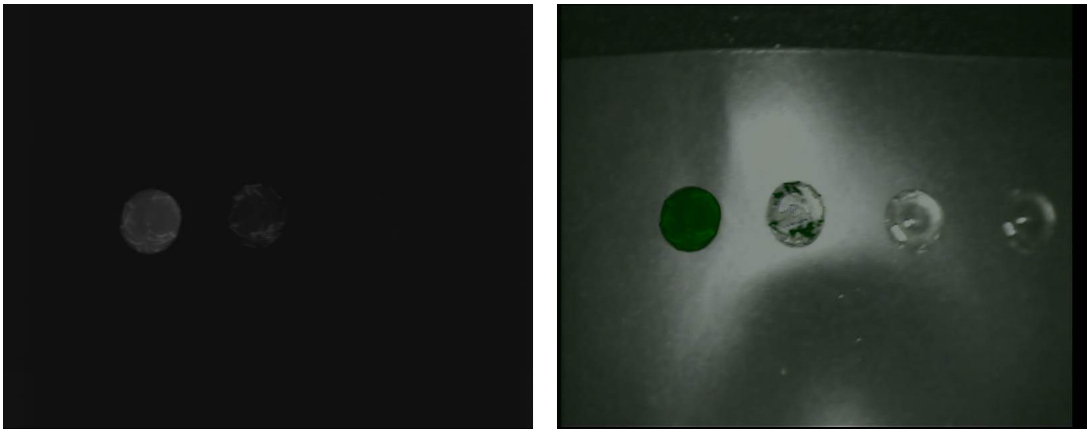

Figure 3.24: Drops of ICG, on the left fluorescence only, on the right color and fluorescence overlaid

3.4.2 In-vivo evaluation

First evaluation on Porcine model

Evaluation context and goals

As a prior in-vivo evaluation of the system, a preclinical test has been performed in February 2014 at Clinatec, Grenoble. A digestive and hepatic surgeon was the operator of the test. The goal of this first evaluation was to experience the ergonomics of the system. Indeed, the choice was made to operate a pig in an

operating room. The other aim of the test was to obtain clues about the relevance of fluorescence imaging for the cholecystectomy, the procedure chosen there. It was also the first occasion to test the color image in a reality-like situation.

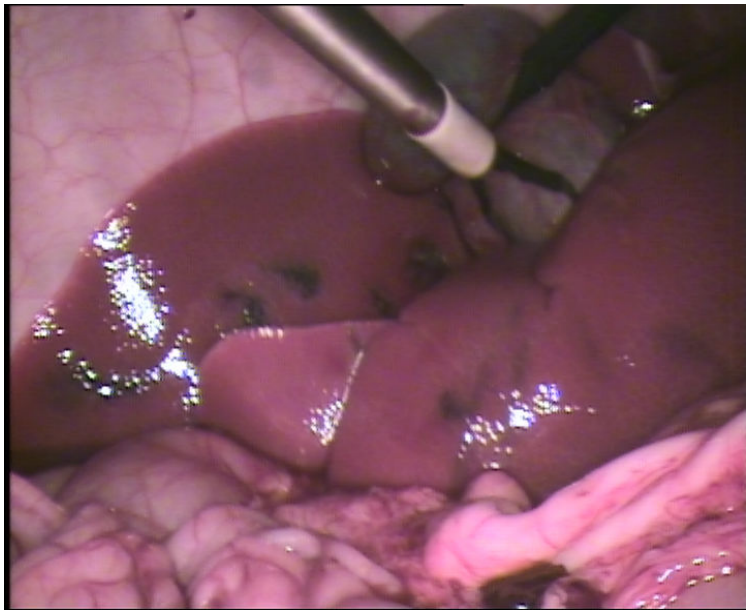

Figure 3.25: Image acquired with the FluoMIS^{TM}system on a pig

The figure 3.25 shows a color image acquired with the system. The image displays different anatomical structures accessible during laparoscopy. The liver is in he center of the field of view. The stomach and the biliary vesicle are at the top of the field. The main issue identified during the test was the poor quality of the colors displayed. There was not enough definition in the colors given by the system and colors of anatomical structures appeared far away from what they are in direct eye visualization.

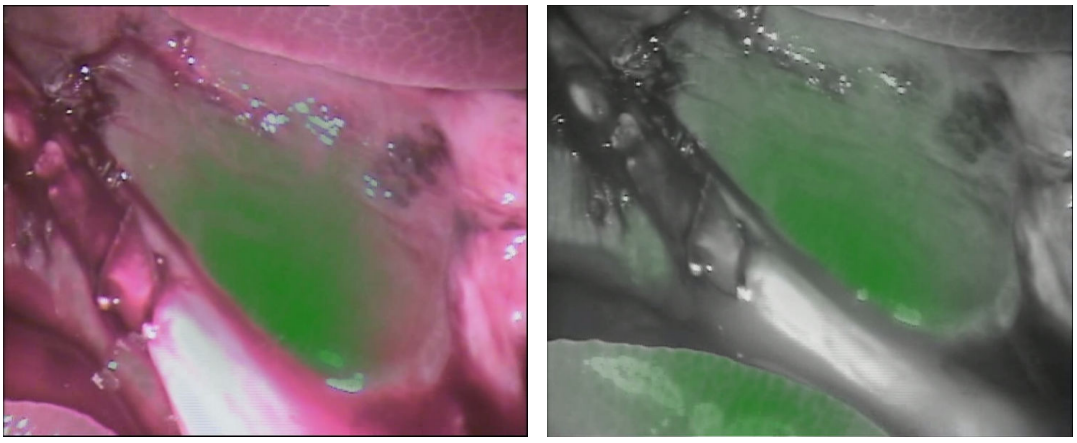

Figure 3.26: Comparison of two setup of acquisition, FluoMIS^{TM} system on a pig. Left fluorescence overlaid on color image, right fluorescence overlaid on N&B image.

In terms of ergonomics, both the maneuverability of the system and the way of displaying the fluorescence information on the screen were evaluated. There is 3 ways of displaying the fluorescence. First, the classic fluorescence only mode which is the only one which appears in the Fluobeam^{TM} or Fluostick^{TM} systems. Then, two color & fluorescence combined modes are proposed in the FluoMIS^{TM} system. The figure 3.26 shows the two modes. One is composed of the overlay of the color and the fluorescence images. The fluorescence information is displayed in false color. Green has been chosen because of its low presence in the anatomy. The second combined mode consists of the superposition of the color information transformed in a B&W image and the fluorescence in green.

Results

As said before, the surgeon was disappointed by the quality of the colors provided by the system. Nevertheless, the relevance of the fluorescence information for the cholecystectomy was assessed. Also, no remarks has been emitted about the ergonomics of the system. The color and fluorescence overlay has been judged the best way to display the fluorescence information on the screen.

Second evaluation on Porcine model

Evaluation context and goals

A evaluation of the FluoMIS^{TM} system has been performed in April 2014. The test has been set at the Institut Mutualiste Montsouris in Paris, France. The operator was a digestive and hepatic surgeon, specialist in minimally invasive surgery.

The evaluation had several goals. As said before, the system has two simultaneous modalities and the first goal of the test was to evaluate the first modality of the FluoMIS^{TM} which is the color image. For the color image, several aspects are considered such as the resolution, the refresh rate and the size and the depth of the field of view.

The second goal was to demonstrate the utility and the quality of the fluorescence modality of the system. Two types of procedures have been considered for this evaluation. First the cholecystectomy and then the hepatectomy. For the cholecystectomy, the aim of fluorescence imaging is to image the biliary vessels and avoid to hurt them in the resection of the biliary vesicle. For the hepatectomy, the aim is to discriminate, thanks to the fluorescence, a part of the liver to be to resected or preserved.

Finally, because it was used in operating room conditions, the test was a good way to evaluate the global ergonomics of the system. The size and shape of the optical head and the general ergonomics of the FluoMIS^{TM} has been evaluated by the surgeon.

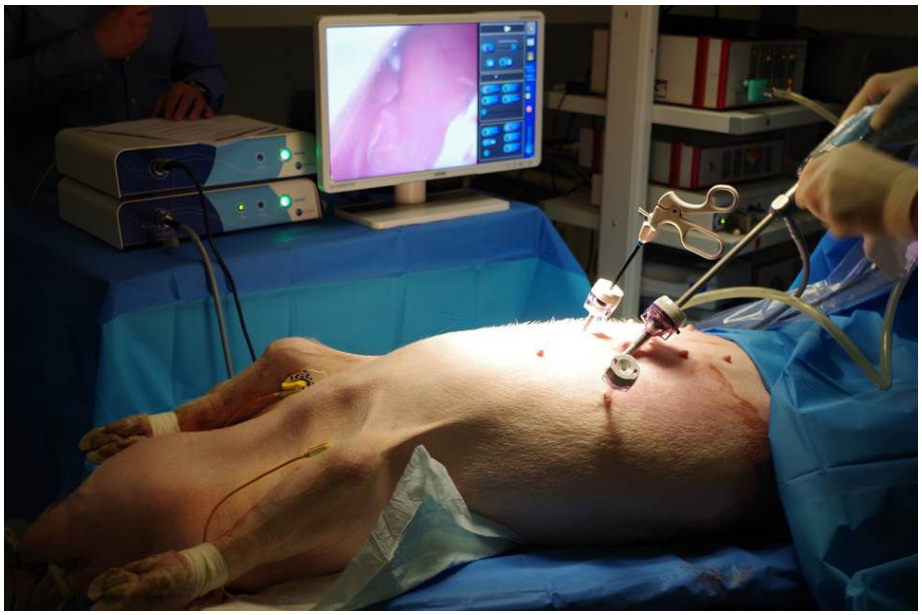

Figure 3.27: The FluoMIS^{TM}system in situation

Evolution of the system

The main changes made on the system between the previous test performed at Clinatec and this one concern the color channel. The main issue identified during this previous session was the poor overall quality of the color channel of the system. The colors appeared false on the screen and the surgeon was

unable to perform his procedure correctly because of the lack of information provided by the color channel. An optimization of the spectral response must been performed. Gains of the sensor on the separate channels Red, Blue and Green could be adjusted in order to give the best response for the system. Then, once the color image acquired by the software of the system, a color optimization is performed. The aim of the color optimization is, for each pixel of the image, to match the color acquired to an other color, supposed to be the true color. The tabulation of the corresponding acquired colors versus true colors is calculated during a calibration where standard color charts are used.

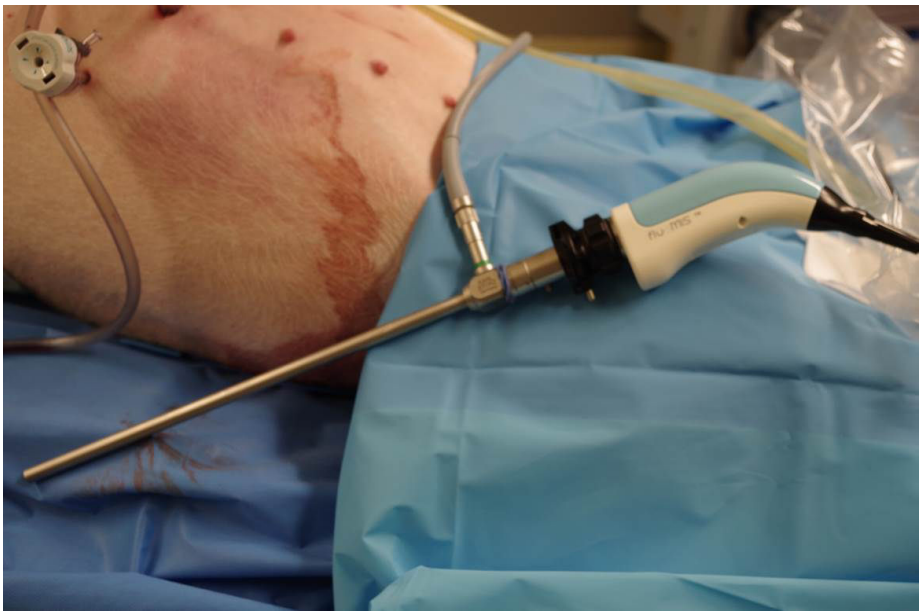

Figure 3.28: The FluoMIS^{TM}system

Results

Overall quality of the color image No issues have been identified concerning the resolution and the frame rate of the color image given to the surgeon. Nevertheless, the image froze 2 or 3 times during the test (approximately 2 hours). Two mains issues have been identified about the color image during the test. First, the depth of field seems to be too short according to the surgeon. Indeed, it has been measured as $3cm$. The value of the depth of field should be at least $6cm$ to perform the surgery in good condition. The surgeon noticed that the Olympus Endoeye® system gives a consequent depth of field from $2cm$ to infinity without the need of focus adjustment. The second identified issue concerns

the exposition of the color image which seems too high for surgeon during the whole operation. It resulted strong reflections on the tissue which make the surgeon exhausted watching the images. The evaluation of the colors themselves has been perturbed because of this surexposition problem. Nonetheless, the surgeon judged good the colors but only in the center of the field of view. He noticed color distortions on the edge of the field of view and when moving back and forth the laparoscope.

Pertinence of the fluorescence information given Because of the poor quality of the color image, the whole cholecystectomy has not been performed during the test. Nonetheless, the biliary canal has been identified and it confirmed the usefulness of fluorescence imaging in cholecystectomy. The figure 3.29 shows an image acquired during the operation. It is a view of the cystic canal marked by the fluorescence in green overlaid in the color image. A complete hepatic segmentation has been performed. Fluorescence was useful in identifying positively and negatively segments of the liver. The figure 3.30 shows sample images of the test performed on the liver segmentation.

Display modalities Between the several display modalities, which are color only, fluorescence only, color plus fluorescence combined and B&W plus fluorescence, the fluorescence alone has been preferred when precise fluorescence information was needed. The surgeon did not found the same level of information in the color and fluorescence or B&W and fluorescence channels than in the fluorescence only display.

Ergonomics The ergonomics of the system has been well evaluated. No drawbacks has been identified in the setup. The shape and the weight of the optical head of the system were satisfying. In the classic configuration of the system, 2 boxes, one for the control and the other for the light, an optical head and a classic laparoscope, resulted no issue in the comprehension of the system. No adaptation is needed between the use of a classic laparoscopic system and the FluoMIS^{TM}. The figure 3.27 illustrates the system's ergonomics.

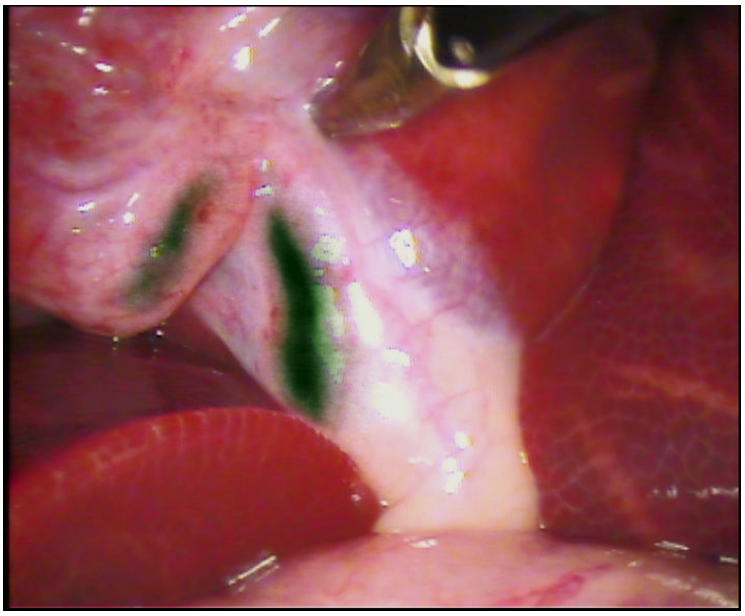

Figure 3.29: Cystic canal below the gallbladder

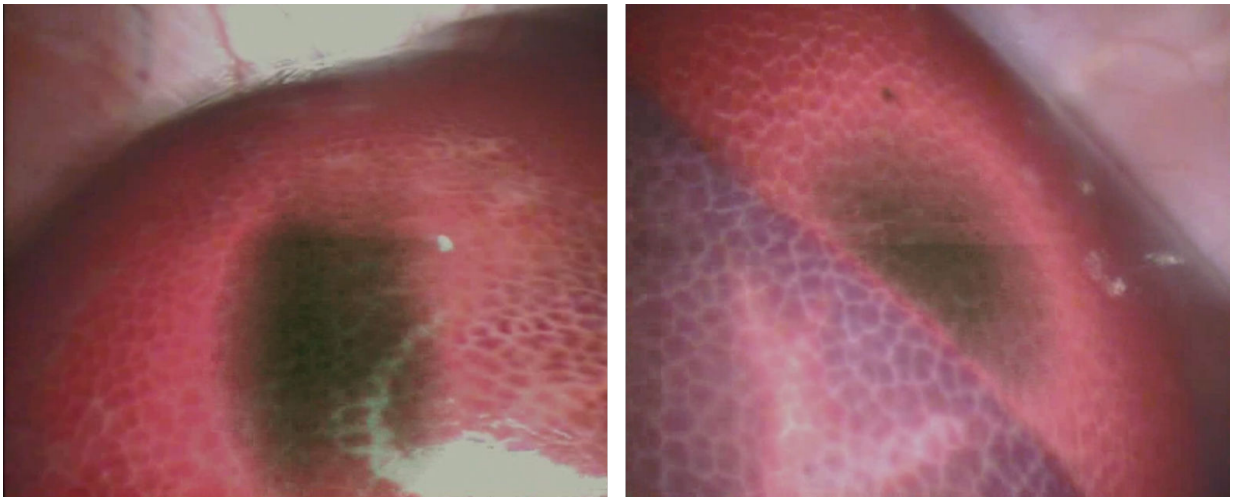

Figure 3.30: Hepatic segmentation determination. Left, positively. Right, negatively.

Conclusion about the evaluation The final evaluation of the FluoMIS^{TM} confirmed the utility of fluorescence for mini-invasive procedures. It also provides us with clues about the ergonomics of mini-invasive systems. Nevertheless, works is still needed to improve the quality of the color image given to the surgeon and it is now the main challenge and issue for the translation of the technology from open surgery to mini-invasive surgeries.

3.5 Conclusion of the chapter

This chapter presented the development of a fluorescence image-guided device for mini-invasive procedures, the FluoMIS^{TM}. The technical development of the system included concepts validated during the development of th Fluostick^{TM} system exposed in chapter 2 of this thesis and innovative aspects, for instance the design of a light source or the addition of a color channel in the fluorescence acquisition chain. Cholecystectomy and hepatectomy indications has been validated experimentally during preclinical evaluations.
These evaluations also demonstrated the need of further investigation. Indeed, the overall quality of the color image and the depth of field of the FluoMIS^{TM} have been judged not good enough by surgeons. These particular points will be the purpose of the development presented in chapter 4 of this thesis.

Bibliography

[1] B. Page, J. Ocampo, M. Nutis, and A. Luciano, *Nezhat Operative Gynecologic Laparoscopy and Hysteroscopy, Third Edition* (Cambridge University Press, 2008).

[2] M. Yoshida, T. Furukawa, Y. Morikawa, Y. Kitagawa, and M. Kitajima, "The developments and achievements of endoscopic surgery, robotic surgery and function-preserving surgery," Japanese Journal of Clinical Oncology **40**, 863–869 (2010).

[3] J. G. Zhang and H. F. Liu, "Functional imaging and endoscopy," World Journal of Gastroenterology **38**, 4277–4282 (2011).

[4] M. Ankersmit, M. H. van der Pas, D. A. van Dam, and W. J. Meijerink, "Near infrared fluorescence lymphatic laparoscopy of the colon and mesocolon," The association of Coloproctology of Great Britain and Ireland **13**, 70–73 (2011).

[5] Y. Ashitate, A. Stockdale, H. S. Choi, R. G. Laurence, and J. V. Frangioni, "Real-time simultaneous near-infrared fluorescence imaging of bile duct and arterial anatomy," Journal of Surgical Research **176**, 7–13 (2012).

[6] R. A. Cahill, F. Ris, and N. J. Mortensen, "Near-infrared laparoscopy for real-time intra-operative arterial and lymphatic perfusion imaging," The Association of Coloproctology of Great Britain and Ireland **13**, 12–17 (2011).

[7] D. C. Gray, E. M. Kim, V. E. Cotero, A. Bajaj, V. P. Staudinger, C. A. Tan Hehir, and S. Yazdanfar, "Dual-mode laparoscopic fluorescence image-guided surgery using a single camera," Biomedical Optics Express **3**, 1 (2012).

[8] A. Matsui, E. Tanaka, H. S. Choi, V. Kianzad, S. Gioux, S. J. Lomnes, and J. V. Frangioni, "Real-time near-infrared fluorescence-guided identification of the ureters using methylene blue," Surgery **148(1)**, 78–86 (2010).

[9] A. Matsui, E. Tanaka, H. K. Choi, J. H. Winer, V. Kianzad, S. Gioux, R. G. Laurence, and J. V. Frangioni, "Real-time intraoperative near-infrared fluorescence identification of the extrahepatic bile ducts using clinically-available contrast agents," Surgery **148(1)**, 87–95 (2010).

[10] I. Miyashiro, K. Kishi, M. Yano, K. Tanaka, M. Motoori, M. Ohue, H. Ohigashi, A. Takenaka, Y. Tomita, and O. Ishikawa, "Laparoscopic detection of sentinel node in gastric cancer surgery by indocyanine green fluorescence imaging," Surgical Endoscopy **25**, 1672–1676 (2011).

[11] E. C. Rossi, A. Ivanova, and J. F. Boggess, "Robotically assisted fluorescence-guided lymph node mapping with icg for gynecologic malignancies: A feasibility study," Gynecologic Oncology **124**, 78–82 (2012).

[12] S. Tobis, J. Knopf, C. Silvers, J. Yao, H. Rashid, G. Wu, and D. Golijanin, "Near infrared fluorescence imaging with robotic assisted laparoscopic partial nephrectomy: Initial clinical experience for renal cortical tumors," The Journal of Urology **186**, 47–52 (2011).

[13] J. Glatz, J. Varga, M. Garcia-Allende P. B. ad Koch, F. R. Greten, and V. Ntziachristos, "Concurrent video-rate color and near-infrared fluorescence laparoscopy," Journal of Biomedical Optics **18(10)** (2013).

[14] S. Demos and S. Urayama, "Enhanced visualization of the bile duct via parallel white light and indocyanine green fluorescence laparoscopic imaging," (2014).

[15] J. Heemskerk, N. Bouvy, and C. Baeten, "The end of robot-assisted laparoscopy? a critical appraisal of scientific evidence on the use of robot-assisted laparoscopic surgery," Surgical Endoscopy and Other Interventional Techniques **28**, 1388–1398 (2014).

[16] T. Ishizawa, S. Tamura, K. Masuda, T. Aoki, K. Haseqawa, H. Imamura, Y. Beck, and N. Kokudo, "Intraoperative fluorescent cholangiography using indocyanine green: A biliary road map for safe surgery," Journal of the American College of Surgeons **208**, 1–4 (2009).

[17] R. Schols, N. Bouvy, R. Van Dam, and L. Stassen, "Advanced intraoperative imaging methods for laparoscopic anatomy navigation: An overview," Surgical Endoscopy and Other Interventional Techniques **27**, 1851–1859 (2013).

[18] R. Schols, T. Lodewick, N. Bouvy, D. Van Dam, W. Meijerink, G. Van Dam, C. Dejong, and L. Stassen, "Near-infrared fluorescence laparoscopy of the cystic duct and artery in pigs: Performance of a preclinical dye," Journal of Laparoendoscopic and Advanced Surgical Techniques **24**, 318–322 (2014).

[19] H. Takeyama, T. Hata, J. Nishimura, R. Nonaka, M. Uemura, N. Haraguchi, I. Takemasa, T. Mizushima, H. Yamamoto, Y. Doki, and M. Mori, "A novel endoscopic fluorescent clip visible with near-infrared imaging during laparoscopic surgery in a porcine model," Surgical Endoscopy and Other Interventional Techniques **28**, 1984–1990 (2014).

[20] F. Verbeek, J. Van Der Vorst, B. Schaafsma, M. Hutteman, B. Bonsing, F. Van Leeuwen, J. Frangioni, C. Van De Velde, R.-J. Swijnenburg, and A. Vahrmeijer, "Image-guided hepatopancreatobiliary surgery using near-infrared fluorescent light," Journal of Hepato-Biliary-Pancreatic Sciences **19**, 626–637 (2012).

[21] L. Li, Y. Ebihara, R. Shirogane, and M. Saito, "Near infrared fluorescence imaging and spectrum of indocyanine green for laparoscopy diagnosis in gastric cancer," Chinese Optics Letters **10** (2012).

[22] H. Kudo, T. Ishizawa, K. Tani, N. Harada, A. Ichida, A. Shimizu, J. Kaneko, T. Aoki, Y. Sakamoto, Y. Sugawara, K. Hasegawa, and N. Kokudo, "Visualization of subcapsular hepatic malignancy by indocyanine-green fluorescence imaging during laparoscopic hepatectomy," Surgical Endoscopy and Other Interventional Techniques **28**, 2504–2508 (2014).

[23] Y. Kondo, Y. Murayama, H. Konishi, R. Morimura, S. Komatsu, A. Shiozaki, Y. Kuriu, H. Ikoma, T. Kubota, M. Nakanishi, D. Ichikawa, H. Fujiwara, K. Okamoto, C. Sakakura, K. Takahashi, K. Inoue, M. Nakajima, and

E. Otsuji, "Fluorescent detection of peritoneal metastasis in human colorectal cancer using 5-aminolevulinic acid," International Journal of Oncology **45**, 41–46 (2014).

[24] T. Ishizawa, N. Zuker, N. Kokudo, and B. Gayet, "Positive and negative staining of hepatic segments by use of fluorescent imaging techniques during laparoscopic hepatectomy," Archives of Surgery **147**, 393–394 (2012).

[25] M. Diana, E. Noll, P. Diemunsch, B. Dallemagne, M. Benahmed, V. Agnus, L. Soler, B. Barry, I. Namer, N. Demartines, A.-L. Charles, B. Geny, and J. Marescaux, "Enhanced-reality video fluorescence: A real-time assessment of intestinal viability," Annals of Surgery **259**, 700–707 (2014).

[26] M. Bouvet and R. Hoffman, "Laparoscopic fluorescence imaging for identification and resection of pancreatic and hepatobiliary cancer," Frontiers of Gastrointestinal Research **31**, 92–99 (2013).

[27] C. Chi, . Du, J. Ye, D. Kou, J. Qiu, J. Wang, J. Tian, and X. Chen, "Intraoperative imaging-guided cancer surgery: From current fluorescence molecular imaging methods to future multi-modality imaging technology," Theranostics **4-11**, 1072–1084 (2014).

[28] F. H. Netter, *Atlas d'anatomie humaine, 3eme edition* (Masson, 2004).

[29] D. Golijanin, J. Marshall, A. Cardin, E. Singer, R. Wood, J. Reeder, G. Wu, J. Yao, S. Passamonti, and E. Messing, "Bilitranslocase (btl) is immunolocalised in proximal and distal renal tubules and absent in renal cortical tumors accurately corresponding to intraoperative near infrared fluorescence (nirf) expression of renal cortical tumors using intravenous indocyanine green (icg)," The Journal of Urology **179(4)**, 137 (2008).

Chapter 4

Improve the FluoMIS^{TM}, breakthrough in the technology and prospective studies

What you will find in this chapter:

In this chapter, based on the results of the prior development of the FluoMIS^{TM}, a improvement in the performances of the FIGS system for mini-invasive surgery is proposed. The innovation is in the use of a single CMOS color image sensor and a pulsed acquisition mode.

Contents

Figures

Tables

4.1 Introduction

The chapter 3 of this thesis presented the utility of fluorescence image-guided surgery for mini-invasive procedures. The advantages of mini-invasive procedures themselves have also been exposed, [1, 2]. The FluoMIS^{TM} imaging system has been evaluated on preclinical models and successfully demonstrated the utility of the technology in cholecystectomy and hepatic related surgeries. Nevertheless, evaluations also revealed that the overall quality of the color image of the system was not good enough and the depth of field of the imaging device too short.

During the last three years, technologically innovative devices has been presented in the literature. Some devices involved the use of two, or more, imaging sensors [3, 4, 5, 6, 7, 8]. These systems presented an architecture similar to the FluoMIS^{TM}, although the FluoMIS^{TM}presents a smaller footprint. Only one system in literature involves the use of one sensor to acquire both color and fluorescence images, see Gray et al [9]. In this particular paper, a video camera is used to acquire sequentially the color image and the fluorescence of nerves marked by a specific probes which emits red light under a $405nm$ excitation.
The one camera architecture is also the choice made to solve the issues identified during the evaluation of the FluoMIS^{TM}. The system presented in chapter 4 will differ from the one presented by Gray et al. because it will be able to acquire a color image and ICG fluorescence in the NIR area of the spectrum.

This chapter will present an innovative way to furnish the color and the fluorescence information simultaneously to the surgeon with only one image sensor. The development of this new device will also demonstrate the pertinence of digital CMOS sensor for fluorescence imaging purpose. The system will be fully characterized and compared with the FluoMIS^{TM}. An improvement will be exposed in terms of color image quality and depth of field, the main drawbacks identified during the evaluation of the FluoMIS^{TM}. At the end of the chapter, prospective studies will be exposed and discussed.

4.2 The development of a single imager fluorescence imaging device for mini-invasive surgery

4.2.1 Principle and purpose of the development

The development of the FluoMIS^{TM}, exposed in the Chapter 3 of this thesis, shows the pertinence of the use of fluorescence imaging for mini-invasive procedures. Nevertheless, the use of two cameras and a dichroic filter, reveals issues in the acquisition of a color image with a sufficient quality for the operating room. Several aspects have to be improved concerning the color image of the system :

- The fidelity of the colors proposed to the surgeon
- The depth of field of the image
- The exposure control and the overall dynamic of this image
- The definition of the image

The drawbacks of the FluoMIS^{TM} will be part of the initial specifications of the system presented in this chapter. Almost every limitations cited here are due to the implication of two analog sensors and the use of a lens with an extended back focal length. So the use of only one image sensor and standard C-mount optics will help in improving the system.
A sequential acquisition is proposed in order to be able to acquire color and fluorescence information with only one sensor. The color image and the fluorescence image are acquired one after the other and the white light and excitation light are activated in function. A single camera is linked to the laparoscope thanks to a standard C-mount video-coupler. The figure 4.1 is a schematics of the system. The system still involves standard rigid laparoscope.
It is also important to notice that the fluorescence performance must be similar or possibly better than the one of the FluoMIS^{TM}.

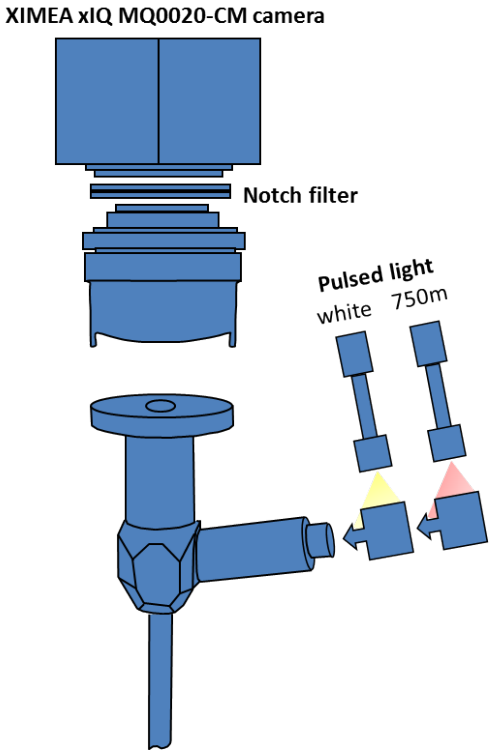

Figure 4.1: Schematic, principle of the system

Also, the use of a single imager gives the possibility to make a step further in the miniaturization of the fluorescence imaging technologies which is one of the main purpose of this thesis. Finally, we hope that the new system will resolve the issues identified in the development process of the FluoMIS^{TM} and will be the basis of a clinical translation of the fluorescence imaging technologies to mini-invasive surgeries procedures.

4.2.2 System architecture

The evolution between the FluoMIS^{TM}system described in the chapter 3 and the new system is mainly located in the optical head of the system and the whole image acquisition chain. The new system will keep the same outer ergonomics and the same white light and excitation light generation. The figure 4.2 presents a schematic of the architecture of the system. One box is dedicated to the control of the device and the generation of the excitation light. With few modification, this control box is similar to the one used to drive the Fluostick^{TM}(see Chapter 2 of this thesis). The control box is linked to the computer through an USB3 connection for the images and a serial bus for the commands.

The light box of the system is composed of LEDs white light emission which is mixed to the laser excitation light thanks to an optical combination and a dichroic separator. Chapter 3 of this thesis presents a complete description of this system with the references of the materials and filters involved. The light is sent to the laparoscope thanks to a standard $5mm$ fiber light cable. The laparoscope selected is a Storz laparoscope optimized for NIR imaging. The complete evaluation procedure of the laparoscope is presented in Chapter 3 of the thesis.

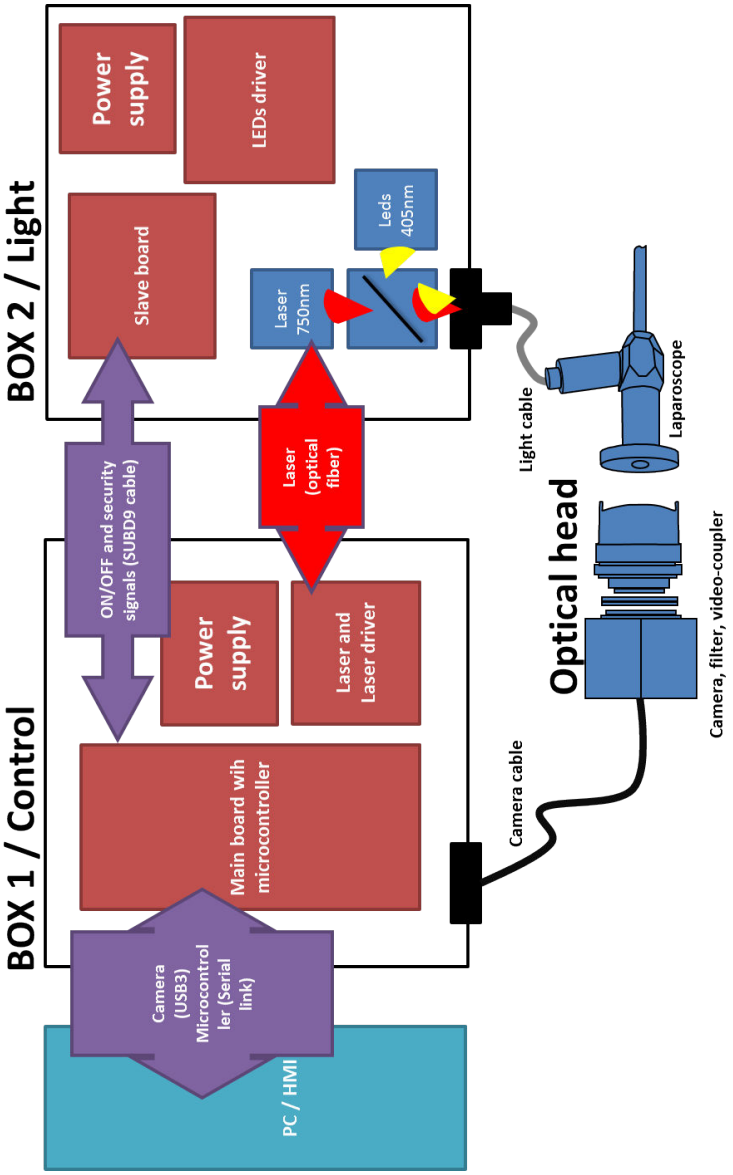

Figure 4.2: Architecture of the system

The control and light boxes of the system are directly issued from the FluoMIS^{TM}

previous development. Both white light and Laser sources will be driven by a hardware trigger signal and there is no need of further electronics development. The figure 4.3 is a picture of the control and the light boxes.

Figure 4.3: Control and Light boxes

4.2.3 Camera and sensor evaluation

The characteristics of the camera are directly transposed from the system requirements described below. We described a single imager system with a sequential acquisition mode. The images should be displayed real-time to the surgeon. Also, the camera should be sensitive to visible light and near-infrared light.
About 12 different cameras and sensors have been benchmarked for the system. The appendix A of this thesis presents theoretical concepts and a method of sensor characterization. The camera selected for this prototype is the Ximea Xiq MQ022CG-CM, see figure 4.4. Results of its evaluation are also presented in appendix B. Data about the noise and the quantum yield of the camera are presented and compared to other systems. The main characteristics of the camera are listed below in table 4.1:

Sensor	Cmosis CMV2000
Framerate max	$170fps$
Definition	$2048\times1088px$
Resolution	$70\mu m$ at a $10cm$ working distance
Size	$35\times35\times35mm$

Table 4.1: Characteristics of the Ximea camera selected for the system

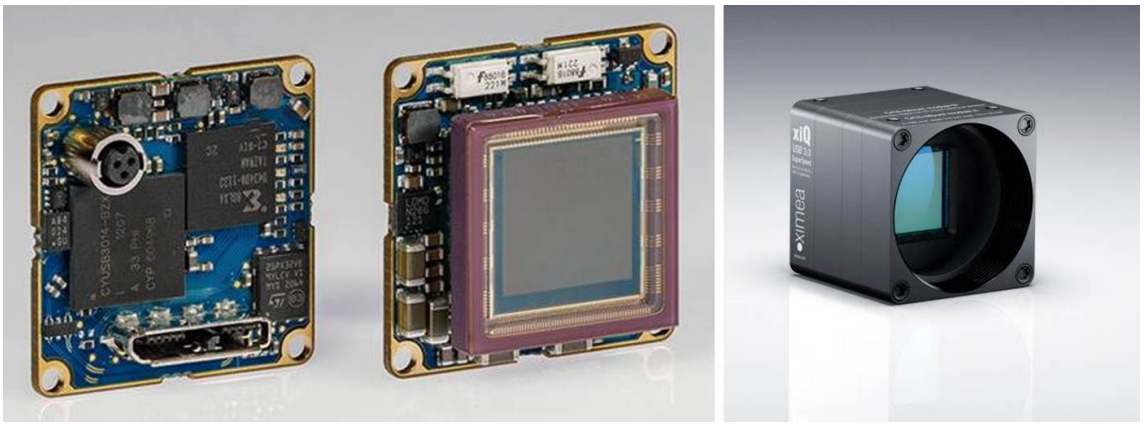

Figure 4.4: Ximea Xiq MQ022CG-CM camera and Cmosis CMV2000 sensor

Because the goal of the system is to acquire color and fluorescence images with the same sensor, it must be a color one. Color images are acquired by a monochrome native sensor thanks to a color filter array (also called Bayer filter mosaic). One colored filter is placed in front of each pixel. The more classic Bayer filter involves red, green and blue filters. More complex mosaic filters with yellow, green, cyan and magenta complementary colors also exist. A step called demosaicing is required to reconstruct a full color image ((R,G,B) values for each pixel) from the incomplete color samples output from an image sensor overlaid with a color filter array.
The camera selected for this development uses a classic RGB Bayer filters array. The particularity of these filters is to be transparent to wavelength above $800nm$. This phenomenon is shown in figure 4.5. After $800nm$, the spectral response of the sensor matches the curve of the monochrome version of the sensor. Fluorescence measurement will not be affected by the Bayer filtering if performed in this area of the spectrum.

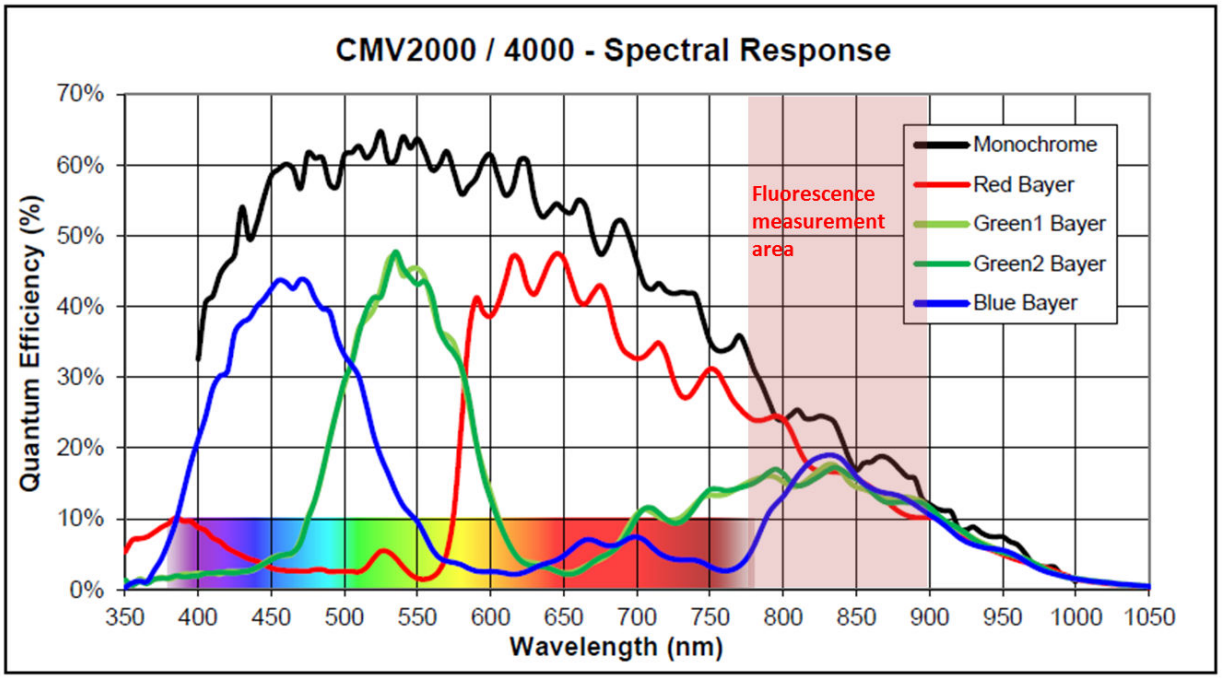

Figure 4.5: CMV2000 Bayer filters distribution

The following figure, 4.6, shows color and fluorescent images acquired sequentially with the device. The video coupler used with the system is a non-specific commercialized product. A video coupler able to image a $2/3inch$ sensor without vignetting artifact had not been identified. Nevertheless, the one selected performs properly except for the edge of the sensor. Because the camera integrates a CMOS sensor, a precise and efficient cropping is permitted (cf appendix B for further details and explanation). A cropped image of $1440\times1080px$ (Full-HD definition with a 4/3 ratio)could be furnished to the surgeon without vignetting artifact.

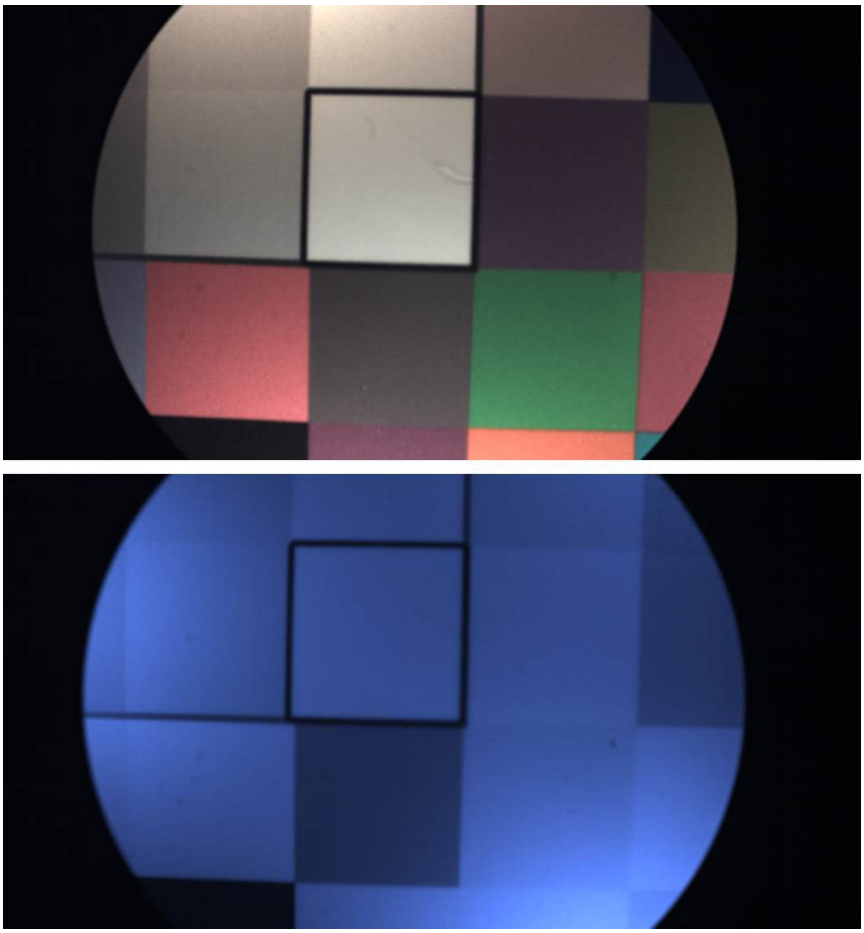

Figure 4.6: A color image and a fluorescence acquired with the video coupler selected, full-frame

4.2.4 Sequence and image acquisition

As said before, the system works in a sequential mode of acquisition. Color and fluorescence images are acquired sequentially. The camera acquisition has to be synchronized with the white light and excitation light sources.
The system has to provide the surgeon with real-time images of the field of operation. A critical requirement of the system arises from this statement. It must be able to acquire a couple of fluorescence and white light images in less than $40ms$ which will corresponds to a $25fps$ framerate. Also, the lag between the actual acquisition and the display of images should be inferior to $70ms$ to keep the system reliable for the surgeon.
The implementation of a dedicated microcontroller is the choice which was made in order to properly drive the system. The microcontroller is the master of the

synchronous system. The lights' drivers and the camera work as slave units. The software of the system will mostly work asynchronously from the timed sequence of acquisition.
The figure 4.7 presents the sequence of acquisition with the several signals generated by the microcontroller and the resultant images acquired by the camera and sent to the software.

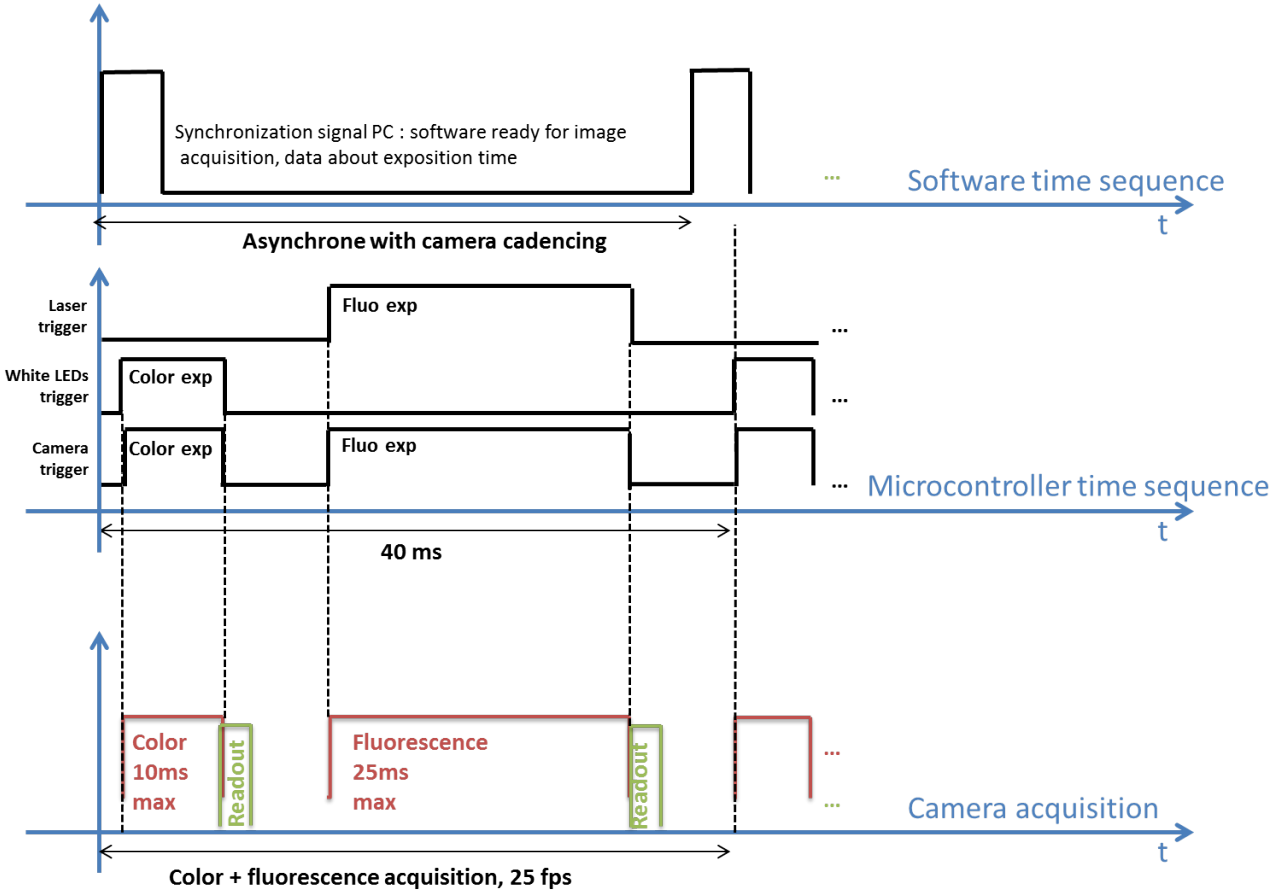

Figure 4.7: Sequences and acquisition

Exposure times are different for the fluorescence and the color images. Because the sensor is much more sensitive in the visible part of the spectrum, there is no need of exposition time longer than $10ms$. One goal of the timing sequence is to allow the fluorescence exposition to be as long as possible for the $40ms$ total time sequence. As defined, the fluorescence exposure time could be $30ms$ long, which is similar to the exposure time used by FIGS system for open-surgery and longer than the $20ms$ used for the FluoMIS^{TM} system. It results a $50fps$ video flux sent to the software with color and fluorescence images alternated.

In this master/slave configuration, the microcontroller is able to set the exposure time of the camera. In fact, the length of high state of the camera's trigger signal will correspond to the effective exposure time of the sensor. Several exposure times have been implemented in the microcontroller's firmware and the software can address the exposure time of the camera by requesting directly the microcontroller. Software and microcontroller are linked thanks to a serial protocol. This communication is asynchronous to the generation of trigger signals by the microcontroller and the $50fps$ cannot be perturbed by incoming commands.

4.2.5 Filtering

A specific filter has been developed for this project. The filtering approach is here different from the one presented in chapter 2 and 3 of this thesis. The system described here must be able to see the visible incoming light. The only part of the spectrum which has to be filtered is the region of the spectrum which correspond to the excitation light emitted by the system.
The excitation light is generated the same way as it is in the FluoMIS^{TM} system. The Laser emission is centered at the $748nm$ wavelength.
A filter able to discriminate only a small part of the spectrum is called a notch filter. The technology involved is an interferential coating. The following figures, 4.8 and 4.9, show respectively the transmission and the optical density measurement made on the filter thanks to a spectrometer. The optical density of the filter is around 4 which is below the value of OD6 which corresponds to the emission filter of the Fluostick^{TM}. Nonetheless, because it will be used between the sensor and the lens and not in front of the lens of an open surgery system, the requirements in terms of filtering capacity are not equally demanding.

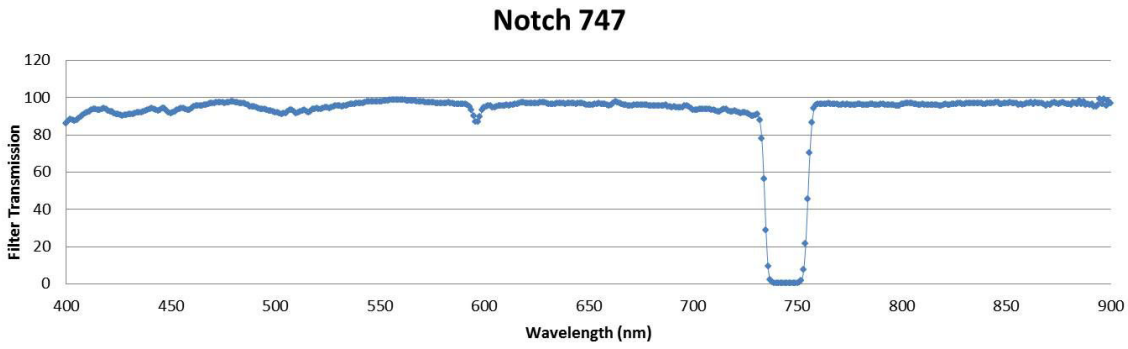

Figure 4.8: Custom notch filter, transmission

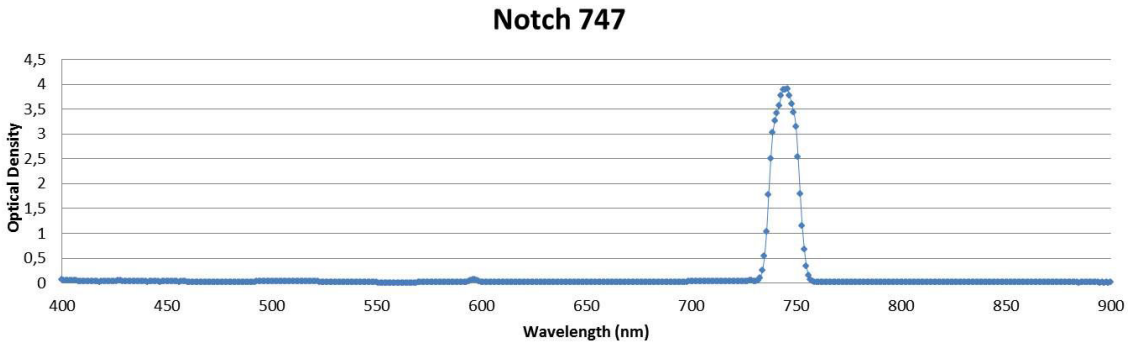

Figure 4.9: Custom notch filter, optical density

4.2.6 Mechanics

The main mechanical development concerned the optical head of the system. The ergonomics of the FluoMIS^{TM} have been successfully evaluated by surgeons during in-vivo experiments. The choice is made to keep the external design of the system and only work on the inner structure of the head in order to integrate the new camera. The figure 4.10 shows the inner structure developed for the system. Thanks to its small package, the camera selected fit well the shell of the FluoMIS^{TM} previously developed with few modification.
Enough spare space is available in the shell for the USB3 and trigger connections. A specific cable is used to combine the USB3 and the trigger wires and connect the optical head to the control box. The cable has a $9mm$ external diameter and is flexible enough for a hand-held manipulation. The PVC outer sheath of the cable is medical grade in order to facilitate maintenance and decontamination.

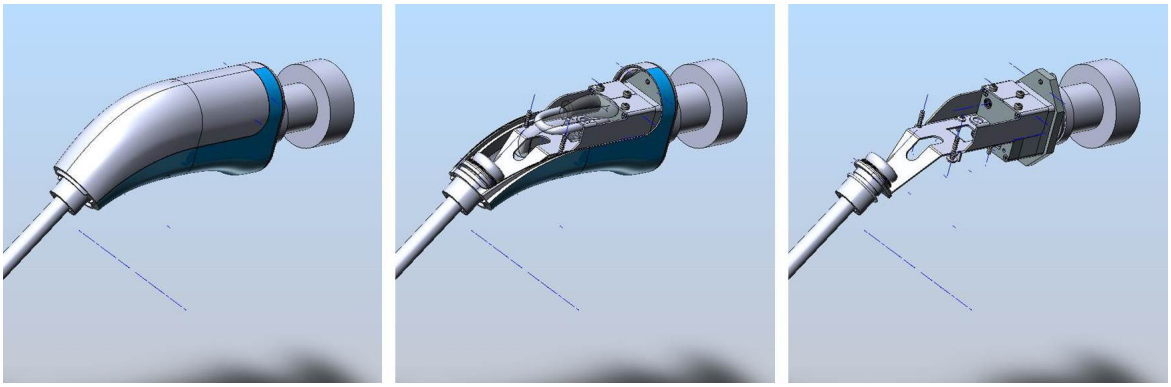

Figure 4.10: Inner architecture of the optical head of the system

4.3 System evaluation, comparison with the FluoMIS^{TM} system

Differences with the FluoMIS^{TM} must be significant for the following characteristics, which are the purpose for the development of a new system:

- The fidelity of the colors proposed to the surgeon
- The depth of field of the image
- The exposure control and the overall dynamic of this image
- The definition of the image

Also, we must guaranty that the system is, at least, as sensitive as the FluoMIS^{TM} . Indeed, the fluorescence efficiency and pertinence have been successfully evaluated with the FluoMIS^{TM} and it will be the basis for the fluorescence evaluation of the new system.

4.3.1 Color image

The color image proposed to the surgeon is one of the main issue of the FluoMIS^{TM} system. The sequential acquisition mode and the filter used in the system described in this chapter allow the sensor to collect a wider part of white light spectrum when acquiring the color image. Also, the sensor has been recently developed and the system is fully taking advantage of the latest improvements in term of overall sensitivity that have been achieved the past 3 years. It is particularly true for CMOS sensors.
Finally, it results that the native quality of the color image proposed by the system seems to be better than the FluoMIS^{TM}.Quantitative evaluation involving DeltaE94 measurements on reference color targets (MacBeth) have been performed. Nonetheless, experience shows that the comprehension of colors for mini-invasive procedures is very subjective and mostly only the feedback of surgeons will help in determining the color quality of a system. The figure 4.11 shows color images of the same lamb heart taken by three different systems. One system is a Storz Tricam® tri-CCD camera for laparosopy. Storz systems are references for laparoscopic procedures. It is the major actor with Olympus on the market. In this figure, both the FluoMIS^{TM} and the new system are compared to the Storz camera.

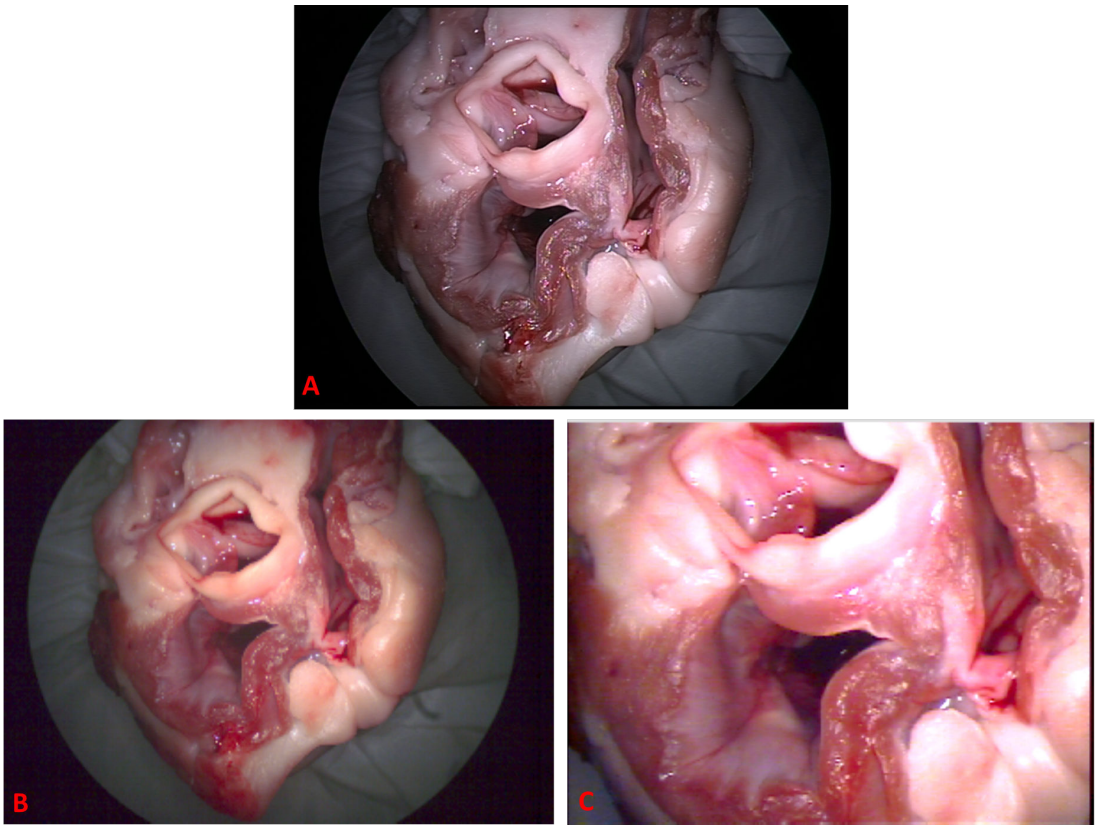

Figure 4.11: Color comparison between the new system (B), the FluoMIS^{TM} (C) and a Storz reference system (A). Same images of a lamb heart

At least, we are able to say that there is no loss of quality between the FluoMIS^{TM} ans the new system. Also there is clearly an improvement in the red part of the spectrum but in-vivo evaluations by surgeons have to be performed in order to be able to conclude on this point.

4.3.2 Depth of field

In-vivo evaluations on the FluoMIS^{TM}stress the fact that the actual depth of field of the system was too narrow to correctly perform surgeries. One goal of the development of the new system is to improve that point.
Calculation has been performed using USAF1951 resolution target. The aim of the test was to determine if the new system has a better depth of field than the FluoMIS^{TM}. The figure 4.12 shows sample images of the resolution targets at several working distances. Both systems, using the same rigid laparoscope, had been focused on a $5cm$ working distance. Then, without adjusting the focus, systems had been set to longer working distance, up to $10cm$. The resolution of

$250\mu m$ has been chosen as the limit of resolution to determine the depth of field. This limit corresponds to about 10 times the circle of confusion given for $2/3inch$ sized sensor. The depth of field expressed here is around 1.5 times the distance between the optimized resolution at $5cm$ and the working distance where the 250 μm resolution is reached.

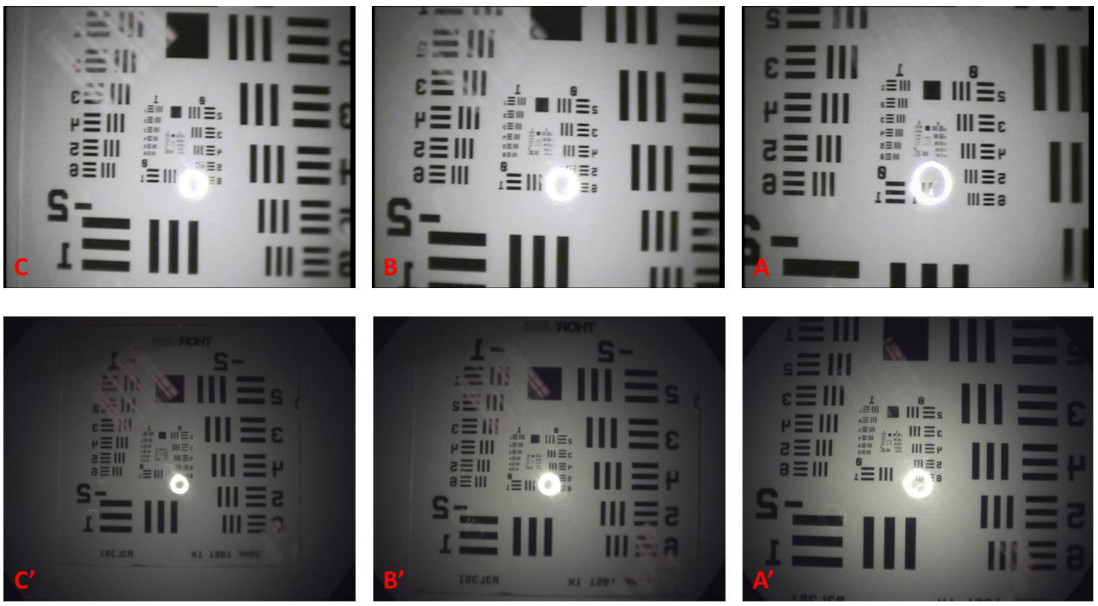

Figure 4.12: Images acquired for the depth of field comparison between the systems. A,B and C acquired with the FluoMIS^{TM} at 5, 6.5 and 8 cm working distance. A', B' and C' acquired with the new system at 5, 6.5 and 8 cm working distance

The table 4.2 displays the results of the depth of field evaluation. The $250\mu m$ resolution limit is reached at $2cm$ from the optimized working distance for the FluoMIS^{TM} . It is commonly stated that approximately 1/3 of the depth of field is in front of the subject imaged and approxiately 2/3 is beyond. It means that its depth of field should be around $2.7cm$. For the new system, limit is reached at $4.5cm$ from the optimized working distance. The depth of field of this system should be around $6cm$.
Finally, even if the calculation of the depth of field could be more rigorous, we are able to conclude that the depth of field of the new system is about twice larger than the depth of field of the FluoMIS^{TM}.

FluoMIS^{TM}	**Working distance (cm)**	10	9,5	9	8,5	8	7,5	7	6,5	6	5,5	5
	Element/Group (USAF1951)	X	X	X	X	0/5	1/1	1/1	1/2	1/3	1/5	1/6
	LinePair/mm	X	X	X	X	1,78	2,00	2,00	2,24	2,52	3,17	3,56
	Resolution (μm)	X	X	X	X	280,90	250,00	250,00	223,21	198,41	157,73	140,45
New System	**Working distance (cm)**	10	9,5	9	8,5	8	7,5	7	6,5	6	5,5	5
	Element/Group (USAF1951)	1/1	1/1	1/2	1/4	1/5	1/5	1/6	2/1	2/2	2/3	2/4
	LinePair/mm	2,00	2,00	2,24	2,83	3,17	3,17	3,56	4,00	4,49	5,04	5,66
	Resolution (μm)	250,00	250,00	223,21	176,68	157,73	157,73	140,45	125,00	111,36	99,21	88,34

Table 4.2: Evaluation of the depth of field, system comparison

4.3.3 Fluorescence sensitivity, comparison with previous development

The new system developed in this chapter must have at least the same level of sensitivity to ICG than the FluoMIS^{TM} . We compare the overall sensitivity in ICG visualization of the new device, the FluoMIS^{TM} and the Fluostick^{TM} . The methods implies drops of 10 μL of ICG at different concentrations. Description of the test method is made in Appendix B, section B.1. The quantities of ICG imaged are respectively 1000 *pmol*, 100 *pmol*, 50 *pmol*, 10 *pmol* and 5 *pmol*. The figure 4.13 displays the results of the experiment. The mini-invasive systems have been evaluated at $5cm$ and $3cm$ working distance. The $750nm$ Laser excitation was measured as $5mW/cm^2$ at $5cm$ and $6.5mW/cm^2$ at $3cm$. In this configuration both systems are Class1 Laser systems (see Chapter 3 for more explanation about the calculation of the Laser class for the mini-invasive system). The Fluostick^{TM} is also a Class1 Laser system. The excitation his about $18mW/cm^2$ at the nominal $8cm$ working distance.

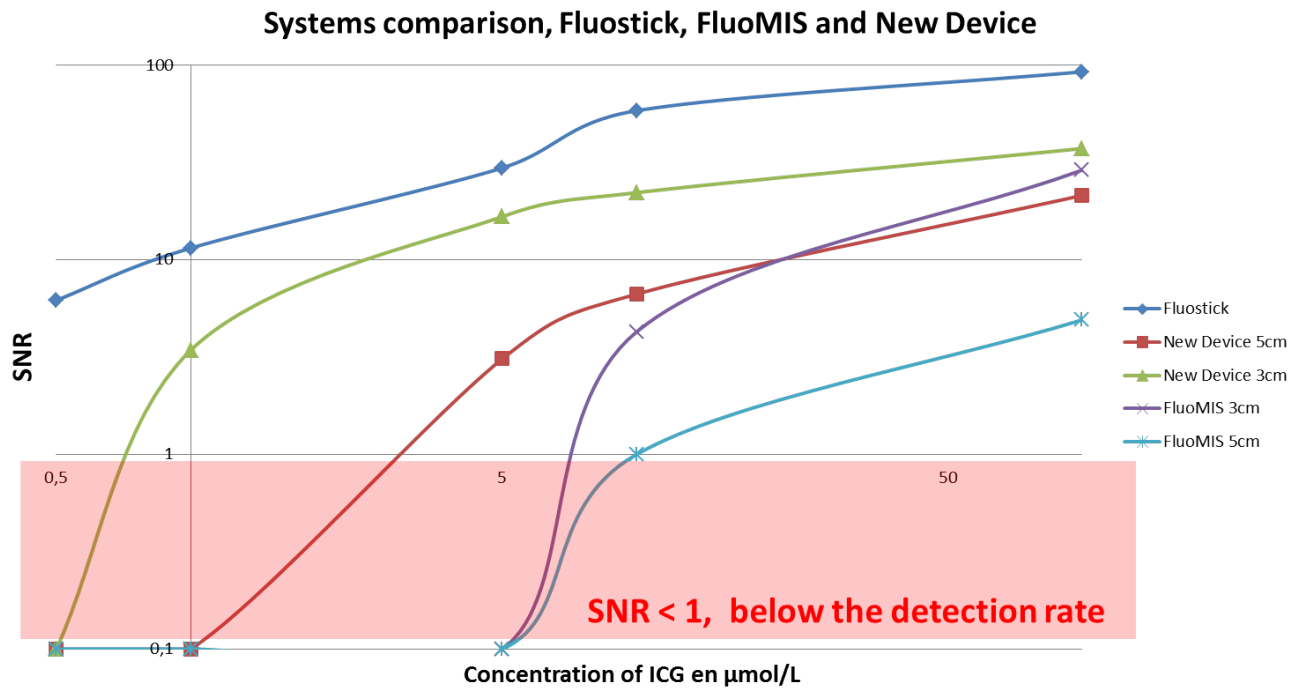

Figure 4.13: ICG limit of detection comparison between the new system, the FluoMIS^{TM} and the Fluostick^{TM}

Results of the test show that the ICG limit of detection for the new system is around $10pmol$ when the FluoMIS^{TM} stops at $100pmol$. Even if the ICG sensitivity of the system does not reach the level of FIGS system for open surgery (the Fluostick^{TM}), the improvement in comparison of the FluoMIS^{TM}is noticeable and should be compatible with the measurement of targeted molecules such as the Angiostamp^{TM} from Fluoptics.

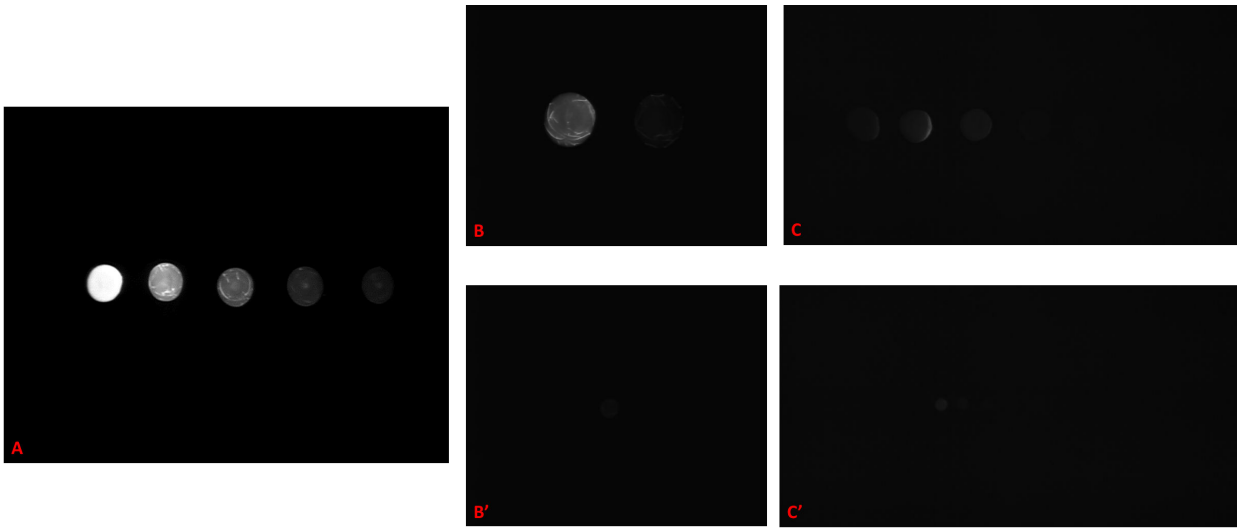

Figure 4.14: ICG sensitivity drops test comparison between the systems. A is the Fluostick^{TM}, B and B' are the FluoMIS^{TM}at 3 and 5cm working distance, C and C' are the new system at 3 and 5cm working distance. The 5 drops of ICG have the following concentrations, from left to right 100$\mu mol/L$, 10$\mu mol/L$, 5$\mu mol/L$, 1$\mu mol/L$ and 0.5$\mu mol/L$

4.4 Distal sensor and perspective studies

4.4.1 In-vivo evaluation

In-vivo evaluation must be conducted in order to finally evaluate the performance of the new system. A cholecystectomy performed on a pig model, as presented in chapter 3, is the method selected. The test should be set in Q1 2015 and conducted by the same surgeons that tested the FluoMIS^{TM} device. Improvements about the color image and the depth of field of the device have to be assessed. Also, the reliability of the pulsed acquisition methods could only be validated by a real and representative in-vivo procedure.

4.4.2 Distal sensor

Prospective studies have been conducted in order to improve the fluorescence sensitivity of the system. It has been presented in chapter 3 that the laparoscope itself induces a great light loss between the field of operation and the sensor of the camera. Indeed, such a system is composed of numerous optical elements which are rarely optimized for near infrared imaging. It results that the numbers of

photons which actually reach the sensor is low in comparison to the total amount of photons emitted. The figure 4.15 is a reminder of the architectures involved in this thesis. The configuration open surgery has been presented in chapter 2 with the development of the Fluostick^{TM}. The direct translation to mini-invasive with the use of a rod-lens type laparoscope is developed in chapter 3 and chapter 4.

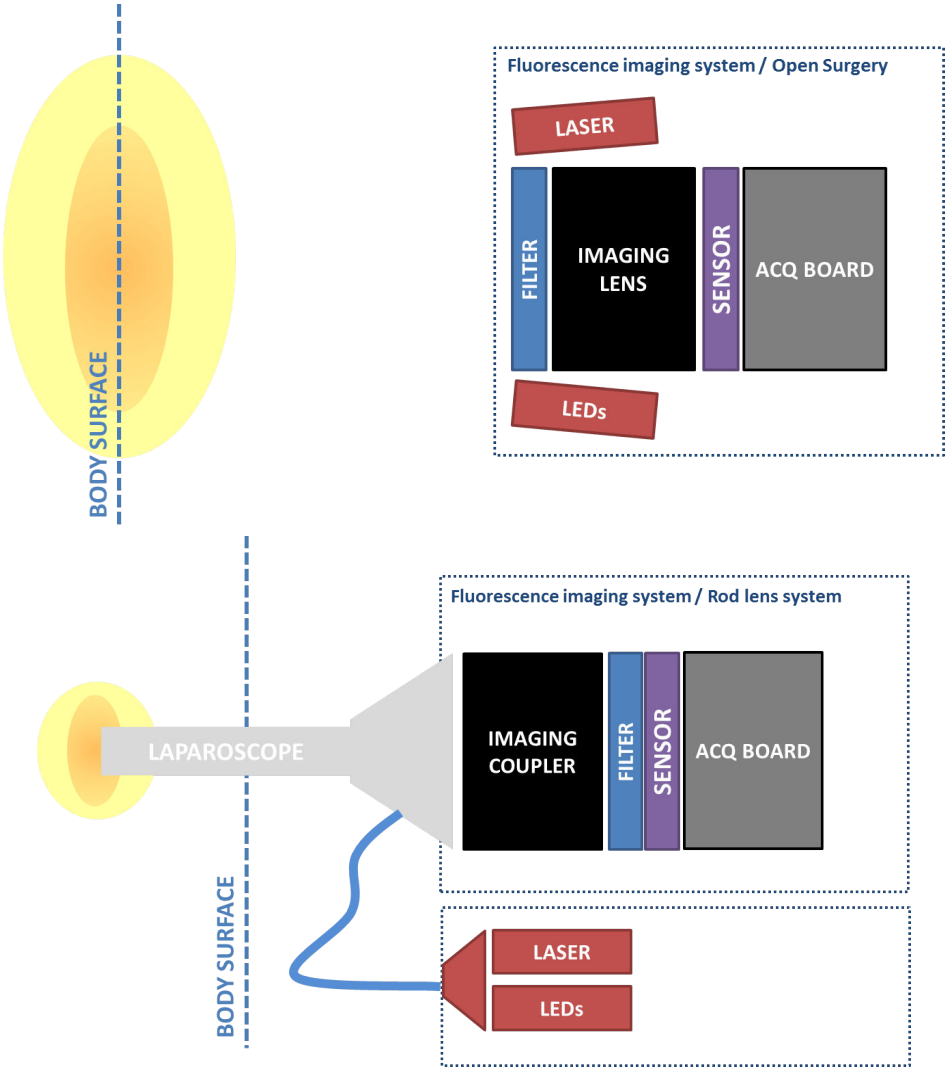

Figure 4.15: Description of FIGS systems architecture as presented in this thesis

A solution to the photons loss issue could be an image sensor placed at the distal tip of the laparoscope. Such an integration could avoid numerous of optical combinations found in rod lens laparoscope. According to measurement performed in chapter 3 of the thesis, at least a factor 5 in terms of light aperture could be gained. The figure 4.16 presents the potential architecture of such a system. Micro sensors have been evaluated. By micro sensor, it is meant a sensor

packaged with dimension inferior to the diameter of a standard rigid laparoscope, i.e. $10mm$. The test performed show that these sensors, all developed for color imaging and high illuminated environments, are irrelevant for NIR-imaging due to a real lack of sensitivity. None of the sensors evaluated were able to acquire a fluorescence image of ICG at a $20ms$ exposition time. The sensors tested included references from Omnivision and Awaiba companies. Nonetheless, improvements in the sensor's field could occur and a constant benchmarking of newcomers must performed.

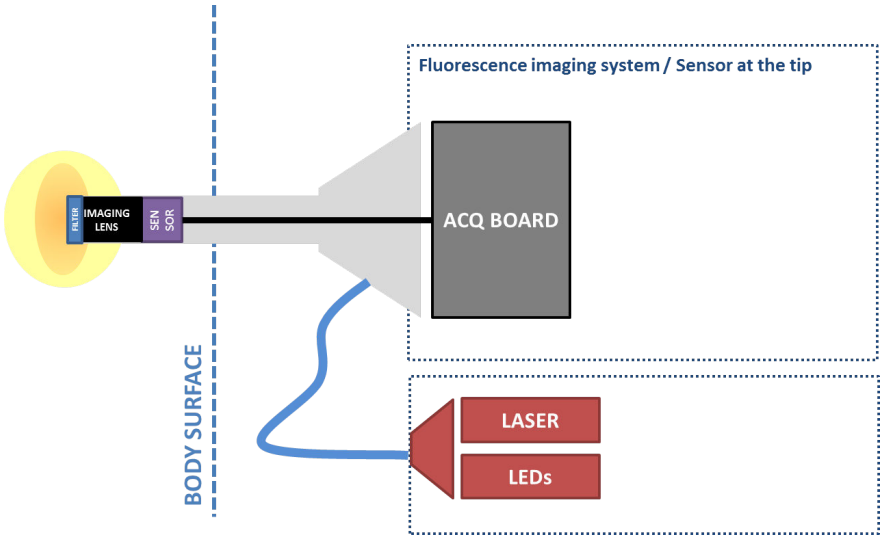

Figure 4.16: Evolution of the FIGS system mini-invasive architecture with a distal sensor

4.5 Conclusion of the chapter

The last chapter of this thesis presented the development of a single imager fluorescence laparoscopic system for mini-invasive surgeries. The system has been characterized and compared to the FluoMIS^{TM}system previously developed. Results and images acquired with the system show an improvement and the quality of the color image proposed should correspond to surgeons requirements. Although preclinical and clinical evaluation are still needed in order to completely evaluate the system, the technology presented will be implemented as a CE Medical system by the Fluoptics company.

Bibliography

[1] J. G. Zhang and H. F. Liu, "Functional imaging and endoscopy," World Journal of Gastroenterology **38**, 4277–4282 (2011).

[2] M. Yoshida, T. Furukawa, Y. Morikawa, Y. Kitagawa, and M. Kitajima, "The developments and achievements of endoscopic surgery, robotic surgery and function-preserving surgery," Japanese Journal of Clinical Oncology **40**, 863–869 (2010).

[3] V. Vanugopal, M. Park, Y. Ashitate, F. Neacsu, F. Kettenring, J. V. Frangioni, P. Gangadharan, and S. Gioux, "Design and characterization of an optimized simultaneous color and near-infrared fluorescence rigid endoscopic imaging system," Journal of Biomedical Optics **18(12)**, 126018 (2013).

[4] H. Takeyama, T. Hata, J. Nishimura, R. Nonaka, M. Uemura, N. Haraguchi, I. Takemasa, T. Mizushima, H. Yamamoto, Y. Doki, and M. Mori, "A novel endoscopic fluorescent clip visible with near-infrared imaging during laparoscopic surgery in a porcine model," Surgical Endoscopy and Other Interventional Techniques **28**, 1984–1990 (2014).

[5] R. Schols, N. Bouvy, R. Van Dam, and L. Stassen, "Advanced intraoperative imaging methods for laparoscopic anatomy navigation: An overview," Surgical Endoscopy and Other Interventional Techniques **27**, 1851–1859 (2013).

[6] J. Glatz, J. Varga, M. Garcia-Allende P. B. ad Koch, F. R. Greten, and V. Ntziachristos, "Concurrent video-rate color and near-infrared fluorescence laparoscopy," Journal of Biomedical Optics **18(10)** (2013).

[7] S. Demos and S. Urayama, "Enhanced visualization of the bile duct via parallel white light and indocyanine green fluorescence laparoscopic imaging," (2014).

[8] Y. Ashitate, A. Stockdale, H. S. Choi, R. G. Laurence, and J. V. Frangioni, "Real-time simultaneous near-infrared fluorescence imaging of bile duct and arterial anatomy," Journal of Surgical Research **176**, 7–13 (2012).

[9] D. C. Gray, E. M. Kim, V. E. Cotero, A. Bajaj, V. P. Staudinger, C. A. Tan Hehir, and S. Yazdanfar, "Dual-mode laparoscopic fluorescence image-guided surgery using a single camera," Biomedical Optics Express **3**, 1 (2012).

Conclusion

We have seen in the thesis how fluorescence image-guided surgery could help the surgeon in numerous procedures. With this technology the surgeon performs faster and decrease the complication rate in open surgeries such as hepatic tumor resection or sentinel lymph node biopsy. Even though, the number of minimally invasive procedures drastically increase since 1983 and the first laparoscopic appendectomy. There is a very small amount of mini-invasive surgeries performed with fluorescence devices. Nevertheless, the interest in this technology is tremendous because it may provide complementary information to the surgeon who cannot anymore sense the tissues. This thesis has been an opportunity to address almost all the aspects and technical points on which fluorescence image-guided surgery is based. This has been performed in translating devices from open to mini-invasive surgeries.

Working on this thesis illustrated that the scaling down of the technology, from open to mini-invasive procedures, involved purely technical aspects, related to the miniaturization process, but also contextual issues, linked to the particular surgical context. For example, the technical issues identified are the sensitivity and the size of the image sensors, the integration of the different light sources, the depth of field of the imaging system or the need to acquire images at a high framerate due to the real-time constraint and the high magnification factor of the laparoscopic device.

In view of these elements, this work mostly focused on systems architectures, electronics, sensors characterizations, cameras integrations and some optical and filtering aspects. Fluoptics expertise was very helpful concerning filtering, software and colorimetry optimization.
The miniaturization approach has been conducted into two main stages. First of all, the work was focused on the size of the optical head of the fluorescence imaging device, see chapter 2. It resulted a new miniaturized FIGS imager, called the

Fluostick^{TM}. The main challenge was to reduce the size of the sensor and ensure that the ICG fluorescence limit of detection of the system is compatible with the use of molecular imaging probes. The second stage consisted in the integration of the color information into the device. Two methods have been implemented. One consisted in the use of two sensors and a simultaneous acquisition of fluorescence and color information, see chapter 3. The other method included only one sensor and a pulsed sequential acquisition mode to overlaid color and fluorescence images, see chapter 4.

The approach based on a color sensor device and its white light / excitation light pulsed acquisition is the most efficient device for ICG visualization during mini-invasive surgeries. Other ways of acquisition has been tested, such as a red, green, blue and excitation lights pulsed mode with a monochrome sensor. This solution was too slow for a real-time acquisition of the images. These approaches are today in use for prospective studies on multi-spectral pulsed acquisition mode. The two sensors system, the FluoMIS^{TM}, still has some advantages in comparison to the one sensor pulsed system. In fact, even if it is not the case for ICG visualization, the single sensor system could be susceptible to image bias created by endogenous auto-fluorescence of images tissues because light from all the spectrum except for the fluorescence excitation light is acquired. In the dual sensors device, a monochrome camera is dedicated to the acquisition of the fluorescence contrast agent emission only. Filtering can be designed in order to avoid autofluorescence issues.
The pulsed device was supposed to become the solution of a research project where Fluoptics was involved. The subject was the tumor ablation in case of bladder cancer. The procedure exists for this type of surgery and implies the visualization of the protoporphyrin IX, a fluorescence molecule expressed by bladder tumor under certain condition. The fluorophore emits red light when excited by a wavelength around $400nm$. A review of the literature shows that urine is fluorescent in the green part of spectrum when illuminated with a deep blue light. Because of this particular problem, the use of a single imager was not possible because autofluorescence would introduce a bias in the the fluorescence signal to noise ratio. A two sensors system was chosen for this particular project and optimized for the visualization of the protoporphyrin IX.

The work performed in this thesis resulted into actual products. The Fluostick^{TM} is currently a commercialized product of Fluoptics. It received a CE-mark in 2013. The evolution of the FluoMIS^{TM}, as presented in chapter 4, will be in-

volved into clinical trial in 2015. Nonetheless, improvements and challenges are still pending for the technology. One o the challenge is the limit of detection and the overall sensitivity of the system. The thesis identified a factor 100 to be gained in ICG limit of detection at a $5cm$ working distance in order to be able to image tumor specific targeted fluorescence contrast agents. As presented in chapter 4, the use of a distal sensor architecture could be a way to solve this limit of detection gap. Also, a specific works on optics (anti-reflection coating specially focused on ICG fluorescence emission) could help by increasing the amount of light that reach the image sensor of the system. An improved ICG limit of detection also allow to decrease the dose injected to the patient. A lower dose of ICG will directly reduce the cost of the procedure and potential toxicity issues for the patient.
Besides, 3D mini-invasive systems recently appeared on the market. In terms of fluorescence imaging, these 3D devices lead to a loss in resolution and a deterioration of the limit of detection because of the complex optical path needed to acquire 3D images. Nevertheless, the perspective of a 3D fluorescence image-guided surgery system for mini-invasive procedures is tremendous.

The translation of the fluorescence technology from open surgery to mini-invasive procedures was the guideline of the thesis. From an other point of view, the technologies developed in the thesis could go back from mini-invasive to open surgery. Indeed, the achievements about general miniaturization and ergonomics, CMOS sensors and pulsed acquisitions could be the core technologies for the design of a color and fluorescence image-guided surgery device for open surgeries.

Appendix A

Image sensor characterization

A.1 Imaging technologies

A.1.1 CCD sensor

Generalities

The CCD sensors (Charge-coupled Devices) were developed by George E. Smith and Willard Boyle in Bell laboratories in 1969. This invention leaded to the Nobel Prize in Physics in 2009. CCDs appeared on the market in the 70s with the advent of semiconductors and progress both in solid-state physics and electronics.
The basic principle of an image sensor, CCD or CMOS APS, is to transform incident light from a source into electron/hole couples using the photoelectric effect induced by the contact of incoming photons with semiconductor material. Once the charges accumulated, they are stored in a register and then transmitted to an analog to digital converter. CCD and CMOS image sensors are both issued from mono-crystalline silicon blocks. The technology used is the MOS capacitor. If the energy of an incident photon is greater than the gap between the valence band and the conduction band, then an electron/hole couple is created. This is the principle of the photoelectric effect. The total number of electrons that the potential well will be able to garner is proportional to the voltage applied. The maximum number of electrons that can garner the well is called the well capacity. The notion of sensor dynamic is directly related to the well capacity and the maximum number of electrons that a photosite can store.
Each well corresponds to a photosite and a photosite corresponds a pixel of the image. The CCD sensor is composed of a matrix of pixel responsible for transforming the incidents photons in electron/hole couples. There is 3 different families of CCD sensors : the Full-Frame CCDs, the Block-Transfer CCDs and

the Interline CCDs. These architectures will be describe below.
More precisely, the following diagram shows the architecture of a classic CCD's photosite. In the case of a CCD sensor, the incidents photons pass through the superficial layers of the sensor whose presence is explained by the technologies used for its manufacture. The electron/hole couples are formed at the surface layer (or epi-layer). The thickness of this layer is around $15\mu m$ for the majority of CCD sensors.
The ratio between the number of photons hitting the cell at a given energy (i.e. a specific wavelength) and the number of electrons effectively created is called the quantum efficiency of the sensor. The evaluation of the quantum efficiency of a full range of wavelengths evaluate the global efficiency of a sensor. The quantum yield depends largely on the materials used to build the sensor as well as its own design.

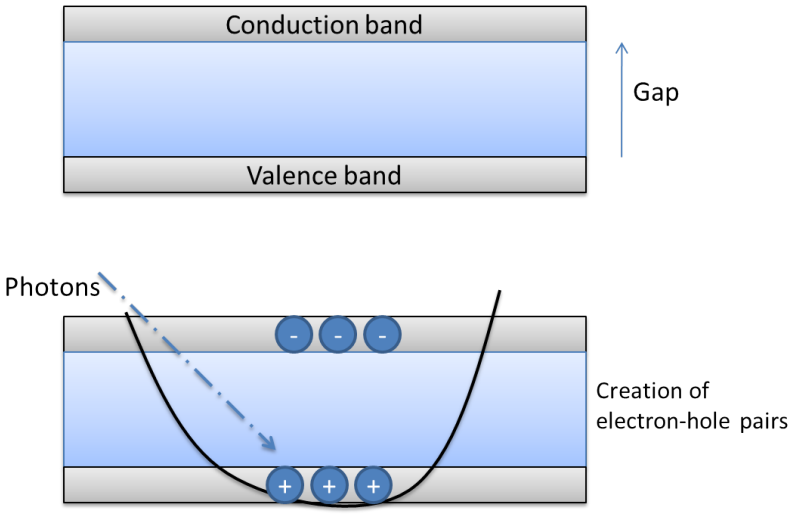

Figure A.1: MOS capacity, photoelectric effect in a photo-diode

Of course, the quantum efficiency can not alone assess for the performance of a sensor in its entirety. The signal collected and exploitable from a sensor involves a complex acquisition chain influencing greatly the performance of the imager itself. Behind the function of photon collection and creating electron-hole couples there is a signal conversion stage of charges in voltage. It is from this stage that we can assess the sensitivity of an imager. The other important parameter to be quantified when evaluating a sensor is the noise. All the noise characteristics of an imager will be discussed in more detail later.

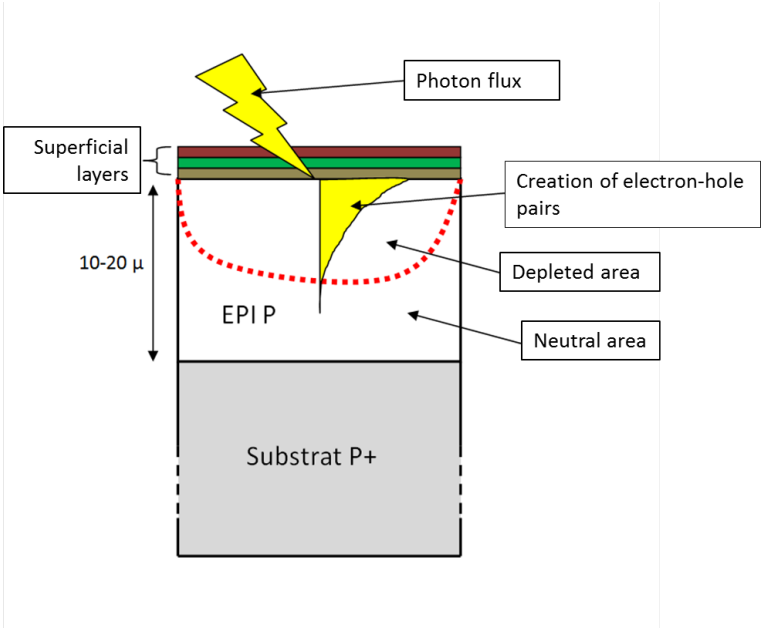

Figure A.2: CCD's photo-site architecture

Full-Frame CCD sensor As previously announced, there are different types of CCD sensors. The oldest type of CCD sensor is the Full-Frame one. The principle is, for an acquisition and therefore a given exposure time, to read the entire surface of the detector pixels at once. We distinguish two phases. First of all, an acquisition stage where the sensor is exposed to light depending on the exposition time. Then takes place a readout stage, where the sensor is occulted. During this step the collected information is transmitted line by line to a register and then treated. This mode of operation involves the use of a mechanical shutter which physically hides the sensor reading part which collects the data in order to avoid any kind of artifact. In thus case, the CCD cells have a dual role, photosensitive and charge transfer capacity.
This mode of operation has the advantage of offering a wide dynamic because the entire sensor's surface is dedicated to the collection of photons. The fill-factor is the ratio between the physical size of the sensor and the surface actually dedicated to the acquisition of light. For a full-frame type CCD it goes from 70 to almost 100%. It's the most sensitive type of CCD sensor. However, the Full Frame does not allow short exposure time, therefore, important operating speeds are excluded. The frame rate of this type of CCDs barely exceed 10 frame per second. In addition, this type of sensor is exposed to the phenomena of blooming and smearing due to the glare of neighboring pixels of a saturated photosite. This

is actually an overflow of electrons between photosite since there is no physical barrier between the pixels. Finally, because of the nature of the surface layers of the photosites and the fact that electrons flow over the areas of the photosensitive sensor during signal acquisition, a large part from blue spectrum collected is absorbed when transferring charges. Nevertheless, this lack of sensitivity in the blue part of the spectrum is not an issue for Near Infrared fluorescence imaging.

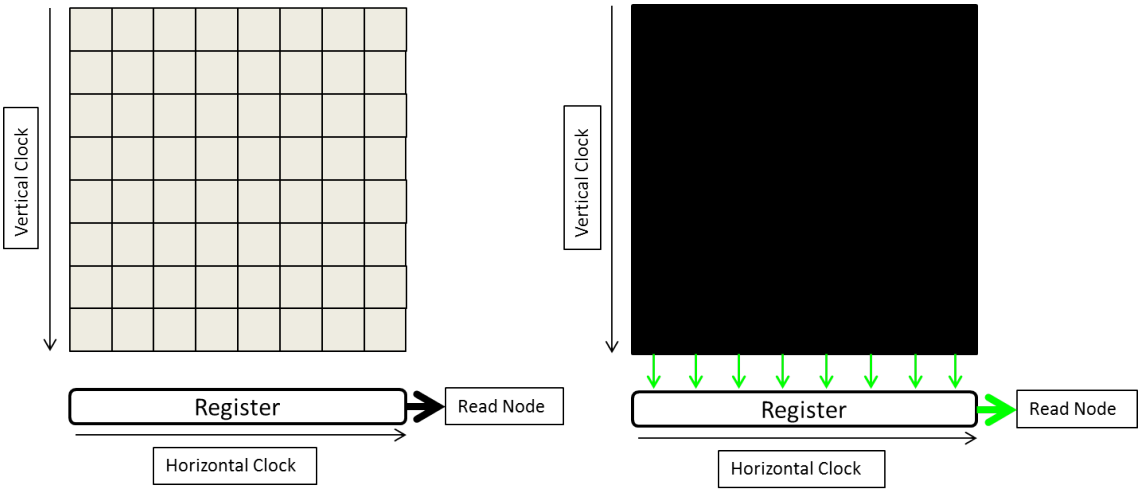

Figure A.3: Diagram of a Full-Frame CCD sensor

Block-Transfer CCD sensor

The block transfer CCD differs from the full-frame type by a surface discriminated into two areas, one dedicated for the acquisition and the other for the storage and the transfer of the data acquired. This mode of operation, compared to a full-frame CCD, offers the advantage of reducing the time required for transferring data and thus allows a higher frame rate of images acquired per second. Despite the possibility offered to achieve shorter acquisition time, this kind of sensor can not perform properly without mechanical shutter to avoid problems artifact during data processing. Operation always requires two phases, one acquisition and another reading which is performed sensor obstructed. However, the reading phase becomes shorter by the addition of the buffer reading zone. Of course, the cost of production of this type of sensor is important because only half of its surface is effectively dedicated to the photons detection.
A loss of sensitivity due to the use of this technique seem somewhat obvious. Indeed, with an equal sensor surface, a reduction of the fill-factor is noted(theoretically less than 50%). A way to correct this problem is the use of an array of micro

lenses which can refocus the incident light to the sensitive part of the sensor and thus reach a value of fill-factor similar to a full-frame CCD.

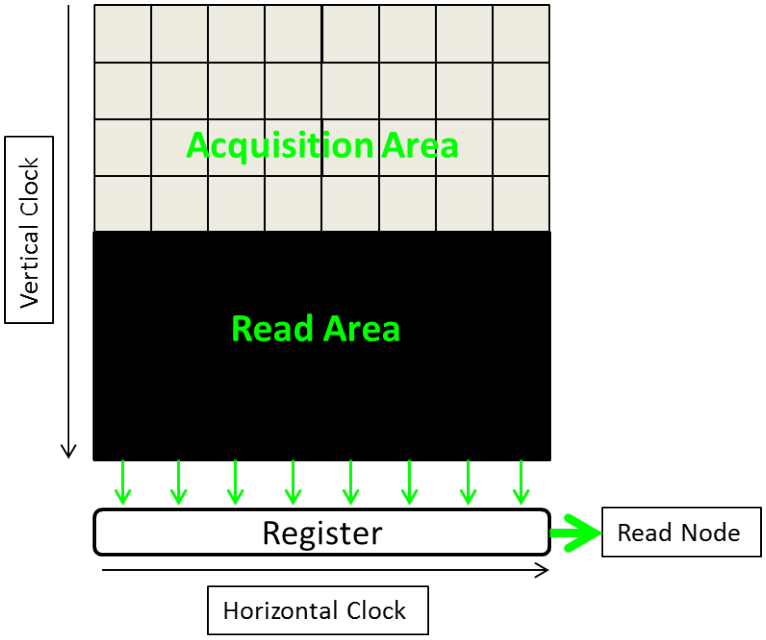

Figure A.4: Diagram of a Block-Transfer CCD sensor

Interline CCD sensor

The interline CCD is the fastest type of CCD sensor. The sensor is discriminated by pairs of columns, one is dedicated to the acquisition and the other to the storage and transfer of the data to the register(s). This configuration allows to avoid shutters and thus reduces the charges transfer time.
Despite the problem of the cost of production (exactly the same as the Block-Transfer CCD), the gain on the maximum number of frames per second is noticeable. This method eliminates the need for mechanical shutter. The transfer of information between the acquisition column and the storage column is about $1\mu s$, which avoids artifacts while in continuous acquisition (this functionality is also called electronic shuttering). As for the Block-Transfer CCD, an array of micro-lenses could be used to redistribute the incident light to the sensitive part of the sensor in order to achieve a correct fill-factor value. Another advantage is that the sensor is less sensitive than its predecessors to glare phenomena, smearing and blooming, thanks to the physical boundaries created by the columns dedicated to the reading between photosites.
This type of CCD is the most common. It offers a compromise between sensitivity

and real-time imaging performances.

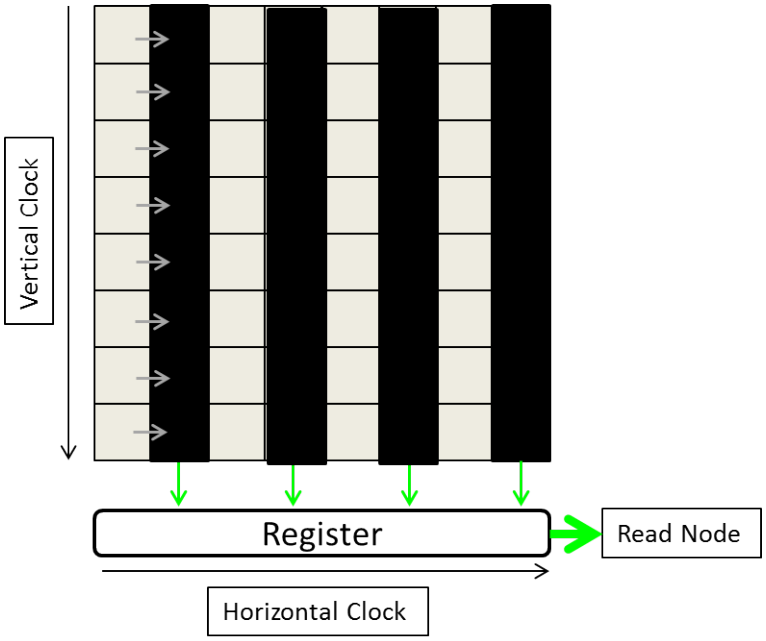

Figure A.5: Diagram of an Interline CCD sensor

CMOS-APS technology

For fifteen years now a new technology becomes highly competitive in front of CCD sensors. This is the CMOS-ASP for Complementary Metal Oxide Semi-Conductor Active Pixel Sensors, name rather related to the manufacturing technique (taken directly from the microelectronics computer chip type) as the imaging technology itself. The CMOS sensor is different from the CCD in that the electronics dedicated to information processing (amplification, analog to digital conversion) are located directly on the pixel, alongside the photosite. Obviously, the surface dedicated of the pixel to the detection light is diminished. Also, as mentioned before, a micro-lenses array can solve part of the problem, as the Interline CCD, by redirecting the luminous flux to the sensitive part of the pixel and thus significantly increase the fill-factor. The figure A.8 shows shows the basic architecture of a CMOS sensor with its electronics and addressing row and column.

Besides the fact that CMOS sensors allow short acquisition time and fast imaging, they are also completely insensitive to artifacts glare as smearing or blooming by the fact that there is no connection possible between the pixels. The figure A.6 shows an example of glare artifacts,

b presents an image from a CCD sensor with glare at a light source. The picture

a shows the behavior of a CMOS sensor in a similar situation, smearing or blooming artifacts are not present.

Another advantage of CMOS compared to CCD is the ability to reach the value of each pixel individually, hence the possibility to perform a windowing of a region of interest. The frame rate of the CMOS sensor will be directly linked to the number of pixels selected in the region of interest. The figure A.7 represents the type of windowing possible on a CMOS sensor

a and CCD sensor

b.

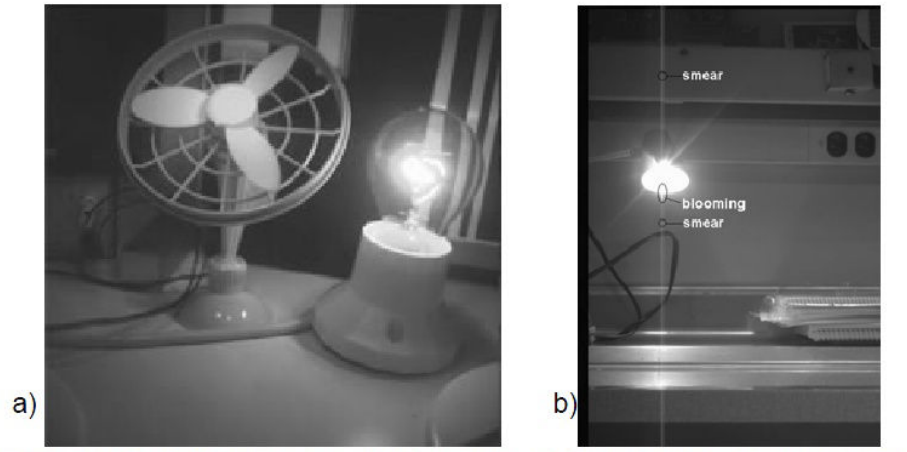

Figure A.6: Examples of glare artifacts

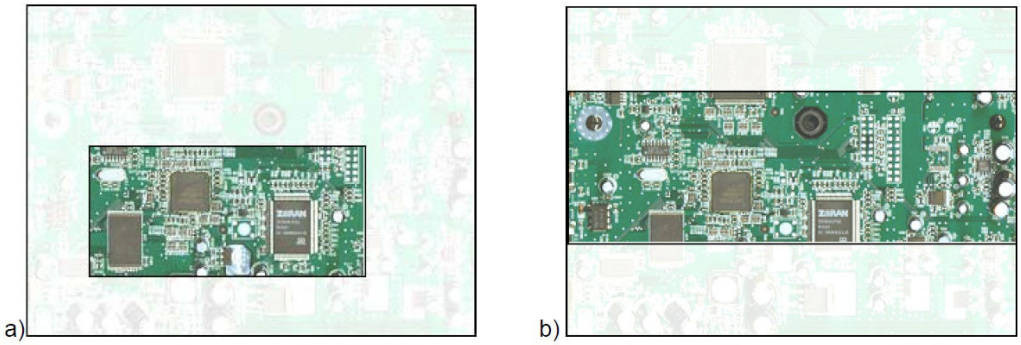

Figure A.7: Several windowing achievable on CMOS and CCD sensor

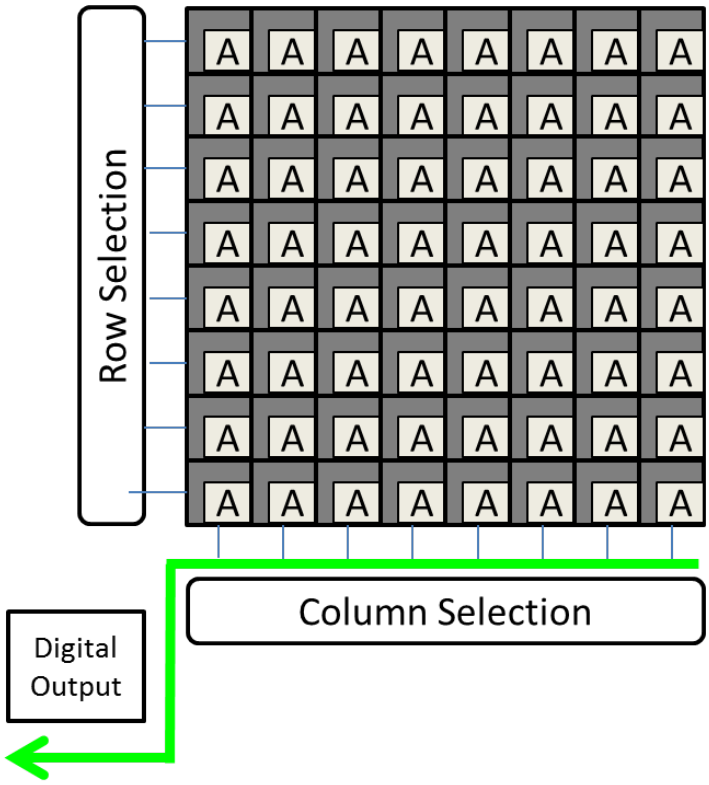

Figure A.8: Diagram of a CMOS sensor

From a constitutive point of view, the CMOS sensor differs pretty much from the CCD. Although both from single-crystal silicon and using the photoelectric effect described above to detect photons, the two technologies are opposed by their target of manufacture, composition of cells and the thickness of the epi-layers. The Photon flux must pass through several layers at the surface before being actually absorbed by the silicon. Different refractive index (Si: 3-5; SiO2: 1.45; (Magnan, 2003)), and the nature and thickness of the different cell materials that induce the sensor response are strongly dependent of the wavelength of the incident light.
The figures A.9 and A.10 are two types of cell architectures that can be encountered in CMOS technology. The complexity of the CMOS sensor is that one must ensure that the pixel data transmission, multiple levels of interconnection and dielectrics are used to allow this. In comparison, the structure of the CCD sensor, much simpler (see Figure A.2), optimizes the transmission for larger values. This results in a dynamic generally higher in CCD technology compared to CMOS technology.

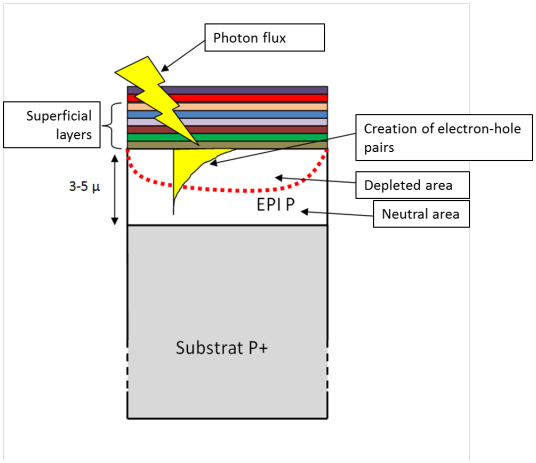

Figure A.9: CMOS' photo-gate architecture

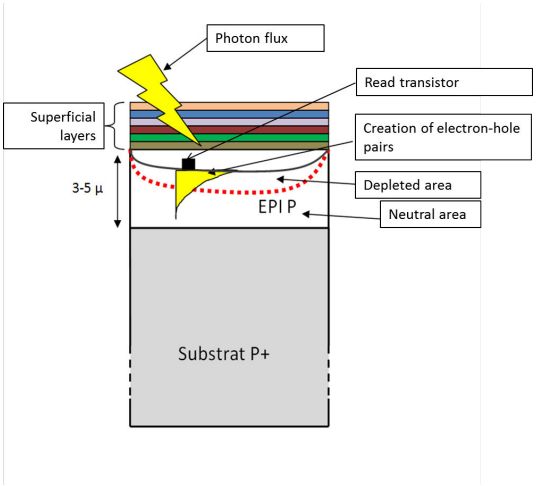

Figure A.10: CMOS' photo-diode architecture

The figure A.9 is the architecture of CMOS-type photogate. This is the same type of detector as the CCD and it is characterized by a transmission of the read data by layer and thus a reduction of the response to low wavelengths, including the blue.

The figure A.10 presents an architecture of CMOS-type photodiode. Compared to the photogate, it includes a read transistor with a common node shared by the photosensitive area. This design results in an overall decrease in sensitivity between the photodiode and photogate. However, there is no loss in sensitivity for lower wavelengths in the case of a photodiode.

Although the photodiode architecture is more complex due to the presence of an additional transistor, it is better integrated and achieves a better fill-factor with less electronics on the pixel. In addition, the use of photogates requires an additional control signal which increase the power consumption of the device and the noise. Finally, more technologically accomplished, the photodiode is the best choice for CMOS APS- although not allowing multiple integrations unlike photogates.

A.2 Characteristic values of an image sensor

For the performance characterization of imagers, sensors, or, more generally, cameras, it is necessary to evaluate a set of parameters. Experiments are used to compare the different solutions according to intrinsic aspects. The goal of a first series of tests will be to extract these characteristic values, the experimental

approach will be discussed later in this report. The parameters to be evaluated are:

- **The Quantization Step** : the number of electrons needed to move from one level of gray to another for a pixel and is expressed as the number of electrons per gray level.
- **The Quantum Yield** : the ratio between the number of incident photons and the number of electrons actually transcribed for a given wavelength, and is expressed in percentage as a function of the wavelength.
- **The Sensor's Response Uniformity** : the difference in response to a single excitation between the pixels of the sensor, the characteristic value is called Non Uniformity Photo Response or PRNU. This value expresses the dispersion of the response of a sensor, as a percentage.
- **The Linearity** : the curve representing the average gray level of a pixel of the sensor as a function of the illumination should be a straight slope.
- **The Noise** : noise characteristics of an imager are numerous and are discussed in detail in the camera characterization method. We include the readout noise, dark current, the photon noise or quantization noise.
- **The Dynamic Range** : it represents the number of values that can be discriminated by the sensor. It is expressed in number of electrons which are directly related to the number of incident photons and the well depth of photosites.

The EMVA (European Machine Vision Association), bringing together the main manufacturers and users of industrial cameras and publishes standards for the characterization of cameras (European Machine Vision Association, 2010). The parameters evaluated by the standard are similar to those exposed in this report. The following graph, A.11, shows the evolution of the response of a sensor to a growing number of incoming photons. It is characteristic of a test from the standard EMVA. The slope of the line represents the quantum efficiency of the sensor. The dynamic is here the delta of values that can discriminate the sensor. The noise grows with the increase of the signal, however, an offset is always present and dominates at low exposure. The signal to noise ratio is the ratio of the two curves. We choose to represent the results independently for easier reading rather than all together like on this type of curve.

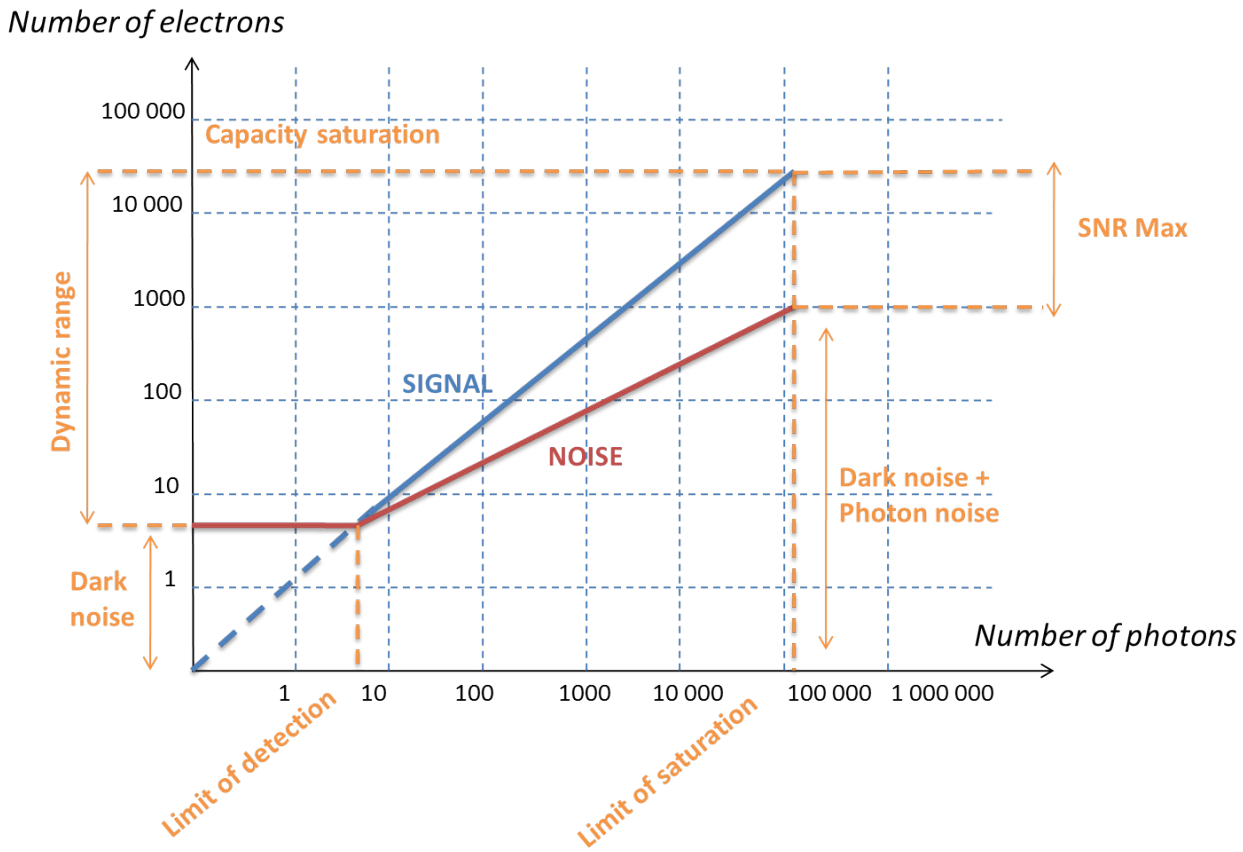

Figure A.11: Sensor global response, noise evolution, EMVA type

A.3 Characterization methodology

A.3.1 Experimental setup

The experiments are designed to extract the intrinsic parameters of a camera, all in order to properly evaluate and to define the strengths and weaknesses. What will follow is to describe and explain the tests to characterize a digital camera, whether it is a CCD or a CMOS. It is important to note that to perform these tests the camera should not be subject to any correction or gain or binning. The material used is a light gun with a controllable voltage source and a diffuser, a power meter, a set of monochromatic filters and software to acquire images from the camera and control parameters such as exposure time or gain of the sensor, see figure A.12. ImageJ software is used to extract from the images acquired useful information such as the average values of gray levels or variance between images.

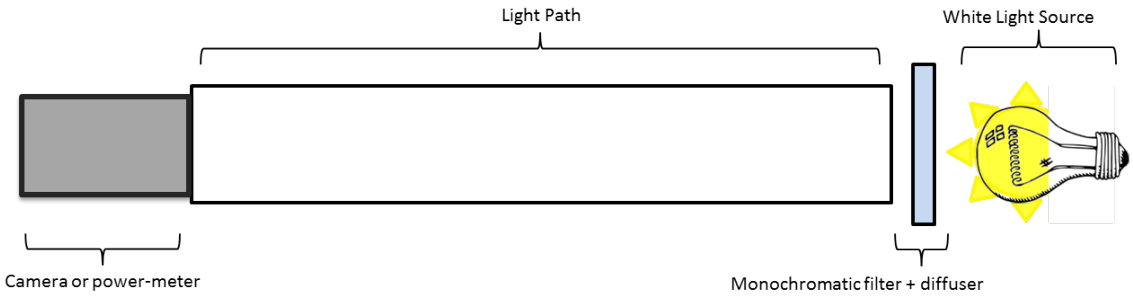

Figure A.12: Diagram of the measurement setup

A.3.2 Quantization step

The quantization step corresponds to the number of electrons per gray level for a pixel of the sensor. In other words, it is the number of electrons needed to move from one level of gray to another. This number, unique to each sensor, corresponds approximately to the total potential well capacity (expressed by a number of electrons) divided by the number of possible levels (corresponding to the dynamics of the image, for example 4096 gray levels possible for a 12 bits sensor). It is obtained by the slope of the straight $N_g = q\sigma^2 + cst$, with N_g the gray level and q the quantization step, cf figure A.13.

$$\begin{cases} N_g = q\sigma^2 + cst \\ With\ \sigma = \frac{1}{\sqrt{2}} \times StandardDeviation[Image1 - Image2] \end{cases} \tag{A.1}$$

The constant value of the equation corresponds to the read offset resulting from the readout noise and dark noise of the camera.

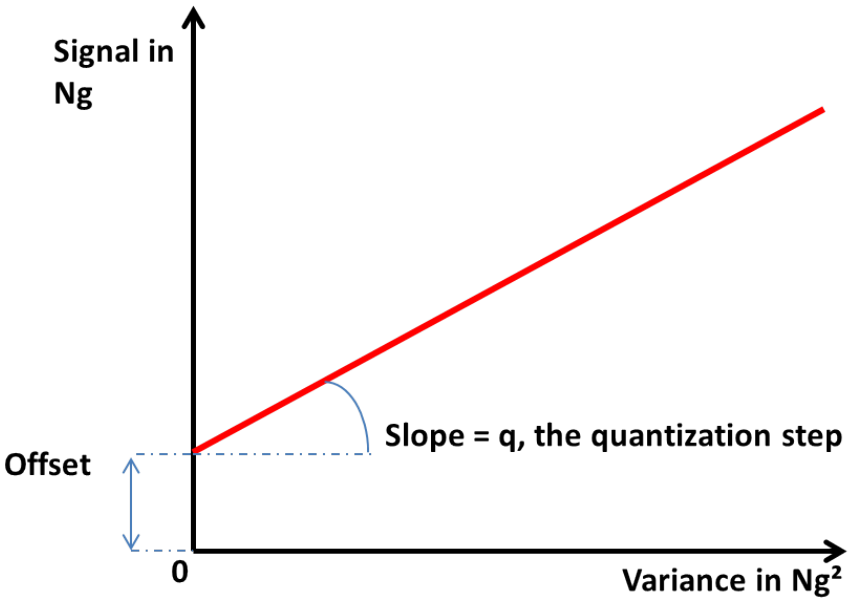

Figure A.13: Curve quantization step

We can write N_g as a function of the quantization step and the number of electrons transcribed by the sensor. This number of electrons being itself a function of the number of photons emitted by the source and the quantum efficiency, defining the percentage of photons transcribed into electrons by the sensor. We define the gray level N_g as follows:

$$\begin{cases} N_g = \frac{1}{q} N_e = \frac{1}{q} Q_e N_{ph} \\ N_e : \textit{number of electrons per pixel} \\ Q_e : \textit{quantum yield} \\ N_{ph} : \textit{number of photons per pixel} \end{cases} \tag{A.2}$$

The photon emission follow a Poisson distribution, this rule is also applied to the electrons transcribed. Knowing that a random variable X follows a Poisson distribution with parameter λ, X $P(\lambda)$, its variance $V(X)$ is equal to λ. The variance between two gray-level images, σ^2, is equal to $\frac{1}{q^2} var(N_e)$. Since N_e follows a Poisson distribution :

$$\sigma^2 = \frac{1}{q^2} N_e \tag{A.3}$$

The combination of the above equations gives us the following relation :

$$q = \frac{N_g}{\sigma^2} \tag{A.4}$$

This shows that q is the slope of the straight line defined by $N_g = q\sigma^2 + cste$. In addition, the following relation about the quantum yield is also defined :

$$Q_e = q\frac{N_g}{N_{ph}} \tag{A.5}$$

In practice, to determine the quantization step, a series of images is acquired by varying the illumination of the sensor from a high value to extinction. The acquisition of a pair of images by illuminance value is sufficient in the context of determining the variance between these two images and thus able to trace the curve. ImageJ software can process images to extract useful information such as average gray level images or the standard deviation of the subtraction of two images.

A.3.3 Noise

The noise characterization of a sensor is an important and critical evaluation. For a CCD or CMOS sensor type there are several types of noises.

Readout noise and Dark noise : The readout noise of a sensor depends on the efficiency of the charge transfer and the associated analog amplification. In the case of a CMOS sensor, the readout noise is rather replaced by a noise called kT/c representing the charges fluctuation to the terminals of a capacity (k Boltzmann constant, T temperature and c capacitance at the input of the amplifier transistor which is generated during the reset of the photosite). The readout noise, depending on the sensor's electronics, occurs once during each measurement and independently of the integration time.

The dark noise is a random phenomenon and it is generally negligible with ill-defined origin (electrons detached spontaneously from the die, or else black body radiation or photon noise associated with dark current). The readout noise is the offset of the curve representing the variance between two images based on the time of acquisition.

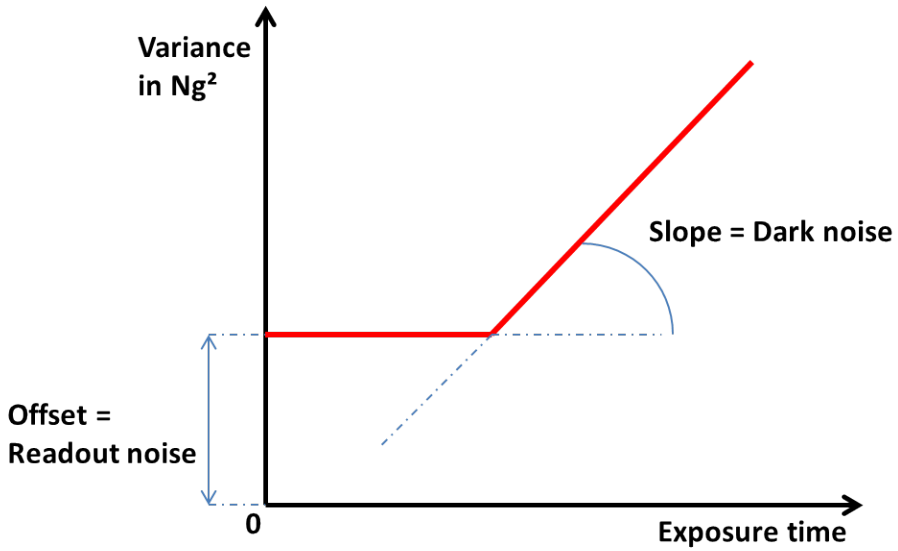

Figure A.14: Curve readout noise and dark current

The variance is expressed by the following equation : $(\frac{1}{\sqrt{2}} \times StandardDeviation[Black1 - Black2])^2$, images are acquired camera obstructed.

Dark current and thermal noise : The dark current, like the dark noise is not a random phenomenon. It is the expression of the natural increase in the black level as a function of the exposure time. It is very temperature dependent and is related to the so-called thermal noise of a sensor (or noise photon conversion electrons). It follows from the appearance of this phenomenon

Hot pixels during long exposure time, usually greater than $1s$. This is generally due to the leakage currents that generate additional electrons at a single pixel site.

The value of the dark current for a sensor is given by the slope of the curve representing the gray level of an image acquired by the camera obstructed in function of the exposition time. The reading offset obtained (different from the readout noise) is due to imperfections of the camera (pre-load of the sensor for instance).

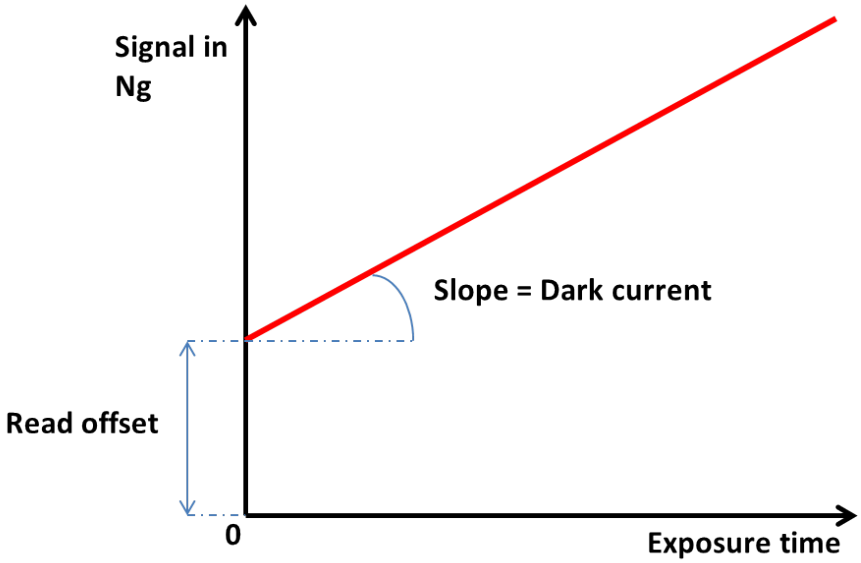

Figure A.15: Curve dark current and offset

Photon noise and quantization noise : The photon noise is independent of the camera. It finds its origin in the fact that any regulated source emits a number of photons per second depending on a Poisson statistics. Its value is equal to the square root of the signal obtained by electrons. The quantization noise is the loss of information on the received signal during the gray-scale electrons conversion. It's expressed in electrons and is equal to $\sqrt{\frac{q^2}{b}}$,q the quantization step previously defined and b the dynamic range expressed in bits (for instance 12 for a 12 bits camera, i.e 4096 levels of gray.
Finally, the gray level of a pixel corresponds to :

$$N_g = N_{ph}\frac{Q_e}{q} + Read\ Offset + Dark\ Current \times \frac{Exposure\ Time}{q} \tag{A.6}$$

The uncertainty in this gray level is the sum of the noises previously defined :

$$\sqrt{Read.Noise^2 + Photon.Noise^2 + Quantization.Noise^2 + (Dark.Current \times Exposure\ Time)^2} \tag{A.7}$$

For very short exposure times, the determining noise factor is the readout noise. However, for long exposure, the thermal noise becomes critical (Dark Current × Exposure Time).

In practice, camera obstructed, the sensor response on integration time short to long is tested. We seek to determine the dark current of the camera corresponds to the natural increase in the black level depending on the exposure time. A series of 5 pictures per integration time can accurately determine the parameters related to the readout noise and dark current. The mean values of gray level of these images are used to plot the two curves as defined above.

A.3.4 Linearity

The linearity evaluation checks whether the gray level obtained is proportional to the luminous flux received. To do this, we plot the average gray level of the images (multiple shots) based on the luminous flux. Note that if the illumination of the camera is not homogeneous, the measurement will be effected only on a portion of the image. Images close to saturation are sensitive, an anti blooming system could be an issue (for the CCDs only, no blooming phenomenon of CMOS sensors).

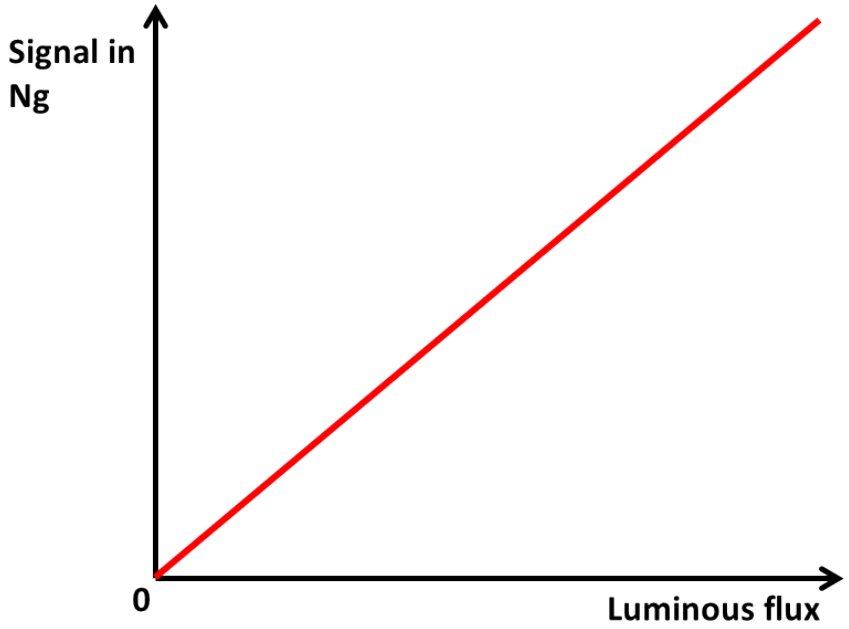

Figure A.16: Curve linearity

A.3.5 Photo Response Non-Uniformity

The PRNU reflects a difference in sensitivity between pixels of a sensor, whether CCD or CMOS technology. This is not a random aspect, it is intrinsic to the

sensor studied. It is therefore the evaluation of the uniformity of the response of a sensor.
To verify this PRNU, the camera is exposed to a constant luminous flux and several acquisitions are made at different rotations of the camera. We quantify this value by a notion of dispersion on the sensor (standard deviation divided by the mean percentage for a series of images, i.e. a position of the camera). We calculate the dispersion for 4 different angles, 12h, 3h, 6h and 9h.

A.3.6 Quantum Yield

The quantum yield, as seen previously, allows to deermine the relationship between the number incoming photons and the number of electrons transcribed by the sensor. This efficiency depends on the wavelength of the beam received. Also, a measurement of the luminous power of the incoming beam is necessary to perform the measure (in nW, this value is measured thanks to a power-meter). The integration time and the light intensity are fixed, only the wavelength varies. Once this data collected, we translate the received power from Watt to Joule as follows: $1W = 1J.s^{-1}$ with s the exposure time. A photon emitted by a source at a wavelength λ has an energy $E = \frac{hc}{\lambda}$ expressed in Joule (h Planck constant and c the celerity). We can therefore express the power received by the power meter into photons, considering the surface of the photo-detector of the power-meter used.
The average gray level per pixel of the camera is recorded, knowing the physical size of each pixel. Thanks to the value of the quantization step evaluated before, this value can be converted in number of electrons. Hence, knowing the surface ratio between the power-meter and a pixel, we are able to determine the quantum yield of a pixel of the camera's sensor for a given wavelength.

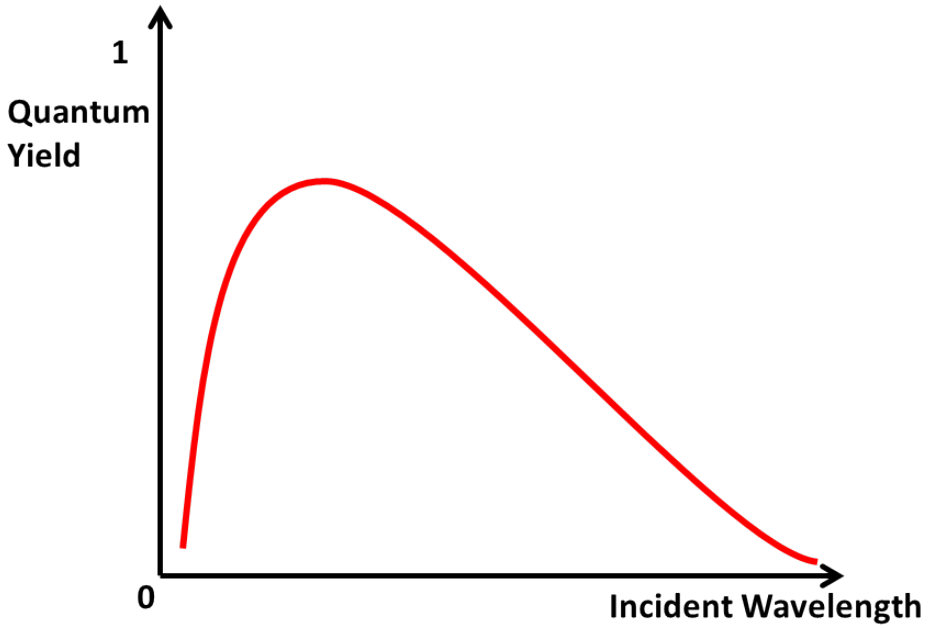

Figure A.17: Curve quantum yield

A.4 Sample results of evaluations

More than 20 different cameras have been evaluated during this thesis for the needs of the development projects. Sample results will be presented in the following section. The data presented have been acquired according to the methods detailed previously.
The NET KS6600 is a custom camera developed for the Fluostick^{TM} project. The camera is also used in the FluoMIS^{TM}. This camera integrates a Sony CCD sensor ICX659ALA. The Ximea MQ022CG-CM is the camera of the pulsed mini-invasive device presented in chapter 4 of this thesis. It compounds a state of the art CMOS sensor from CMOSIS, the CMV2000. Two other systems are compared to these cameras. One is the Lumenera LM165m camera, which integrates a reference CCD sensor in scientific imaging, the Sony ICX285. The other camera is Dalsa HM1400, which is a good illustration of CMOS systems back in 2011 when first camera evaluation had been performed.

The table A.1 presents characteristics and sample results about overall noise of the different systems. The two CCD sensors presented are quite similar in term of characteristics. The main difference resides in the fact that the ICX659 is a smaller sensor and requires less electronics to be interfaced than the ICX285.

System	**Lumenera LM165m**	**Dalsa HM1400**	**NET KS6600 (Fluostick™& FluoMIS™)**	**Ximea MQ022CG-CM (New device chapter4)**
Sensor	CCD Sony ICX285, 2/3"	CMOS Dalsa 1"	CCD Sony ICX659ALA 1/3"	CMOS Cmosis CMV2000 2/3"
Definition	1392×1040px	1400×1024px	752×582px	2048×1088px
Pixel size	6.45μm	7.4μm	6.5μm	5.5μm
Framerate max (fps)	20	64	25	170
ADC definition ($bits$)	14	12	10	12
Dark current ($Ng.px^{-1}.s^{-1}$)	1.54	733	2.5	39
Read noise ($Ng.px^{-1}$)	2	11	2.4	3.8
Offset ($Ng.px^{-1}$)	2	200	3	2
Theorical noise, 1s exposition time (Ng)	5.54	944	7.9	46.8
Theorical noise, 20ms exposition time (Ng)	4.03	225.66	5.45	8.58

Table A.1: Comparison of the cameras integrated in the systems described in the thesis more reference CCD et CMOS systems. Noises are given for a 10$bits$ equivalent dynamic

The noise is low for both CCD sensors.
The noise of the CMOS imagers presented here are higher than the noise of CCDs. Nevertheless, the value of the overall noise is way bigger for the Dalsa camera, from an older sensor generation. Globally, all CMOS sensors tested in 2011 and 2012 were not adapted to a fluorescence imaging use because of too important noise and a truncated Signal-To-Noise ratio. Recent improvements have been performed and CMOS cameras such as the Ximea selected present very good characteristics for an integration in a FIGS systems.

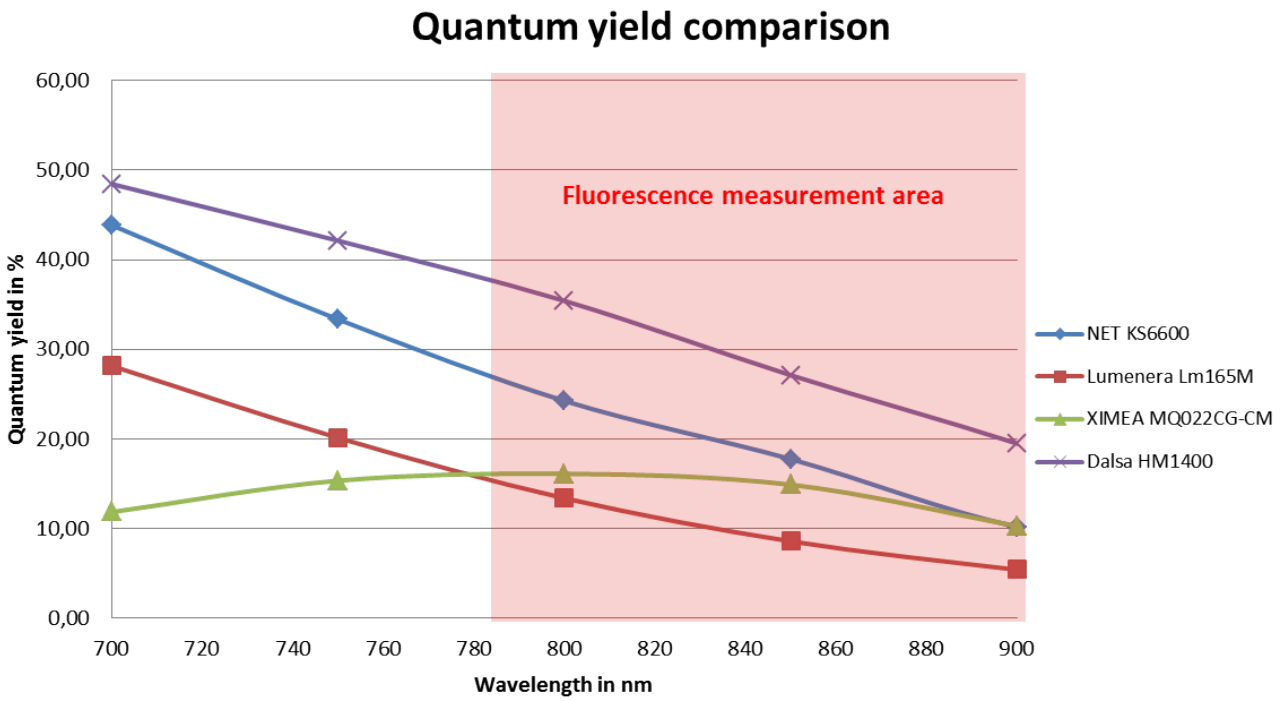

Figure A.18: Quantum yield comparison
Quantum yield comparison between 4 tested systems

The figure A.18 displays the quantum yield characteristics of the 4 systems in the NIR region of the spectrum. The particular response of the Ximea camera is due to the fact that the camera integrates a color sensor and not a monochrome one like the other systems, see figure 4.5 in chapter 4. Althought its quantum yield is the best of the systems, the Dalsa is penalized by its noise too high.

Appendix B

Optics characterization tools

B.1 ICG limit of detection : drops test

A critical aspect which has to be determined to properly evaluate a FIGS system is the fluorescence limit of detection. In the case of ICG visualization, the limit of detection could be expressed as a concentration or a quantity of ICG.
To go further, Fluoptics had performed experiments in order to establish a correlation between a quantity of ICG visualized ex-vivo and in-vivo small tumors targeted by specific fluorescent contrast agent, as the Angiostamp^{TM} developed by the company. The goal was to set an ICG correspondence to more demanding fluorescent contrast agent. It means that a limit of detection measured with ICG could give a information about the overall system sensitivity in NIR fluorescent imaging. Indeed, manipulating ICG in development stages is easy and cheap.
A method of characterization of ICG limit of detection has been designed. The method implies drops of 10 μL of ICG at different concentrations and disposed on a piece of Parafilm®(Pechinet, USA). The ICG used is the Infracyanine®from Serb and is diluted in a 20 % albumin solution (Albunorm^{TM}, Octapharma). The concentration of ICG chosen for the thesis are 100 $\mu mol/L$, 10 $\mu mol/L$, 5 $\mu mol/L$, 1$\mu mol/L$ and 0.5 $\mu mol/L$. So, the quantities of ICG imaged are respectively 1000 $pmol$, 100 $pmol$, 50 $pmol$, 10 $pmol$ and 5 $pmol$. The systems developed in the thesis are mainly designed for ICG visualization and no need to go to lower quantities of product has been identified. Nonetheless, the ability to image a quantity of 5$pmol$ of ICG has been identified as a good indicator to determine if a system is sensitive enough to deal with specific targeted contrast agents. The figure B.1 is image issued from test according to the method described here.

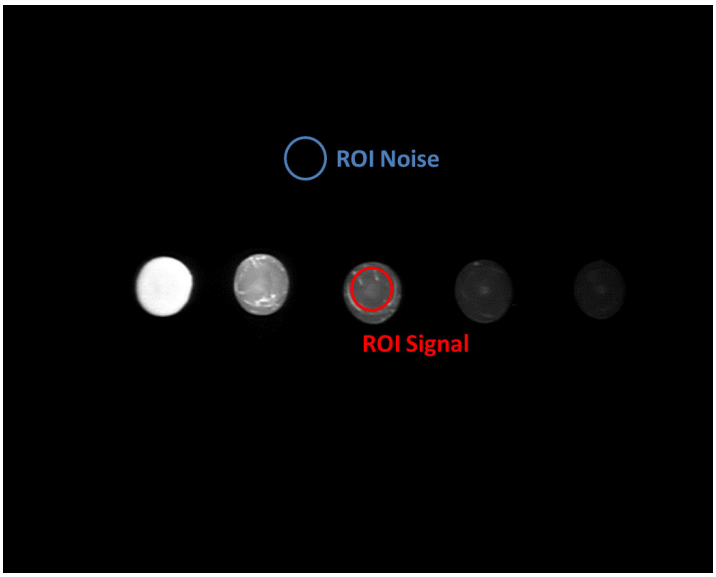

Figure B.1: Image acquired with the Fluostick^{TM}during the drops test. Quantities of ICG visualized are, from left to right, 1000$pmol$, 100$pmol$, 50$pmol$, 10$pmol$ and 5$pmol$.

The calculation of the Signal to Noise Ratio (SNR) is a good indication in order to determine a limit of detection. For one drop of ICG imaged, two Region Of Interest (ROI) are defined, see figure B.1. One gives information about the fluorescence signal collected, the other is informative about the noise and the background level of the image. When the SNR value of a drop is greater than 1, we consider that the system is able to detect the corresponding quantity of ICG. The calculation is performed as follow:

$$SNR = \frac{Average\ value\ in\ Ng(ROI\ Signal) - Average\ value\ in\ Ng(ROI\ Noise)}{Deviation\ of\ ROI\ Noise} \tag{B.1}$$

When the SNR value of a drop is greater than 1, we consider that the system is able to detect te corresponding quantity of ICG.

B.2 Resolution determination

The evaluation of the resolution or the resolving power of an imaging device is an important characteristic. The most common way to determine it involves an USAF1951 resolution test target. The name of the test comes from the fact that it was established by US Air Force in 1951. The pattern consists of banks of

three bars with dimensions from big to small. The smallest bank of bars the imaging device can discern sets its resolving power. The figure B.2 is an example of a USAF1951 test chart imaged by the Fluostick^{TM} system.

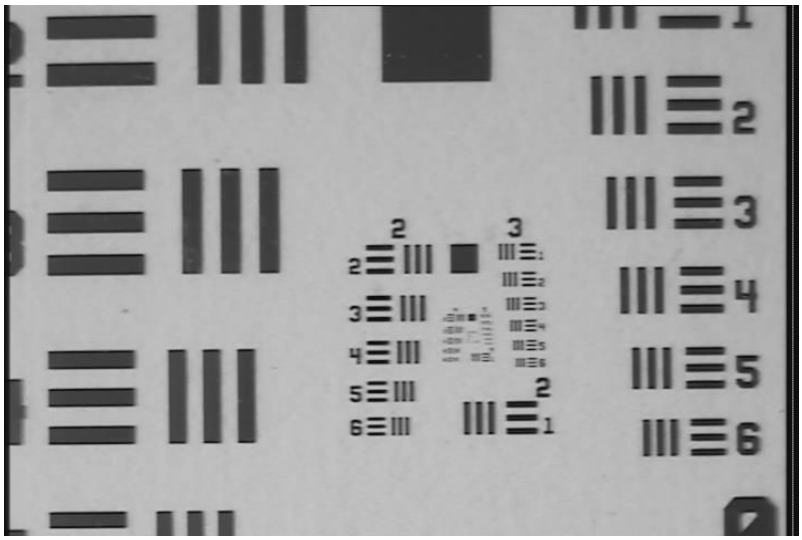

Figure B.2: Image of an USAF1951 resolution chart acquired with the Fluostick^{TM}

Groups of 6 distinctive banks of bar are defined. A correspondence between a Group/Element imaged and a resolution expressed in line pairs per mm is given by the figure B.3.

Number of Line Pairs / mm in USAF Resolving Power Test Target 1951												
Group Number												
Element	-2	-1	0	1	2	3	4	5	6	7	8	9
1	0.250	0.500	1.00	2.00	4.00	8.00	16.00	32.0	64.0	128.0	256.0	512.0
2	0.280	0.561	1.12	2.24	4.49	8.98	17.95	36.0	71.8	144.0	287.0	575.0
3	0.315	0.630	1.26	2.52	5.04	10.10	20.16	40.3	80.6	161.0	323.0	645.0
4	0.353	0.707	1.41	2.83	5.66	11.30	22.62	45.3	90.5	181.0	362.0	-----
5	0.397	0.793	1.59	3.17	6.35	12.70	25.39	50.8	102.0	203.0	406.0	-----
6	0.445	0.891	1.78	3.56	7.13	14.30	28.50	57.0	114.0	228.0	456.0	-----

Figure B.3: Number of line pairs / mm in USAF resolving power test target 1951

Theoretical equations give access to the resolution value expressed in μm, see below. Nevertheless, a rapid correspondence between the number of line pairs per mm given by the tab and the resolution in μm can be made.

$$Resolution(lp/mm) = 2^{Group+(Element-1)/6} \tag{B.2}$$

$$Resolution(\mu m) = \frac{\frac{32000}{2(6+Group)}}{2^{1/6}(Element-1)} \approx \frac{1000}{2 \times Resolution(lp/mm)} \tag{B.3}$$

B.3 Depth of field

The depth of field of an imaging system, such as a FIGS system, is a critical characteristics. The experimental values of the depth of field have been given for all the systems presented in this thesis. There is also a theoretical way to calculate the depth of field of a system. The calculation of the depth of field involved the aperture, N, the focal length, f and the circle of confusion, c of a system. The terms of the equations presented below justify the technical choices made in chapter 4 in order to improve the depth of field of the laparoscopic device.

B.3.1 Hyperfocal

The hyperfocal, H, of an imaging setup is distance beyond which all objects will be considered sharp when the focus of the system is set at infinity.

$$H = \frac{f^2}{N \times c} + f \approx \frac{f^2}{N \times c} \tag{B.4}$$

B.3.2 Depth of field, $d \gg f$

The depth of field is the distance around the focus point where an object would appear sharp. The nearest distance from the first sharp object and the lens of the camera, Dn and the farther distance from a sharp focused object and the lens, Df, are given by the equation below :

$$Dn = \frac{H \times d}{H + d} \tag{B.5}$$

$$Df = \frac{H \times d}{H - d} \tag{B.6}$$

The depth of field itself, Dof, is the difference between these two distances. The following equation is available when $d \gg f$ because of the approximation made on the hyperfocal value.

$$Dof = Df - Dn = \frac{2H \times d^2}{H^2 - d^2} \tag{B.7}$$

B.3.3 Depth of field, $d \approx f$

When the observed object is at a distance close enough to the focal length of the lens, $d \approx f$, the value of the magnification of the imaging system, m, is more accurate to determine the depth of field.
The magnification could be expressed as:

$$m = \frac{f}{f - d} \tag{B.8}$$

In this case, the depth of field is:

$$Dof = 2N \times c \times \frac{m + 1}{m^2} \tag{B.9}$$

B.3.4 Discussion and application

In both cases, the depth of field is function of $\frac{1}{f}$, which than greater the focal value is, lower the depth of field. Concerning the fluorescence imaging systems for mini-invasive surgeries, we have previously seen that with an increase of the value of the back focal length of the system the depth of field decrease. Indeed, increase the back focal length results in virtually increase the focal value of the lens used.
Calculation performed in chapter 4 shows that the back focal length of the new device is twice larger than the back focal length of the FluoMIS^{TM}($2.7cm$ for the FluoMIS^{TM} and $6cm$ for the new device). Indeed, the main difference between the systems is a back focal length which goes from $35mm$ for the FluoMIS^{TM} to $20mm$ for the new development. It is almost the same ratio as the depths of field. The other parameter that differs in the calculation of the depth of field is the circle of confusion which is function of the size of the sensor used.

Communications

SPIE Proceedings paper: The Fluostick, a real hand-held system for near-infrared fluorescence image-guided surgery
Authors: Paul Dorval, Nornam Mangeret, Stephanie Guillermet, Christian Adrien Righini, Gabriele Barabino, Philippe Rizo and Patrick Poulet
Doi: 10/1117/12.2037577
Proc. SPIE8935, Advanced Biomedical and Clinical Diagnostic Systems XII, 89350F (27 February 2014)

Concepts and Applications of Fluorescence Imaging for Surgeons, T. Ishizawa and F. Dip, be published by Springer Science and Business Media (New York) in 2015.
Section IV: New Frontiers In Fluorescence Imaging
Chapter 41: Miniaturized Clinical Imaging Device for Optical Surgery
Authors: Paul Dorval, Ihab Atallah, Gabriele Barabino, Maxime Henry, Michele Keramidas, Fabien Stenard, Clement Millet, Christian Righini, Philippe Rizo, Stephanie Guillermet, Veronique Josserand and Jean-Luc Coll

Résumé

Introduction

Lors de ces 10 dernières années, de progrès significatifs ont eu lieu concernant le domaine de l'imagerie médicale. L'imagerie médicale regroupe tous les outils permettant au médecin d'obtenir des représentations de la surface ou de l'intérieur de corps humain ou d'organes spécifiques. Pour le chirurgien, il s'agit d'obtenir de l'information qui permettra de poser un diagnostic ou de guider une intervention complexe.

L'imagerie de fluorescence est une modalité particulière d'imagerie médicale. La technologie exploite les propriétés de sources lumineuses dans le but d'imager en temps réel durant une intervention des particularités anatomiques des tissus grâce à l'injection préalable d'agents de contraste fluorescents au patient. De manière plus précise, la technologie d'imagerie de fluorescence peropératoire a montré un potentiel important pou la chirurgie oncologique, vasculaire et lymphatique. Plus spécifiquement, la fluorescence est utile pour des procédures comme la détection et la biopsie du ganglion sentinelle, la visualisation de la perfusion pour la chirurgie des lambeaux, la résection de tumeurs ou encore l'identification des réseaux vasculaires et lymphatiques.

Depuis 1983 et la première appendicectomie réalisée à l'aide d'un système laparoscopique, les interventions en chirurgie dite minimalement invasive n'ont cessé de se développer. Les avantages d'une opération mini-invasive sont nombreux. Tout d'abord, une diminution des traumatismes de l'opération ainsi qu'une limitation des pertes sanguines sont les premiers bénéfices notés. Bien qu'une chirurgie réalisée de manière mini-invasive peut prendre plus de temps qu'un geste équivalent en ouvert, le temps d'hospitalisation est lui toujours plus court. Expérimentant moins de douleurs et moins de cicatrices, le patient récupère plus rapidement de l'opération et moins de complications post-opératoires sont relevées.

Aujourd'hui, la majorité des indications cliniques de l'imagerie de fluorescence sont relatives aux procédures de chirurgie ouverte. Cependant, le potentiel de la technologie pour la chirurgie mini-invasive est très important. En effet, l'une des particularités de cette chirurgie réside dans le fait que le chirurgien, au cours de son opération, ne peut se fier qu'à l'image que lui renvoie le système. Par ex-

emple, il lui est impossible d'avoir une information de structure des tissus par le toucher, chose qu'il pouvait faire en ouvert. L'imagerie de fluorescence pourrait offrir au praticien ce complément d'information et aider à améliorer et diversifier les interventions de type mini-invasives. De récentes études cliniques ont mis en évidence un apport prometteur de l'imagerie de fluorescence pour des indications comme la cholécystectomie ou encore la néphrectomie, des gestes mini-invasifs courants. Dans ces études, l'imagerie de fluorescence est utilisée pour identifier certaines structures anatomiques comme les canaux biliaires pour la cholécystectomie ou les marges tumorales dans le cas de la néphrectomie. Cependant, très peu de systèmes permettant l'intervention mini-invasive ainsi que le recueil de l'information de fluorescence sont aujourd'hui disponibles sur le marché. Un des principaux problèmes au développement de la technologie réside dans la taille et la limite de détection des systèmes d'imagerie de fluorescence pour la chirurgie ouverte qui empêche la translation directe aux interventions mini-invasives.

Le propos et le but de la thèse est d'identifier les points bloquants et les principaux jalons qui permettront la translation de la technologie d'imagerie de fluorescence de la chirurgie ouverte vers la chirurgie fermée mini-invasive. A titre de validation, la thèse consiste aussi à présenter le développement d'un système performant d'imagerie de fluorescence spécifiquement dédié au mini-invasif. Le titre de la thèse, la miniaturisation des technologies d'imagerie de fluorescence pour assister la chirurgie mini-invasive, décrit bien le challenge que représente la translation de la chirurgie ouverte vers la chirurgie mini-invasive. Il s'agit en effet de partir de technologies existantes, mais trop encombrantes, et de les adapter à une utilisation en chirurgie mini-invasive. Le chemin emprunté passe par une première étape d'optimisation des technologies existantes avec la réalisation d'un système miniature pour la chirurgie ouverte. Le développement de ce système, appelé le Fluostick^{TM}, est le propos du deuxième chapitre de la thèse. Le troisième chapitre présente un premier système spécifique aux interventions mini-invasives et directement basé sur le Fluostick^{TM}, le FluoMIS^{TM}. Le quatrième chapitre de la thèse fait état des investigations effectuées dans le but d'optimiser les caractéristiques et corriger les problèmes du prototype FluoMIS^{TM}. Le premier chapitre du manuscrit est lui une introduction générale sur l'interaction entre la lumière et les tissus, les principes de l'imagerie de fluorescence ainsi qu'une revue sur l'instrumentation existante.

Chapitre 1, l'imagerie de fluorescence

L'imagerie médicale, vue comme le moyen de créer des représentations visuelles du corps humain à des fins de diagnostic ou d'intervention, est divisée en plusieurs catégories selon le spectre électromagnétique. L'imagerie de fluorescence, le propos de cette thèse, est composante de ce qu'on appelle l'imagerie optique au sens large, qui s'intéresse à la partie visible du spectre étendue à ses zones limitrophes proche infrarouge et proche ultraviolet (c'est-à-dire des longueurs d'ondes allant de 200 à 1000 nm).

En chirurgie, le premier instrument d'imagerie optique reste l'oeil du praticien qui est capable de distinguer les structures anatomiques, les couleurs et aspects des tissus grâce à un éclairage adéquat. Cependant, l'utilisation de capteurs, de caméras et de lumières spécifiques peut permettre d'atteindre un niveau d'information supplémentaire pour le chirurgien.

A un niveau microscopique, il existe deux types principaux d'interaction entre la lumière et les tissus : l'absorption et la diffusion. L'absorption exprime la disposition d'un milieu à absorber et bloquer la lumière incidente. Elle définit aussi comment l'énergie des photons incidents sera absorbée par le milieu considéré. Le deuxième phénomène d'interaction est la diffusion. Un faisceau de photons incident se diffuse dans le tissu avant d'être absorbé. La lumière réagira différemment avec les tissus en fonction de sa longueur d'onde. L'étude des coefficients d'absorption des principaux constituants des tissus montre une zone, appelée fenêtre thérapeutique, entre 600 nm et 1000 nm ou l'absorption des tissus est la plus faible. La diffusion est également moindre dans cette zone qui est privilégiée par les différentes modalités d'imagerie optique.

La thèse se focalise sur une modalité particulière d'imagerie optique appelée imagerie de fluorescence par réflexion. Une molécule est qualifiée de fluorescente lorsqu'elle est capable d'émettre de la lumière après avoir absorbé un rayonnement de longueur d'onde inférieure, et donc composée de photons d'énergie supérieure. Plusieurs molécules sont actuellement disponibles sur le marché clinique et injectable à l'homme. L'IndoCyanine Green, ICG, est l'une de ces molécules, appelées aussi fluorophores. L'ICG à de plus l'avantage d'opérer dans la fenêtre thérapeutique précédemment définie avec un pic d'absorption autour de 800 nm et une émission entre 800 et 900 nm. On parle plus communément d'imagerie de fluorescence proche infrarouge lorsque l'instrument d'imagerie est

spécifiquement dédié à l'ICG, en restant dans la perspective de l'autorisation d'usage thérapeutique d'autres molécules ; en particulier ciblant des pathologies spécifiques.

Le système d'imagerie de fluorescence à proprement parlé est composé d'un système d'éclairage, de type LED ou Laser, chargé d'exciter la molécule fluorescente cible. Un capteur est chargé d'acquérir la lumière émise par la molécule fluorescente. Un filtrage est placé devant le capteur dans le but de discriminer l'émission du fluorophore de la réflexion de la lumière d'excitation notamment. Après une large exploitation de la technique pour la recherche préclinique, une poignée de systèmes sont actuellement disponibles sur le marché clinique et sont essentiellement dédiés à des procédures de chirurgie ouverte. Les principales indications sont la chirurgie lymphatique et oncologique via notamment la technique du ganglion sentinelle, la chirurgie reconstructive, la chirurgie hépatique et cardiaque. Le système pris en référence pour cette thèse est le Fluobeam® développé par la société Fluoptics à Grenoble. Il servira de base technologique aux développements effectués au cours de cette thèse.

Chapitre 2, le Fluostick^{TM}, un système miniaturisé pour l'imagerie de fluorescence en ouvert

Les systèmes existants d'imagerie de fluorescence sont trop volumineux pour imager les rebords des cavités ou les côtés des organes en chirurgie ouverte. Cependant, l'imagerie de fluorescence appliquée à des indications spécifiques, comme la résection tumorale dans le cas de carcinose péritonéale ou encore certains cas de cancer au niveau de la cavité buccale et des voies aériennes supérieures a montré tout son potentiel sur des études précliniques. Aucun des instruments existants sur le marché ne permet aujourd'hui une translation de ces applications du préclinique au clinique. Le développement d'un système miniature pour la chirurgie ouverte trouve ici tout son intérêt. De plus, dans la cadre de la thèse, un tel développement serait la première étape de miniaturisation de la technologie pour aller vers le mini-invasif.

Le système développé, le Fluostick^{TM}, a été pensé dans l'optique d'être une véritable pièce à main. En effet, la miniaturisation du système d'imagerie de fluorescence concerne uniquement la tête caméra du système, seule partie à entrer dans champ opératoire du chirurgien. Le besoin du chirurgien d'utiliser un système d'imagerie plus petit, plus maniable et plus léger a été rapidement identifié.

Néanmoins, outre l'aspect ergonomique, l'autre but important de ce développement est de conserver un niveau de performance équivalent avec l'existant sur le marché, notamment en termes de limite de détection en fluorescence.
En partant du savoir-faire de Fluoptics sur les aspects filtrage et optique, le principal effort de miniaturisation a été consenti sur le capteur d'image du système.

Le Fluostick^{TM} a tout d'abord été caractérisé sur banc pour s'assurer de ces performances intrinsèques d'imageur de fluorescence. La puissance de la lumière d'excitation, la résolution géométrique des images fournies ou encore la limite de sensibilité en ICG du système ont été évaluées et se sont trouvées comparables avec les performances du Fluobeam®.

Des études précliniques ont été menées sur modèles de tumeurs de type cancer tête et cou et carcinose péritonéale. Ces évaluations sur souris ont notamment permis de valider la pertinence du système sur la visualisation de molécules fluorescentes ciblantes comme par exemple l'Angiostamp^{TM} développé par Fluoptics.

Enfin, un essai clinique a été mené avec le système. L'essai, réalisé au CHU de Saint-Etienne, avait pour but de valider la pertinence de l'utilisation de l'ICG dans la détection de tumeurs disséminées sur le péritoine et dans la cavité abdominale dans le cas de carcinose péritonéale. Dans le cadre du développement du Fluostick^{TM}, l'essai a été le moyen de valider l'ergonomie du système ainsi que ses performances et caractéristiques sur de véritables cas cliniques.

Le système a démontré son intérêt et ses performances se sont montrées au niveau de l'instrumentation existante en imagerie de fluorescence. Les choix effectués, que ce soit concernant l'ergonomie ou encore le capteur utilisé, serviront de base au design d'un système dédié à la chirurgie mini-invasive. En plus de son intérêt intrinsèque, le Fluostick^{TM} est la première étape de miniaturisation vers le véritable but de la thèse : développer un système d'imagerie de fluorescence pour adresser les interventions mini-invasive.

Chapitre 3, du Fluostick^{TM} au FluoMIS^{TM}, un système dédié à la chirurgie mini-invasive

C'est en se basant sur le travail effectué sur le Fluostick^{TM} que le système FluoMIS^{TM} (Fluorescence Minimally Invasive Surgery) a été développé. La voie d'acquisition de l'information de fluorescence est similaire entre les deux systèmes. Ce sont les particularités des interventions mini-invasives qui vont faire la différence entre les deux systèmes.

En effet, lors d'une chirurgie ouverte, le chirurgien a une vision directe de son champ opératoire et l'information de fluorescence en niveaux de gris fournie sur un écran annexe par le système d'imagerie est suffisante. Dans le cas d'une intervention de type mini-invasive le chirurgien ne voit plus directement son champ opératoire et doit se fier à un système d'imagerie couleur pour effectuer son geste. D'un point de vue ergonomique, deux systèmes d'imagerie ne peuvent pas coopérer au cours de l'intervention, le système d'imagerie de fluorescence doit donc jouer deux rôles : recueillir une information de fluorescence et fournir au chirurgien la meilleure image couleur possible du champ opératoire.

Le but de ce développement fut donc de créer un système d'imagerie de fluorescence pour la chirurgie mini-invasive en ajoutant une voie d'acquisition couleur au système Fluostick^{TM} existant. De plus, le nouveau système doit pouvoir s'interfacer avec un laparoscope standard du commerce ce qui implique un travail sur l'optique d'entrée du système ainsi que sur la génération de la lumière qui doit être compatible avec l'utilisation d'un câble fibre pour laparoscope.

D'un point de vue technique, le système se compose de deux capteurs, l'un monochrome pour l'acquisition de la fluorescence et l'autre couleur pour recueillir l'image anatomique du champ opératoire. Malgré l'ajout d'un capteur par rapport au Fluostick^{TM}, la tête caméra du système conserve un caractère de pièce à main, essentiel pour une caméra de chirurgie mini-invasive manipulée pendant toute l'intervention par le chirurgien ou son assistant.

Le système développé au cours de la thèse, le FluoMIS^{TM}, a été caractérisé et comparé aux performances de systèmes d'imagerie de fluorescence dédiés à la chirurgie ouverte. Des évaluations précliniques sur cochons ont permis de valider l'ergonomie du système en le mettant dans les mains de chirurgiens. Ces tests ont également confirmé l'intérêt et la pertinence de la fluorescence sur des

procédures comme la cholécystectomie. Par contre, la qualité de l'image couleur fournie au chirurgien n'a elle pas été jugée satisfaisante. La profondeur de champ du système s'est révélé trop faible pour une utilisation efficac toute au long de l'intervention. Les problèmes identifiés sur le FluoMIS^{TM} sont le propos du développement présenté dans le chapitre 4 de la thèse.

Chapitre 4, un nouveau système pour la chirurgie mini-invasive

Le développement du FluoMIS^{TM} a confirmé l'intérêt de l'imagerie de fluorescence pour la chirurgie mini-invasive. Cependant des problèmes on été identifiés sur la qualité de l'image couleur fournie par le système, d'un point de vue résolution, colorimétrie et profondeur de champ. L'utilisation d'un seul capteur couleur de plus grande taille et d'une meilleure résolution ainsi que l'adoption d'un mode d'acquisition séquentiel de l'information couleur et fluorescence ont permis la résolution de la plupart des problèmes identifiés.

L'utilisation d'un seul capteur, contre deux précédemment avec le système FluoMIS^{TM}, est possible du moment que les différentes informations à recueillir sont bien discriminées de manière spectrale et bien visible par le senseur. C'est le cas avec le capteur sélectionné pour le système. En effet, il dispose d'un filtrage de type Bayer pour l'acquisition de l'image couleur, filtrage devenant transparent dans la zone proche infrarouge du spectre, là où est collectée l'information de fluorescence. L'électronique du système a été développée dans le but de synchroniser les éclairages avec les acquisitions séquentielles du capteur pour ensuite recréer un flux d'images couleur et fluorescence de manière transparente pour l'utilisateur.

La caractérisation du système a bien montré le gain attendu en termes de résolution, profondeur de champ et qualité du rendu colorimétrique par rapport au système FluoMIS^{TM}. De plus, un gain significatif concernant la limite de détection en ICG par rapport au FluoMIS^{TM} est aussi observé. Seule la poursuite d'études précliniques et cliniques plus approfondies permettront de définitivement valider ces développements. A ce moment là seulement un marquage réglementaire et une commercialisation seront engagés par Fluoptics. Néanmoins, le but fixé en début de thèse semble atteint avec ce nouveau système d'imagerie de fluorescence dédié à la chirurgie laparoscopique et aux interventions mini-invasives en général.

Conclusion

Cette thèse à été l'occasion de montrer comment l'imagerie de fluorescence pouvait aider le praticien dans de nombreuses procédures. Grâce à la technologie, le chirurgien peut pratiquer son geste plus rapidement et le nombre de complications postopératoires est diminué comme dans le cas de la résection de tumeurs hépatiques par exemple.

Bien que le nombre d'interventions mini-invasives n'a cessé d'augmenter depuis 1983 et la première appendicectomie laparoscopique, seulement une infime partie des actes chirurgicaux sont réalisés à l'aide d'un instrument d'imagerie de fluorescence. Cependant, l'intérêt dans la technologie est réel et serait un moyen de fournir au chirurgien l'information supplémentaire dont il n'a plus accès par le toucher comme en chirurgie ouverte. Cette thèse fut l'opportunité d'adresser tous les aspects et détails techniques du système d'imagerie de fluorescence avec la démarche d'adapter la technologie à la chirurgie minimalement invasive. Travailler sur cette thèse a illustré que la mise à l'échelle de la technologie, de l'ouvert vers le fermé, implique des problèmes purement techniques, liés à la miniaturisation, mais aussi des soucis d'ergonomie et de mise en IJuvre du fait de la singularité des procédures de chirurgie fermée. Par exemple, les difficultés rencontrées concernent la sensibilité et la taille des capteurs d'images, l'intégration des différentes sources de lumière, la profondeur de champ du système et le besoin d'acquérir des images à haute vitesse à cause de la contrainte temps réel et du grandissement important du système de chirurgie laparoscopique. A la vue de ces éléments, ce travail s'est principalement centré sur l'architecture des systèmes, l'électronique, la caractérisation de capteurs, l'intégration des caméras et quelques aspects relatifs au filtrage et à l'optique. L'expertise de Fluoptics a été très importante sur les éléments liés au filtrage, au software ou encore l'optimisation colorimétrique.

La miniaturisation à proprement parlé a été conduite en deux étapes principales. Tout d'abord, l'effort a été consenti sur la taille de la tête optique du système d'imagerie de fluorescence pour l'ouvert. Il en a résulté un appareil miniature dédié à la chirurgie ouverte, appelé le Fluostick^{TM}, permettant d'adresser de nouvelles indications par rapport à l'instrumentation existante, telles que la résection de tumeurs dans le cadre de carcinose péritonéale,. Le principal challenge fut de réduire la taille du capteur d'images tout en assurant une limite de détection compatible avec l'utilisation de molécules fluorescentes ciblantes. La deuxième étape de miniaturisation a consisté en l'ajout d'une image couleur

au système, étape indispensable pour aller vers un système dédié à la chirurgie mini-invasive. Pour ce faire, deux méthodes ont été implémentées. L'une a consisté en l'utilisation de deux capteurs d'images et une acquisition simultanée de l'information de couleur et de fluorescence. L'autre méthode a été d'utiliser un seul capteur et une acquisition séquentielle pulsée pour superposer la fluorescence à l'image couleur.

L'approche basée sur l'utilisation d'un seul capteur d'images et un mode d'éclairage pulsé est la méthode la plus efficiente pour la visualisation de l'ICG lors de procédures mini-invasives. D'autres méthodes d'acquisition ont été testées, comme l'utilisation d'un éclairage séquentiel rouge, vert, bleu et lumière d'excitation avec un capteur monochrome. Cette méthode jugée trop lente pour la visualisation de l'ICG a tout de même été implémentée dans un système permettant l'imagerie de la protoporphyrine IX (PPIX) dans le cadre d'ablation de tumeurs au niveau de la vessie. La particularité de la méthode fut de permettre la visualisation d'un fluorophore opérant dans le spectre visible, la PPIX émettant de la lumière rouge quand elle est soumise à une longueur d'onde autour de 400 nm. En termes de valorisation, deux produits pour Fluoptics ont été issus de la thèse. Le Fluostick^{TM} est actuellement un produit commercialisé par Fluoptics. Il a reçu la certification CE medical en 2013. L'évolution du FluoMIS^{TM}, tel que présenté dans le chapitre 4 de la thèse, fera l'objet d'un essai clinique en 2015. Cependant, des améliorations et challenges technologiques sont toujours à venir. Un des challenges concerne la limite de sensibilité des systèmes. Le travail de thèse a permis d'identifier un facteur 100 à gagner sur le limite de détection en ICG à une distance de travail de 5 cm pour être capable de travailler avec des molécules fluorescentes ciblantes en procédure mini-invasive. Comme présenté dans le manuscrit, une approche basée sur l'utilisation d'un capteur à l'extrémité distale du laparoscope pourrait être une voie possible pour améliorer la sensibilité du système. Une autre voie pourrait consister en un travail spécifique sur les optiques du système, avec notamment des traitements antireflets adaptés à la fluorescence de l'ICG, pour permettre d'augmenter la quantité de lumière d'émission atteignant le capteur du système. Une limite de sensibilité améliorée est aussi un moyen de diminuer la dose de fluorophore injecté au patient. Une dose plus faible signifie une diminution du coût de la procédure ainsi qu'une potentielle toxicité diminuée.

Récemment, des systèmes d'imagerie mini-invasif 3D sont apparus sur le marché. En ce qui concerne l'imagerie de fluorescence, ces systèmes 3D présen-

tent une perte en résolution et une potentielle détérioration de la limite de détection à cause des trains optiques complexes impliqués dans la formation de ces images 3D. Cependant, la perspective d'un système d'imagerie de fluorescence mini-invasif 3D reste attirante.

Le transfert de la technologie d'imagerie de fluorescence de la chirurgie ouverte vers le fermé a été le fil conducteur de cette thèse. D'un autre point de vue, les solutions mises en IJuvre et les résultats obtenus dans la thèse peuvent aussi servir les interventions ouvertes. En effet, la miniaturisation des systèmes et le travail sur l'ergonomie, l'utilisation de capteurs de type CMOS et de modalités d'acquisition pulsée peuvent être le socle technologique d'un système alliant l'image couleur et l'information de fluorescence pour la chirurgie ouverte.

Paul DORVAL

Miniaturisation des technologies d'imagerie de fluorescence pour assister la chirurgie mini-invasive

Résumé

L'imagerie de fluorescence est une technique d'imagerie médicale permettant de visualiser l'émission d'un traceur, ou fluorophore, à l'aide d'une excitation de type Laser ou LED. Les domaines d'application de la technologie sont la chirurgie oncologique, la chirurgie reconstructive ou encore la chirurgie cardiaque. Bien que les besoins en chirurgie ouverte soient importants, l'évolution des pratiques tend à démocratiser la chirurgie dite minimalement invasive. La chirurgie endoscopique va dans ce sens, le but étant de limiter les traumatismes opératoires rencontrés en chirurgie ouverte. Parmi les avantages de cette techniques on note une diminution des saignements et de la douleur, ou encore une réduction de la durée d'hospitalisation.

Lors d'une intervention de type chirurgie ouverte, le praticien peur se contenter de la seuls information de fluorescence fournie par le système d'imagerie. Cependant, tout l'enjeu de l'imagerie de fluorescence pour la chirurgie mini-invasive est de venir greffer ne information relative au fluorophore sur une image couleur de très bonne qualité, essentielle au chirurgien. Pour une première évaluation, un système deux caméras a été réalisé. Un capteur est dédié à l'acquisition de l'image couleur et un autre à l'information de fluorescence. Cependant, notamment pour conserver pour conserver un système compact et proposer la meilleure ergonomie possible au chirurgien, l'endoscope final ne devra comporter qu'un seul imageur. Le principe de base est d'utiliser des impulsions de lumière d'excitation et de lumière blanche afin de séquentiellement acquérir les données de fluorescence et les images couleur. Il convient ensuite de traiter les informations recueillies pour reconstruire l'image désirée en temps réel.

Mots clés : Imagerie médicale, Imagerie de fluorescence peropératoire, chirurgie mini-invasive

Abstract

Fluorescence image-guided surgery is a medical imaging modality which allows the surgeon to visualize a fluorescent probe previously injected to the patient. The probe could be specific or not and the technology is useful in a wide range of application from oncologic procedures to reconstructive surgeries or cardiac procedures. Despite the important needs of this technology in open-procedures, the surgery in general is more and more minimally invasive. The goal of mini-invasive surgery is to limit patient's per and post operation trauma. The advantages of the technique are a decrease of bleeding and pain and a decreasing hospitalization time.

During an open surgery, the B&W fluorescence information given by the fluorescence image-guided surgery system is enough for the surgeon. For mini-invasive procedures, the in-game is to overlay the fluorescence information to high quality color image, compulsory for the surgeon to perform his procedure. As a first evaluation, a 2-sensors system has been rapidly developed. One sensor is dedicated to the acquisition of the color image and the other to the fluorescence information. In order to make the system more compact and improve the quality of the color image furnished to the surgeon, the final system should be composed of only one sensor. To create the color image and collect the fluorescence information with one sensor, the technique involved pulsed white light and excitation light in a sequential acquisition mode. The two information are combined and a real-time color plus fluorescence video is displayed to the surgeon.

Key words: Medical imaging, Fluorescence Image-Guided Surgery, Mini-invasive surgery